

Chapman University

## Chapman University Digital Commons

---

Pharmaceutical Sciences (Ph.D.) Dissertations

Dissertations and Theses

---

Summer 8-2019

### Sensory Primary Cilium is a Distinct Signaling Compartment

Rinzhin Tshering Sherpa

Chapman University, sherp101@mail.chapman.edu

Follow this and additional works at: [https://digitalcommons.chapman.edu/pharmaceutical\\_sciences\\_dissertations](https://digitalcommons.chapman.edu/pharmaceutical_sciences_dissertations)

 Part of the [Biology Commons](#), [Cell Biology Commons](#), and the [Molecular Biology Commons](#)

---

#### Recommended Citation

Sherpa RT. *Sensory Primary Cilium is a Distinct Signaling Compartment*. [dissertation]. Irvine, CA: Chapman University; 2019. <https://doi.org/10.36837/chapman.000086>

This Dissertation is brought to you for free and open access by the Dissertations and Theses at Chapman University Digital Commons. It has been accepted for inclusion in Pharmaceutical Sciences (Ph.D.) Dissertations by an authorized administrator of Chapman University Digital Commons. For more information, please contact [laughtin@chapman.edu](mailto:laughtin@chapman.edu).

Sensory primary cilium is a distinct signaling compartment

A Dissertation by

Rinzhin Tshering Sherpa

Chapman University

Orange, CA

School of Pharmacy

Submitted in partial fulfillment of the requirements for the degree of

Doctor of Philosophy in Pharmaceutical Sciences

August 2019

Committee in charge:

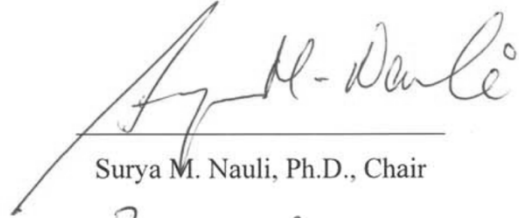
Surya M. Nauli, Ph.D., Chair

Reza Mehvar, Ph.D.

Rennolds Ostrom, Ph.D.

Marco Bisoffi, Ph.D.

The dissertation of Rinzhin T. Sherpa is approved.



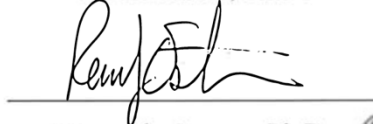
---

Surya M. Nauli, Ph.D., Chair



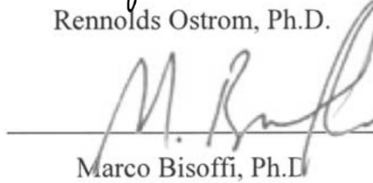
---

Reza Mehvar, Ph.D.



---

Rennolds Ostrom, Ph.D.



---

Marco Bisoffi, Ph.D.

August 2019

Sensory primary cilium is a distinct signaling compartment

Copyright © 2019

by Rinzhin Tshering Sherpa



## ACKNOWLEDGEMENTS

Firstly, I would like to thank my advisor Dr. Surya Nauli for his continuous guidance and support of my Ph.D. study. I appreciate all his contributions of time, ideas, and funding to make my Ph.D. a productive and stimulating experience.

I would also like to thank the rest of my thesis committee members, Drs. Mehvar, Ostrom and Bisoffi for their advice, encouragement and patience. I highly appreciate their time and insightful comments.

My sincere thanks to the support from members of the Nauli lab and the Chapman University School of Pharmacy. I would like to thank my family and others for supporting me throughout this journey.

I would acknowledge the funding support from Congressionally Directed Medical Research Program PR130153, NIH HL131577 and the Chapman University School of Pharmacy. Without the support, it would not have been possible to conduct this research.

## ABSTRACT

Sensory primary cilium is a distinct signaling compartment

by Rinzhin Tshering Sherpa

The primary cilium is a solitary cellular organelle that protrudes from the apical cell membrane. Findings on cilia-dependent mechanosensation have shown that the primary cilium acts as a transducer of fluid-shear stress into intracellular signaling. Over recent years, studies in primary cilia have intensified after determining a causal relationship between dysfunctional primary cilia and cystic diseases. Along with its mechanosensory function, the primary cilium houses a variety of receptors, ion channels and transporter proteins. Studies in cilia biology have shown that primary cilia are coordinators of signaling pathways such as Hedgehog (Hh), Wnt, and platelet-derived growth factor (PDGF) pathways during development and tissue homeostasis. The primary cilium has been established as a mechano, chemo- and osmosensing unit that transmits extracellular cues to the cell, which supports the importance of the primary cilium. As an important organelle involved in sensory functions and signal transductions, we encompass methodology for measuring cilia signaling along with a study of pH sensing function and cAMP signaling dynamics in the cilium. Defects in the structure of cilia or protein complexes located in the primary cilia cause a variety of diseases. With increasing the knowledge of ciliary biology, we can strategize approaches to repair defective cilia. Here we try to contribute to understanding the complex dynamic pathways of the cilia and point to potential pathways in regulating ciliary structure and function.

## TABLE OF CONTENTS

<b>Chapter 1. Introduction.....</b>	<b>1</b>
Motile Cilia.....	2
Primary Cilia.....	3
References.....	7
<b>Chapter 2. Mechanosensory and Chemosensory primary cilia in ciliopathy and ciliotherapy. ....</b>	<b>13</b>
Introduction.....	14
Mechanobiology and diseases.....	14
Primary cilia as biomechanics.....	17
Modulating mechanobiology pathways.....	21
Potential intervention for cilio-therapy.....	22
Potential mechano-therapy.....	23
Summary.....	24
References.....	25
<b>Chapter 3. Measurement of cytoplasmic and cilioplasmic calcium in a single living cell. ....</b>	<b>27</b>
Introduction.....	28
1. Choosing Ca <sup>2+</sup> indicators.....	30
2. Experimental Setup.....	34
2.1. Expression of genetically encoded cilia targeting sensor.....	34
2.2. Cell growth on microwire .....	35
3. Fluorescence Microscopy.....	35
3.1. Overview.....	35
3.2. Experimental setup.....	36
3.2.1. Flow equipment setup.....	37
3.2.2. Monitoring experiment.....	39
3.2.3. Data analysis.....	40
Conclusion.....	41
References.....	42
<b>Chapter 4. The Role of the Primary Cilium in Sensing Extracellular pH. ....</b>	<b>47</b>
Introduction.....	48
Materials and Methods.....	50
Results.....	55
i. Intracellular Acidosis in Response Acidic pH <sub>o</sub> .....	55
ii. MAPK Activation in Response to Acidic pH <sub>o</sub> .....	63
iii. NH <sub>4</sub> Cl Pre-Pulse Induces Intracellular Acidosis.....	67
iv. Intracellular Acidosis Activates MAPK Signaling Pathways.....	71
v. Effects of K <sup>+</sup> on pH <sub>i</sub> Recovery and MAPK Phosphorylation.....	71
Discussion.....	75

References.....	79
<b>Chapter 5. Sensory primary cilium is a responsive cAMP microdomain in renal epithelia.</b> .....	82
Introduction.....	83
Materials and Methods.....	84
Results.....	92
i. Tolvaptan increases ciliary length and enhances shear-stress induced cytosolic calcium increase.....	92
ii. Vasopressin receptor knockdown modulates cilia.....	96
iii. Primary cilia are cAMP responsive microdomain.....	101
Discussion.....	110
References.....	115
<b>Conclusion.....</b>	119
<b>References.....</b>	123

## LIST OF TABLES

Table 1. Mechanical forces within blood vessel.....	15
Table 2. Mechanotransduction diseases.....	16
Table 3. Ciliary proteins and their subcellular localization.....	18
Table 4. Properties of cilia targeting G-CAMP based sensors.....	33
Table 5. Composition of solutions used in the NH <sub>4</sub> Cl pre-pulse.....	52

## LIST OF FIGURES

Figure 1. Primary cilium as a sensory organelle.....	17
Figure 2. Mechanosensory primary cilia are dependent on functional sensory proteins...20	
Figure 3. Intracellular signaling pathways are involved in transducing mechanosensory function of primary cilia.....21	
Figure 4. Ciliary dopamine receptor can regulate cilia length and function through a complex cellular pathway.....22	
Figure 5. Schematic representation of genetically encoded calcium indicator (GECI) constructs. ....34	
Figure 6. Flow equipment setup for live cell and cilia imaging.....37	
Figure 7. Setup of cells grown on microwire in a perfusion chamber.....38	
Figure 8. Single-live cell and cilia imaging with 5HT6-mCherry-G-GECO1.0.....40	
Figure 9. Schematic outline to alter intracellular pH ( $pH_i$ ) and ions channels responsible for pH recovery.....48	
Figure 10. Decreased intracellular pH in response to acidic extracellular pH in wild-type and <i>Tg737</i> cells.....56	
Figure 11. Immunofluorescence staining to study effects of decreasing $pH_o$ on primary cilia.....59	
Figure 12. Immunofluorescence staining to study effects of decreasing $pH_o$ on primary cilia of NIH3T3 cells. ....61	
Figure 13. Histogram showing the lengths of primary cilia from NIH3T3 cells in response to acidified $pH_o$ or Hedgehog activation (Hh).....62	
Figure 14. Cilium length of NIH3T3 cells after Hh activation or acidic $pH_o$ exposure....64	
Figure 15. Electron micrographs of endothelial cells at pH 7.4 and pH 5.5.....65	
Figure 16. ERK1/2 phosphorylation in wild-type and <i>Tg737</i> cells in response to decreasing $pH_o$ .....66	
Figure 17. p38 phosphorylation in wild-type and <i>Tg737</i> cells in response to decreasing $pH_o$ .....67	
Figure 18. Intracellular $pH_i$ changes in response to the $NH_4Cl$ pre-pulse in wild-type and <i>Tg737</i> cells.....68	

Figure 19. Immunofluorescence staining to study effects of NH <sub>4</sub> Cl pre-pulse on primary cilia of wild-type and <i>Tg737</i> cells.....	69
Figure 20. Primary cilia length from wild-type and <i>Tg737</i> cells before and after NH <sub>4</sub> Cl pre-pulse in 0 Na <sup>+</sup> /K <sup>+</sup> solution.....	70
Figure 21. ERK1/2 and p38 phosphorylation during the NH <sub>4</sub> Cl pre-pulse in wild-type and <i>Tg737</i> cells.....	72
Figure 22. Intracellular pH <sub>i</sub> changes in response to the NH <sub>4</sub> Cl pre-pulse including a 5 mM K <sup>+</sup> solution step in wild-type and <i>Tg737</i> cells.....	73
Figure 23. Effect of 5 mM K <sup>+</sup> recovery solution on ERK1/2 and p38 phosphorylation profiles during the NH <sub>4</sub> Cl pre-pulse in wild-type and <i>Tg737</i> cells .....	74
Figure 24. Tolvaptan increases cilia length and enhances mechanosensitivity.....	92
Figure 25. Tolvaptan increases ciliary length in the dose-dependent manner without affecting stages of cell division.....	94
Figure 26. V2R modulates ciliary length and function.....	95
Figure 27. V2R knockdown cells show lower expression of receptor.....	96
Figure 28. V2R is localized to primary cilia.....	97
Figure 29. V2R is localized to primary cilia in renal epithelial cells.....	99
Figure 30. Apical and basolateral distribution of V2R in renal epithelial cells.....	100
Figure 31. Adenylyl cyclase isoforms are differentially expressed to cilia in different cell lines.....	101
Figure 32. Among adenylyl cyclase (AC) isoforms localized to the primary cilia of renal LL-CPK1 cells.....	102
Figure 33. Vasopressin mediates cAMP signaling in cilia.....	103
Figure 34. Forskolin increases cAMP level in cilioplasm and cytoplasm.....	104
Figure 35. Tolvaptan increases cilioplasmic cAMP.....	105
Figure 36. Flow decreases cilioplasmic cAMP level. ....	106
Figure 37. Global cAMP levels measured using colorimetric competitive immunoassay, and 5HT6-mCherry-cADDis and cAMP-cADDis.....	107
Figure 38. Calcium channel blocker, verapamil, does not affect increase in ciliary length induced by tolvaptan treatment.....	108

Figure 39. Cilioplasmic and cytoplasmic cAMP levels are differentially regulated.....111



## Chapter 1. Introduction

Cilia are evolutionarily conserved organelles, extending out from the cell and shaped like a thin cylindrical structure with a diameter around  $0.25\ \mu\text{m}$  (S. Sorokin, 1962; S. P. Sorokin, 1968). They are found as projections from the surface of almost all cell types in the human body. From a compositional aspect, the cilium consists of a cytoskeletal scaffold, the axoneme containing nine peripheral microtubule doublets. Each doublet is made of two connected microtubules, a complete 13-protofilament microtubule, named A tubule fused with an incomplete B tubule. The axoneme is covered with a ciliary membrane that contains receptors, ion channels and holds various other proteins within the cilioplasm (Goetz & Anderson, 2010; Janich & Corbeil, 2007; Pazour, Agrin, Leszyk, & Witman, 2005). Ciliogenesis or cilia formation starts from the basal body, which is derived from the centriole. As the cell enters  $G_0$  phase, the centrosome migrates towards the cell surface and attaches to a Golgi-derived vesicle (Lu et al., 2015; S. Sorokin, 1962). The initiation of axonemal nucleation and addition of tubulin dimers, delivered by intraflagellar transport (IFT) proteins, together with a concert of ciliary components extend the cilia (Taschner & Lorentzen, 2016). The vesicle eventually fuses with the cell membrane, and the cilia protrude out of the cell, growing to several micrometers depending on the cell type.

In terms of classification, the cilia can be broadly divided into two classes, i.e., motile and non-motile or primary cilia. As apparent by the name, motile cilia can generate motion and are found in specialized cells, such as respiratory epithelia and Fallopian tubes among others, where they usually occur in a multiciliate form (Boon et al., 2014; Raidt et al., 2015). As a note, cilia and flagella are the same but were labeled as such before their structures could be studied in detail. The most apparent distinction lies in having one or two long flagella per cell compared to ciliated cells which have  $\sim 200\text{-}300$  short cilia per cell. The primary cilium, on the other hand, exists as a single extension of cell that possesses it. In the motile cilium, there is an extra pair of centrally located microtubule doublets, thus designating it to have a  $9 + 2$  pattern (Zhang & Assouline, 2007). On the other hand, the primary cilium lacks this central pair giving it a  $9 + 0$  configuration.

All proteins that are found in the cilia are synthesized in the cytoplasm. From there, the proteins are shuttled and subsequently pass through a selective "barrier" located at the ciliary base (Gilula & Satir, 1972; Reiter, Blacque, & Leroux, 2012). This "barrier" consists of transition fibers projecting from the basal body. The transition fibers and adjoining ciliary necklace region make up the selective "ciliary pore complex" which are thought to be made of the original docking interactions between the centriole and the Golgi-derived vesicle (Garcia-Gonzalo et al., 2011; Takao, Wang, Boss, & Verhey, 2017). This transition zone, delineating the cytoplasm and cilioplasm, also organizes cargos designated for subsequent transport into the cilioplasm. Motor proteins such as kinesin and dynein carry the IFT bound ciliary components in an anterograde and retrograde direction, respectively.

### **Motile cilia**

According to their specialization, the motile cilia show variable length, beat frequency and even a unique 9 + 0 arrangement in nodal cilia. The motile cilia contain dynein arms, that are permanently attached to the A tubule, and power axonemal beating through ATP hydrolysis. There are Nexin–dynein regulatory complexes (N-DRCs) that link adjacent doublets to regulate dynein-based motility (Heuser, Raytchev, Krell, Porter, & Nicastro, 2009). There are also connections between the central microtubule apparatus and the peripheral microtubules, known as radial spokes (Pigino et al., 2011).

The motor protein and linkages form a basis for motile cilia movement, which can be described as the sliding of microtubules relative to one another (Castleman et al., 2009; Heuser et al., 2009; Olbrich et al., 2015; Pigino et al., 2011). The accepted model of ciliary movement proposes that dynein arms from the A tubule of one doublet are attached to the adjacent doublet's B tubule. The ATPase domain in the dynein arm then undergoes successive binding and hydrolysis of adenosine triphosphate (ATP). This causes the dynein to release from its initial position on the B tubule and attach to a new position along the direction of movement toward the B tubule base, also called the minus end of the microtubule. Coordinated movement of the ciliary microtubules, in the case of 9 + 0 nodal cilia, produce a unidirectional beat while in multiciliate cells, the movement generated

is a wave-like motion. In the sperm flagella, notable differences occur in the distribution of the dynein arms and could be a possible factor in its unique beat pattern compared to regular ciliary beating (Faubel, Westendorf, Bodenschatz, & Eichele, 2016; Ma, Tian, Igarashi, Pazour, & Somlo, 2013). In conclusion, a simple model might not account for the diversity of structure and motion patterns, but it does help us understand the critical components involved in cilia motility.

Motile cilia are found in the epithelial surfaces of the respiratory tracts, the Fallopian tubes and the 9 + 0 nodal cilia, being present in the central nervous system. Disruptions to these nodal cilia lead to brain malformations and hydrocephalus (Banizs et al., 2005). In the airways, the wave-like motion generated by cilia expels mucus with trapped pathogens to be eliminated. Without this clearance, the trapped pathogens and particulate matter accumulate, increasing the risk of airway obstruction and other respiratory infections. Similarly, the multiciliate epithelia of Fallopian tubes generate a wave-like motion transport eggs to the uterus. With their specialized functions, even motile cilia have distinctive and unique properties that need to be studied comprehensively in order to understand the underlying basis of its function.

### **Primary cilia**

Looking at the non-motile or primary cilium, it shares basic composition and structural features with the motile cilium. It has a similar arrangement of nine pairs microtubule doublets, anchored to the cell with a basal body, delineated by a transition zone and served by transport proteins to shuttle ciliary components. The similarities tend to end there and as the name implies the non-motile cilium or primary cilium cannot generate its own movement. Some easily recognizable differences are the absence of ciliary components involved in cilia motility, such as the dynein arms bound to the peripheral doublets and associated proteins including the radial spokes. Compared to the motile cilia, the primary cilia are ubiquitous in most mammalian cells and project out to the lumen from the apical surface of polarized and differentiated cells.

Initially, the primary cilia were thought to be remnants of unicellular ancestral origin, serving no function in the more evolved multicellular organism. Another thought was that the primary cilia

could serve as a sensor and increasing evidence has supported the role of primary cilia as specialized sensory appendages as well as being involved in the coordination of signaling pathways. Primary cilia are responsible for a wide range of functions including transduction of mechanosensory stimuli, regulation of developmental pathways, and modulation of cell polarity as well as cell proliferation (Basten & Giles, 2013; Eggenschwiler & Anderson, 2007; Guemez-Gamboa, Coufal, & Gleeson, 2014; Spassky et al., 2008; Veland, Awan, Pedersen, Yoder, & Christensen, 2010; Zhou, 2009).

In the brain, the primary cilia play a critical role in the development and regulating neuronal cell signaling, migration, and differentiation (Banizs et al., 2005; Faubel et al., 2016; Spassky et al., 2008). Studies have found that components of the Hedgehog pathway (Hh) localize in the ciliary compartment at different stages of pathway activation (Murdoch & Copp, 2010). Dysregulation of Hh signaling, due to defective proteins of the pathway results in hydrocephalus, corpus callosum defects, and similar manifestations of conditions that are observed in ciliopathies (Goetz & Anderson, 2010; Lehman & Michaud, 2008; Spassky et al., 2008; Toriello & Parisi, 2009). Ciliopathies include all inherited human disorders caused by both motile and primary cilia dysfunction (Mitchison & Valente, 2017; Waters & Beales, 2011). Primary cilia dysfunction affects the pancreas causing fibrotic deposition, dysplasia, and ductal cysts. Pancreatic development involves several pathways such as Shh and Wnt, which are dependent on the presence of a functioning primary cilium (Han et al., 2008; Lancaster, Schroth, & Gleeson, 2011). In addition, primary cilia in pancreatic ductal cells have been proposed to sense luminal flow and transduce flow-induced signals, similar to their counterpart in the renal epithelia and vascular endothelia (Abdul-Majeed, Moloney, & Nauli, 2012; Abdul-Majeed & Nauli, 2011a, 2011b; Cano, Sekine, & Hebrok, 2006; Mohieldin et al., 2016). The primary cilia on cholangiocytes also function as sensors to detect biliary flow and composition. Studies have shown that the cholangiocyte cilia respond to sensory stimuli by modulating intracellular calcium and cAMP (Gradilone et al., 2007; A. I. Masyuk et al., 2006). Impaired cilia result in the formation of abnormal bile ducts with excessive extracellular matrix deposition. In the skeletal system, ciliary defects can cause polydactyly and aberrant growth of the cartilage and bones (Malone et al., 2007; McGlashan, Haycraft, Jensen, Yoder, & Poole, 2007).

Many of these discoveries have been based on animal models, namely the hypomorphic mouse mutant Oak Ridge Polycystic Kidney (ORPK) (Lehman & Michaud, 2008; McGlashan et al., 2007; Moyer et al., 1994; Murcia et al., 2000; Pazour et al., 2000; B K Yoder et al., 1995; Bradley K Yoder, Hou, & Guay-Woodford, 2002). The ORPK mice have mutations in the *Tg737* gene, homologous to *IFT88* which is a *Chlamydomonas* IFT protein (Pazour et al., 2000). Analysis of ORPK mouse showed that primary cilia are stunted, and the resulting aberrations of primary cilia based signaling contribute towards many of the abnormalities seen in the mutants. One of the most studies functional ciliary complexes is the mechanosensory polycystins (Nauli et al., 2003). Polycystin 1 (PC1) is a transmembrane glycoprotein has a large extracellular N-terminal domain which includes a G-protein coupled receptor proteolytic site (GPS) (Chae et al., 2006; Geng et al., 1996; Nauli et al., 2008). In the cytoplasmic side, PC1 C-terminal forms a coiled-coiled domain through which it interacts with polycystin 2 (PC2), a transient receptor potential polycystic (TRPP) ion channel permeable to calcium ions ( $Ca^{2+}$ ) (Cai et al., 1999; Casuscelli et al., 2009; Koulen et al., 2002; Pazour, San Agustin, Follit, Rosenbaum, & Witman, 2002). PC1 and PC2, make up a mechanosensory complex and are localized to the primary cilium. Bending of the cilia induced by fluid flow activates the polycystin complex leading to an increase in  $Ca^{2+}$  influx (Praetorius & Spring, 2001, 2003). The absence or dysfunction of cilia, PC1, or PC2 decrease  $Ca^{2+}$  influx and hypersensitize the cell to proliferative signals causing cyst formation in polycystic kidney disease (PKD) (Gattone, Wang, Harris, & Torres, 2003; Joly, 2003; Kuo et al., 2014; Wallace, 2011). This disruption of flow-dependent and steady-state intracellular  $Ca^{2+}$  signaling could affect proliferation, differentiation, and apoptosis in a variety of cell types and tissues such as vascular endothelia, cholangiocytes, and chondrocytes (Abdul-Majeed & Nauli, 2011c; Gattone et al., 2003; Joly, 2003; Kathem et al., 2014; Kuo et al., 2014; A. I. Masyuk et al., 2006; T. V Masyuk et al., 2003; Moser et al., 2005; Nauli et al., 2008, 2013; Wallace, 2011).

Subsequent studies over the years have strengthened the varied roles of primary cilia and found important signaling complexes localized to the primary cilium. The causal relationship between dysfunctional primary cilia multi systematic diseases provides various avenues of study to strategize therapeutic options. As an antenna to sense mechanical stimuli i.e. fluid induced stress of bending, primary cilium has been shown to be potential targets for therapeutic intervention in

cases of ciliopathies. This type of cellular level rescue of ciliary function has been done in PKD mice models treated with cilia specific receptor agonists to increase flow sensitivity of the cilia.

As mentioned before, fluid flow induced ciliary  $Ca^{2+}$  signaling phenomenon has been of great interest and highly studied. To overcome limitations of traditional viewing modalities, a mix of side view imaging and targeted sensors can be used to study  $Ca^{2+}$  changes at a high spatio-temporal resolution. Animal models have also shed light on the heterogeneity of cilia related diseases and suggest regulation of ion transport to be influenced by the cilia. As an important aspect of physiological balance, we study if the primary cilia are involved in pH sensing function and their possible role in pH recovery when challenged with acidosis. Another key finding in animal models of ciliopathies such as PKD and even human derived samples show high levels of cyclic adenosine monophosphate (cAMP). Targeted approaches to tackle high cAMP levels have been promising and as a key organelle in cyst development the cilia need to be studied for their possible role in cAMP signaling. Based on our imaging modality and targeted fluorescent sensors we are able to delineate specific signals arising from the distinct domains of the cilioplasm or cytoplasm. Defects in the ciliary structure or cilia localized protein complexes cause a variety of diseases. With increasing the knowledge of ciliary biology, we can strategize approaches to repair defective cilia.

## References

1. Abdul-Majeed, S., Moloney, B. C., & Nauli, S. M. (2012). Mechanisms regulating cilia growth and cilia function in endothelial cells. *Cellular and Molecular Life Sciences*, 69(1), 165–173. Retrieved March 23, 2015, from <http://link.springer.com/10.1007/s00018-011-0744-0>
2. Abdul-Majeed, S., & Nauli, S. M. (2011a). Polycystic diseases in visceral organs. *Obstetrics and gynecology international*, 2011, 609370. Retrieved September 19, 2014, from <http://www.pubmedcentral.nih.gov/articlerender.fcgi?artid=3253486&tool=pmcentrez&rendertype=abstract>
3. Abdul-Majeed, S., & Nauli, S. M. (2011b). Dopamine receptor type 5 in the primary cilia has dual chemo- and mechano-sensory roles. *Hypertension (Dallas, Tex. : 1979)*, 58(2), 325–31. Retrieved from <http://hyper.ahajournals.org/cgi/doi/10.1161/HYPERTENSIONAHA.111.172080>
4. Abdul-Majeed, S., & Nauli, S. M. (2011c). Calcium-mediated mechanisms of cystic expansion. *Biochimica et biophysica acta*, 1812(10), 1281–90. Retrieved November 10, 2015, from <http://www.pubmedcentral.nih.gov/articlerender.fcgi?artid=3043160&tool=pmcentrez&rendertype=abstract>
5. Banizs, B., Pike, M. M., Millican, C. L., Ferguson, W. B., Komlosi, P., Sheetz, J., Bell, P. D., et al. (2005). Dysfunctional cilia lead to altered ependyma and choroid plexus function, and result in the formation of hydrocephalus. *Development*, 132(23), 5329–5339. Retrieved August 1, 2019, from <http://www.ncbi.nlm.nih.gov/pubmed/16284123>
6. Basten, S. G., & Giles, R. H. (2013). Functional aspects of primary cilia in signaling, cell cycle and tumorigenesis. *Cilia*, 2(1), 6. BioMed Central Ltd. Retrieved August 5, 2015, from <http://www.ciliajournal.com/content/2/1/6>
7. Boon, M., Wallmeier, J., Ma, L., Loges, N. T., Jaspers, M., Olbrich, H., Dougherty, G. W., et al. (2014). MCIDAS mutations result in a mucociliary clearance disorder with reduced generation of multiple motile cilia. *Nature Communications*, 5(1), 4418. Retrieved August 1, 2019, from <http://www.ncbi.nlm.nih.gov/pubmed/25048963>
8. Cai, Y., Maeda, Y., Cedzich, A., Torres, V. E., Wu, G., Hayashi, T., Mochizuki, T., et al. (1999). Identification and characterization of polycystin-2, the PKD2 gene product. *The Journal of biological chemistry*, 274(40), 28557–28565. Retrieved November 10, 2014, from <http://www.ncbi.nlm.nih.gov/pubmed/10497221>
9. Cano, D. A., Sekine, S., & Hebrok, M. (2006). Primary Cilia Deletion in Pancreatic Epithelial Cells Results in Cyst Formation and Pancreatitis. *Gastroenterology*, 131(6), 1856–1869. Retrieved from <http://linkinghub.elsevier.com/retrieve/pii/S0016508506022840>
10. Castleman, V. H., Romio, L., Chodhari, R., Hirst, R. A., de Castro, S. C. P., Parker, K. A., Ybot-Gonzalez, P., et al. (2009). Mutations in Radial Spoke Head Protein Genes RSPH9 and RSPH4A Cause Primary Ciliary Dyskinesia with Central-Microtubular-Pair Abnormalities. *The American Journal of Human Genetics*, 84(2), 197–209. Retrieved August 2, 2019, from <http://www.ncbi.nlm.nih.gov/pubmed/19200523>
11. Casuscelli, J., Schmidt, S., DeGray, B., Petri, E. T., Celić, A., Folta-Stogniew, E., Ehrlich, B. E., et al. (2009). Analysis of the cytoplasmic interaction between polycystin-1 and polycystin-2. *American journal of physiology. Renal physiology*, 297(5), F1310–F1315. Retrieved December 24, 2014, from <http://www.pubmedcentral.nih.gov/articlerender.fcgi?artid=2781345&tool=pmcentrez&rendertype=abstract>
12. Chae, S. W., Cho, E.-Y., Park, M. S., Lee, K.-B., Kim, H., & Kim, U. (2006). Polycystin-1



expression in fetal, adult and autosomal dominant polycystic kidney. *Journal of Korean medical science*, 21(3), 425–9. Retrieved December 1, 2014, from <http://www.pubmedcentral.nih.gov/articlerender.fcgi?artid=2729945&tool=pmcentrez&rendertype=abstract>

13. Eggenschwiler, J. T., & Anderson, K. V. (2007). Cilia and Developmental Signaling. *Annual Review of Cell and Developmental Biology*, 23(1), 345–373. Retrieved August 13, 2017, from <http://www.ncbi.nlm.nih.gov/pubmed/17506691>
14. Faubel, R., Westendorf, C., Bodenschatz, E., & Eichele, G. (2016). Cilia-based flow network in the brain ventricles. *Science*, 353(6295), 176–178. American Association for the Advancement of Science. Retrieved August 1, 2019, from <https://science.sciencemag.org/content/353/6295/176.long>
15. Garcia-Gonzalo, F. R., Corbit, K. C., Sirerol-Piquer, M. S., Ramaswami, G., Otto, E. A., Noriega, T. R., Seol, A. D., et al. (2011). A transition zone complex regulates mammalian ciliogenesis and ciliary membrane composition. *Nature Genetics*, 43(8), 776–784. Retrieved December 19, 2018, from <http://www.ncbi.nlm.nih.gov/pubmed/21725307>
16. Gattone, V. H., Wang, X., Harris, P. C., & Torres, V. E. (2003). Inhibition of renal cystic disease development and progression by a vasopressin V2 receptor antagonist. *Nature medicine*, 9(10), 1323–6. Retrieved December 10, 2014, from <http://www.ncbi.nlm.nih.gov/pubmed/14502283>
17. Geng, L., Segal, Y., Peissel, B., Deng, N., Pei, Y., Carone, F., Rennke, H. G., et al. (1996). Identification and localization of polycystin, the PKD1 gene product. *The Journal of clinical investigation*, 98(12), 2674–82. Retrieved December 22, 2014, from <http://www.pubmedcentral.nih.gov/articlerender.fcgi?artid=507729&tool=pmcentrez&rendertype=abstract>
18. Gilula, N. B., & Satir, P. (1972). The ciliary necklace. A ciliary membrane specialization. *The Journal of cell biology*, 53(2), 494–509. The Rockefeller University Press. Retrieved January 23, 2019, from <http://www.ncbi.nlm.nih.gov/pubmed/4554367>
19. Goetz, S. C., & Anderson, K. V. (2010). The primary cilium: a signalling centre during vertebrate development. *Nature reviews. Genetics*, 11(5), 331–44. Nature Publishing Group. Retrieved July 13, 2015, from <http://dx.doi.org/10.1038/nrg2774>
20. Gradilone, S. A., Masyuk, A. I., Splinter, P. L., Banales, J. M., Huang, B. Q., Tietz, P. S., Masyuk, T. V., et al. (2007). Cholangiocyte cilia express TRPV4 and detect changes in luminal tonicity inducing bicarbonate secretion. *Proceedings of the National Academy of Sciences of the United States of America*, 104(48), 19138–43. Retrieved August 6, 2016, from <http://www.ncbi.nlm.nih.gov/pubmed/18024594>
21. Guemez-Gamboa, A., Coufal, N. G., & Gleeson, J. G. (2014). Primary cilia in the developing and mature brain. *Neuron*, 82(3), 511–21. Retrieved February 13, 2015, from <http://www.sciencedirect.com/science/article/pii/S0896627314003390>
22. Han, Y.-G., Spassky, N., Romaguera-Ros, M., Garcia-Verdugo, J.-M., Aguilar, A., Schneider-Maunoury, S., & Alvarez-Buylla, A. (2008). Hedgehog signaling and primary cilia are required for the formation of adult neural stem cells. *Nature Neuroscience*, 11(3), 277–284. Retrieved August 2, 2019, from <http://www.ncbi.nlm.nih.gov/pubmed/18297065>
23. Heuser, T., Raytchev, M., Krell, J., Porter, M. E., & Nicastro, D. (2009). The dynein regulatory complex is the nexin link and a major regulatory node in cilia and flagella. *The Journal of Cell Biology*, 187(6), 921–933. Retrieved August 1, 2019, from <http://www.ncbi.nlm.nih.gov/pubmed/20008568>
24. Janich, P., & Corbeil, D. (2007). GM1 and GM3 gangliosides highlight distinct lipid microdomains within the apical domain of epithelial cells. *FEBS letters*, 581(9), 1783–7.



- Retrieved August 2, 2019, from <http://www.ncbi.nlm.nih.gov/pubmed/17428477>
25. Joly, D. (2003). Ciliary function of polycystins: a new model for cystogenesis. *Nephrology Dialysis Transplantation*, 18(9), 1689–1692. Retrieved December 20, 2014, from <http://ndt.oxfordjournals.org/cgi/doi/10.1093/ndt/gfg256>
  26. Kathem, S. H., Mohieldin, A. M., Abdul-Majeed, S., Ismail, S. H., Altaei, Q. H., Alshimmari, I. K., Alsaidi, M. M., et al. (2014). Ciliotherapy: a novel intervention in polycystic kidney disease. *Journal of geriatric cardiology : JGC*, 11(1), 63–73. Retrieved September 21, 2014, from <http://www.pubmedcentral.nih.gov/articlerender.fcgi?artid=3981986&tool=pmcentrez&rendertype=abstract>
  27. Koulen, P., Cai, Y., Geng, L., Maeda, Y., Nishimura, S., Witzgall, R., Ehrlich, B. E., et al. (2002). Polycystin-2 is an intracellular calcium release channel. *Nature cell biology*, 4(3), 191–197. Retrieved December 22, 2014, from <http://www.ncbi.nlm.nih.gov/pubmed/11854751>
  28. Kuo, I. Y., DesRochers, T. M., Kimmerling, E. P., Nguyen, L., Ehrlich, B. E., & Kaplan, D. L. (2014). Cyst formation following disruption of intracellular calcium signaling. *Proceedings of the National Academy of Sciences of the United States of America*, 111(39), 14283–8. Retrieved December 5, 2014, from <http://www.ncbi.nlm.nih.gov/pubmed/25228769>
  29. Lancaster, M. A., Schroth, J., & Gleeson, J. G. (2011). Subcellular spatial regulation of canonical Wnt signalling at the primary cilium. *Nature Cell Biology*, 13(6), 700–707. Retrieved August 2, 2019, from <http://www.ncbi.nlm.nih.gov/pubmed/21602792>
  30. Lehman, J., & Michaud, E. (2008). The Oak Ridge Polycystic Kidney mouse: modeling ciliopathies of mice and men. *Developmental ...*, 237(8), 1960–1971. Retrieved December 21, 2014, from <http://onlinelibrary.wiley.com/doi/10.1002/dvdy.21515/full>
  31. Lu, Q., Insinna, C., Ott, C., Stauffer, J., Pintado, P. A., Rahajeng, J., Baxa, U., et al. (2015). Early steps in primary cilium assembly require EHD1/EHD3-dependent ciliary vesicle formation. *Nature Cell Biology*, 17(3), 228–240. Retrieved August 2, 2019, from <http://www.ncbi.nlm.nih.gov/pubmed/25686250>
  32. Ma, M., Tian, X., Igarashi, P., Pazour, G. J., & Somlo, S. (2013). Loss of cilia suppresses cyst growth in genetic models of autosomal dominant polycystic kidney disease. *Nature genetics*, 45(9), 1004–12. Springer. Retrieved August 1, 2019, from <http://www.ncbi.nlm.nih.gov/pubmed/26825807>
  33. Malone, A. M. D., Anderson, C. T., Tummala, P., Kwon, R. Y., Johnston, T. R., Stearns, T., & Jacobs, C. R. (2007). Primary cilia mediate mechanosensing in bone cells by a calcium-independent mechanism. *Proceedings of the National Academy of Sciences of the United States of America*, 104(33), 13325–30. National Academy of Sciences. Retrieved January 17, 2019, from <http://www.ncbi.nlm.nih.gov/pubmed/17673554>
  34. Masyuk, A. I., Masyuk, T. V., Splinter, P. L., Huang, B. Q., Stroope, A. J., & LaRusso, N. F. (2006). Cholangiocyte cilia detect changes in luminal fluid flow and transmit them into intracellular Ca<sup>2+</sup> and cAMP signaling. *Gastroenterology*, 131(3), 911–20. Retrieved December 19, 2014, from <http://www.pubmedcentral.nih.gov/articlerender.fcgi?artid=1866168&tool=pmcentrez&rendertype=abstract>
  35. Masyuk, T. V., Huang, B. Q., Ward, C. J., Masyuk, A. I., Yuan, D., Splinter, P. L., Punyashthiti, R., et al. (2003). Defects in cholangiocyte fibrocystin expression and ciliary structure in the PCK rat. *Gastroenterology*, 125(0016-5085 (Print)), 1303–1310. Retrieved September 22, 2014, from <http://www.sciencedirect.com/science/article/pii/S0016508503013696>
  36. McGlashan, S. R., Haycraft, C. J., Jensen, C. G., Yoder, B. K., & Poole, C. A. (2007). Articular cartilage and growth plate defects are associated with chondrocyte cytoskeletal abnormalities in

- Tg737orpk mice lacking the primary cilia protein polaris. *Matrix Biology*, 26(4), 234–246. Retrieved August 2, 2019, from <http://www.ncbi.nlm.nih.gov/pubmed/17289363>
37. Mitchison, H. M., & Valente, E. M. (2017). Motile and non-motile cilia in human pathology: from function to phenotypes. *The Journal of Pathology*, 241(2), 294–309. John Wiley & Sons, Ltd. Retrieved August 2, 2019, from <http://doi.wiley.com/10.1002/path.4843>
  38. Mohieldin, A. M., Zubayer, H. S. M., Al Omran, A. J., Saternos, H. C., Zarban, A. A., Nauli, S. M., & AbouAlaiwi, W. A. (2016). Vascular Endothelial Primary Cilia: Mechanosensation and Hypertension. *Current hypertension reviews*, 12(1), 57–67. Retrieved August 2, 2019, from <http://www.ncbi.nlm.nih.gov/pubmed/26122329>
  39. Moser, M., Matthiesen, S., Kirfel, J., Schorle, H., Bergmann, C., Senderek, J., Rudnik-Schöneborn, S., et al. (2005). A mouse model for cystic biliary dysgenesis in autosomal recessive polycystic kidney disease (ARPKD). *Hepatology*, 41(5), 1113–21. Retrieved September 22, 2014, from <http://www.ncbi.nlm.nih.gov/pubmed/15830394>
  40. Moyer, J., Lee-Tischler, M., Kwon, H., Schrick, J., Avner, E., Sweeney, W., Godfrey, V., et al. (1994). Candidate gene associated with a mutation causing recessive polycystic kidney disease in mice. *Science*, 264(5163), 1329–1333. Retrieved August 2, 2019, from <http://www.ncbi.nlm.nih.gov/pubmed/8191288>
  41. Murcia, N. S., Richards, W. G., Yoder, B. K., Mucenski, M. L., Dunlap, J. R., Woychik, R. P., Beddington, R. S., et al. (2000). The Oak Ridge Polycystic Kidney (orpk) disease gene is required for left-right axis determination. *Development (Cambridge, England)*, 127(11), 2347–55. The Company of Biologists Ltd. Retrieved August 6, 2016, from <http://www.ncbi.nlm.nih.gov/pubmed/10804177>
  42. Murdoch, J. N., & Copp, A. J. (2010). The relationship between sonic Hedgehog signaling, cilia, and neural tube defects. *Birth Defects Research Part A: Clinical and Molecular Teratology*, 88(8), 633–652. Retrieved August 2, 2019, from <http://www.ncbi.nlm.nih.gov/pubmed/20544799>
  43. Nauli, S. M., Alenghat, F. J., Luo, Y., Williams, E., Vassilev, P., Li, X., Elia, A. E. H., et al. (2003). Polycystins 1 and 2 mediate mechanosensation in the primary cilium of kidney cells. *Nature genetics*, 33(2), 129–37. Retrieved September 12, 2014, from <http://www.ncbi.nlm.nih.gov/pubmed/12514735>
  44. Nauli, S. M., Jin, X., AbouAlaiwi, W. A., El-Jouni, W., Su, X., & Zhou, J. (2013). Non-Motile Primary Cilia as Fluid Shear Stress Mechanosensors. *Methods in enzymology* (Vol. 525, pp. 1–20). Retrieved January 2, 2018, from <http://www.ncbi.nlm.nih.gov/pubmed/23522462>
  45. Nauli, S. M., Kawanabe, Y., Kaminski, J. J., Pearce, W. J., Ingber, D. E., & Zhou, J. (2008). Endothelial Cilia Are Fluid Shear Sensors That Regulate Calcium Signaling and Nitric Oxide Production Through Polycystin-1. *Circulation*, 117(9), 1161–1171. Retrieved December 30, 2014, from <http://www.ncbi.nlm.nih.gov/pubmed/18285569>
  46. Olbrich, H., Cremers, C., Loges, N. T., Werner, C., Nielsen, K. G., Marthin, J. K., Philipsen, M., et al. (2015). Loss-of-Function GAS8 Mutations Cause Primary Ciliary Dyskinesia and Disrupt the Nexin-Dynein Regulatory Complex. *The American Journal of Human Genetics*, 97(4), 546–554. Retrieved August 2, 2019, from <http://www.ncbi.nlm.nih.gov/pubmed/26387594>
  47. Pazour, G. J., Agrin, N., Leszyk, J., & Witman, G. B. (2005). Proteomic analysis of a eukaryotic cilium. *The Journal of cell biology*, 170(1), 103–13. The Rockefeller University Press. Retrieved January 18, 2019, from <http://www.ncbi.nlm.nih.gov/pubmed/15998802>
  48. Pazour, G. J., Dickert, B. L., Vucica, Y., Seeley, E. S., Rosenbaum, J. L., Witman, G. B., & Cole, D. G. (2000). Chlamydomonas IFT88 and its mouse homologue, polycystic kidney disease gene tg737, are required for assembly of cilia and flagella. *The Journal of cell biology*, 151(3), 709–18. Retrieved August 2, 2019, from <http://www.ncbi.nlm.nih.gov/pubmed/11062270>

49. Pazour, G. J., San Agustin, J. T., Follit, J. A., Rosenbaum, J. L., & Witman, G. B. (2002). Polycystin-2 localizes to kidney cilia and the ciliary level is elevated in orpk mice with polycystic kidney disease. *Current Biology*, 12(11), R378–R380. Elsevier. Retrieved September 21, 2014, from <http://www.cell.com/article/S0960982202008771/fulltext>
50. Pigino, G., Bui, K. H., Maheshwari, A., Lupetti, P., Diener, D., & Ishikawa, T. (2011). Cryoelectron tomography of radial spokes in cilia and flagella. *The Journal of Cell Biology*, 195(4), 673–687. Retrieved August 1, 2019, from <http://www.ncbi.nlm.nih.gov/pubmed/22065640>
51. Praetorius, H. A., & Spring, K. R. (2001). Bending the MDCK cell primary cilium increases intracellular calcium. *The Journal of membrane biology*, 184(1), 71–9. Retrieved September 22, 2014, from <http://link.springer.com/10.1007/s00232-001-0075-4>
52. Praetorius, H. A., & Spring, K. R. (2003). Removal of the MDCK Cell Primary Cilium Abolishes Flow Sensing. *Journal of Membrane Biology*, 191(1), 69–76. Retrieved from <http://link.springer.com/10.1007/s00232-002-1042-4>
53. Raidt, J., Werner, C., Menchen, T., Dougherty, G. W., Olbrich, H., Loges, N. T., Schmitz, R., et al. (2015). Ciliary function and motor protein composition of human fallopian tubes. *Human Reproduction*, 30(12), 2871–2880. Retrieved August 1, 2019, from <https://academic.oup.com/humrep/article-lookup/doi/10.1093/humrep/dev227>
54. Reiter, J. F., Blacque, O. E., & Leroux, M. R. (2012). The base of the cilium: roles for transition fibres and the transition zone in ciliary formation, maintenance and compartmentalization. *EMBO reports*, 13(7), 608–618. Retrieved August 6, 2016, from <http://embor.embopress.org/cgi/doi/10.1038/embor.2012.73>
55. Sorokin, S. (1962). Centrioles and the formation of rudimentary cilia by fibroblasts and smooth muscle cells. *The Journal of cell biology*, 15(2), 363–377. Rockefeller University Press. Retrieved January 9, 2018, from <http://www.ncbi.nlm.nih.gov/pubmed/13978319>
56. Sorokin, S. P. (1968). Reconstructions of centriole formation and ciliogenesis in mammalian lungs. *Journal of cell science*, 3(2), 207–30. Retrieved September 22, 2014, from <http://www.ncbi.nlm.nih.gov/pubmed/5661997>
57. Spassky, N., Han, Y.-G., Aguilar, A., Strehl, L., Besse, L., Laclef, C., Romaguera Ros, M., et al. (2008). Primary cilia are required for cerebellar development and Shh-dependent expansion of progenitor pool. *Developmental Biology*, 317(1), 246–259. Retrieved August 2, 2019, from <http://www.ncbi.nlm.nih.gov/pubmed/18353302>
58. Takao, D., Wang, L., Boss, A., & Verhey, K. J. (2017). Protein Interaction Analysis Provides a Map of the Spatial and Temporal Organization of the Ciliary Gating Zone. *Current Biology*, 27(15), 2296–2306.e3. Retrieved December 19, 2018, from <http://www.ncbi.nlm.nih.gov/pubmed/28736169>
59. Taschner, M., & Lorentzen, E. (2016). The Intraflagellar Transport Machinery. *Cold Spring Harbor perspectives in biology*, 8(10). Cold Spring Harbor Laboratory Press. Retrieved August 1, 2019, from <http://www.ncbi.nlm.nih.gov/pubmed/27352625>
60. Toriello, H. V., & Parisi, M. a. (2009). Cilia and the ciliopathies: an introduction. *American journal of medical genetics. Part C, Seminars in medical genetics*, 151C(4), 261–2. Retrieved September 22, 2014, from <http://www.ncbi.nlm.nih.gov/pubmed/19876932>
61. Veland, I. R., Awan, A., Pedersen, L. B., Yoder, B. K., & Christensen, S. T. (2010). Primary cilia and signaling pathways in mammalian development, health and disease. *Nephron Physiology*, 111(3), 39–53.
62. Wallace, D. P. (2011). Cyclic AMP-mediated cyst expansion. *Biochimica et biophysica acta*, 1812(10), 1291–300. Retrieved August 20, 2015, from

<http://www.pubmedcentral.nih.gov/articlerender.fcgi?artid=3081913&tool=pmcentrez&rendertype=abstract>

63. Waters, A. M., & Beales, P. L. (2011). Ciliopathies: an expanding disease spectrum. *Pediatric nephrology (Berlin, Germany)*, 26(7), 1039–56. Retrieved September 22, 2014, from <http://www.pubmedcentral.nih.gov/articlerender.fcgi?artid=3098370&tool=pmcentrez&rendertype=abstract>
64. Yoder, B K, Richards, W. G., Sweeney, W. E., Wilkinson, J. E., Avenier, E. D., & Woychik, R. P. (1995). Insertional mutagenesis and molecular analysis of a new gene associated with polycystic kidney disease. *Proc Assoc Am Physicians* , 107(3), 314-323. Retrieved September 22, 2014, from <http://www.ncbi.nlm.nih.gov/htbin-post/Entrez/query?db=m&form=6&dopt=r&uid=8608416>
65. Yoder, Bradley K, Hou, X., & Guay-Woodford, L. M. (2002). The polycystic kidney disease proteins, polycystin-1, polycystin-2, polaris, and cystin, are co-localized in renal cilia. *Journal of the American Society of Nephrology : JASN*, 13(10), 2508–16. Retrieved September 21, 2014, from <http://www.ncbi.nlm.nih.gov/pubmed/12239239>
66. Zhang, M., & Assouline, J. G. (2007). Cilia containing 9 + 2 structures grown from immortalized cells. *Cell Research*, 17(6), 537–545. Nature Publishing Group. Retrieved August 2, 2019, from <http://www.nature.com/articles/7310151>
67. Zhou, J. (2009). Polycystins and primary cilia: primers for cell cycle progression. *Annual review of physiology*, 71, 83–113. Retrieved December 19, 2014, from <http://www.ncbi.nlm.nih.gov/pubmed/19572811>

## **Chapter 2. Mechanosensory and Chemosensory primary cilia in ciliopathy and ciliotherapy.\***

### **Abstract**

Mechanobiology is the study of cellular processes by which cells are able to sense and respond to extracellular physical forces and translate those mechanical signals into intracellular biochemical reactions, molecular responses, gene expressions and tissue developments. Over the past few decades, the field within mechanobiology has been advanced by the discovery and recognition of a new sensory organelle, termed primary cilium. Primary cilia serve as antennae to sense small changes in the microenvironment surrounding the cells. Abnormalities in primary cilia can lead to various clinical diseases, termed ciliopathies, which are characterized by gross anatomical defects in cellular and tissue structures. Medical exploitation of ciliotherapies is underway in attempt to assess primary cilium as a potential mechanobiology target at the cellular level for therapeutic intervention.

---

\* Nauli SM, Sherpa RT, Reese CJ, Nauli AM. Mechanosensory and Chemosensory Primary Cilia in Ciliopathy and Ciliotherapy. *Mechanobiology: Exploitation for Medical Benefit*. Hoboken, NJ, USA: John Wiley & Sons, Inc.; 2016. p. 75–99. <https://doi.org/10.1002/9781118966174.ch5>

## Introduction

Over the past few decades, we have been able to integrate mechanobiology into the molecular basis of disease. Mechanical forces in the cellular microenvironment have been recognized as critical regulators for molecular responses, biochemical reactions, gene expressions and tissue developments. Recent insights into cellular mechanotransduction point to primary cilium as the cellular organelle, which enables a cell to sense and respond to mechanical fluid-shear stress.

Primary cilia are among the organelles possessed by cells. As mechanosensory organelles, primary cilia are usually classified into a “9+0” type, a classification based on their structural microtubule arrangement (Figure 1). Based on the motility characteristic, primary cilia are generally classified as non-motile organelles. Like any other organelle within a cell, cilia have many important and specialized cellular functions. Classification of cilia can thus provide a broad spectrum of understanding on their role in cellular function.

Structural or functional abnormalities of primary cilia can result in a spectrum of clinical diseases that are associated with gross anatomical changes in tissue and/or organ structure (Hildebrandt, Benzing, and Katsanis 2011, Waters and Beales 2011). It is therefore not hard to understand that a single cell is required to sense and respond to mechanical signals mediated from the extracellular micro-environment and translate those stimuli into intracellular signaling events. Furthermore, this mechanotransduction process is crucial for maintaining a healthy cellular structure and function and cannot be disrupted. With this understanding, we have an abundance of knowledge to exploit medical intervention in hope to remedy mechano-associated diseases.

## Mechanobiology and diseases

Although genetic mutations or abnormal functions of various proteins can be traced back to mechanotransduction signaling, the etiology of mechano-pathophysiology has been difficult to analyze, primarily due to two main challenges. The **first challenge** described previously by Nauli illustrates that mechanical forces are very difficult to analyze and differentiate in a complex physiological system *in vivo* (Nauli, Jin, and Hierck 2011). Although different



mechanical forces are known to be distinct from one another in cell culture or *ex vivo* studies (Prasad et al. 2014, Nauli et al. 2013), the biophysical properties that these forces possess are extremely complex and can alter the property of one another *in vivo*. For example, there are at least five different mechanical forces that a blood vessel could encounter (Table 1). If pressure force were terminated through occlusion in one segment of an artery, the other four mechanical forces in the same artery would be altered. In other words, if pressure were prevented from occurring in an artery, the artery would not have the ability to experience stretch, strain, compression or shear-stress forces, as a consequence.

Table 1. Mechanical forces within blood vessel (adapted from (105))

<b>Types of forces</b>	<b>Differentiations of forces</b>
Stretch	Distention force by surrounding muscle
Cyclic strain	Pulsatile force by turbulent flow of blood
Compression	Contractile force by differential pressure in the vessel
Pressure	Systolic force on intima surface by kinetic flow of blood
Shear stress	Drag force along intima surface by kinetic flow of blood

The ***second challenge*** proposed previously by Ingber expresses that mechanotransduction does not necessarily contain a classic coupling “stimulus-response” (Ingber 2003). Any external mechanical forces would need to impose on the pre-existing force balance. In other words, the pre-existing force coupled with additional force stimuli applied to the system governs the overall cellular response. Thus, the existing forces have already complicated our studies on mechanotransduction, and if not assessed, would undermine the overall importance of the role of pre-existing physical forces in the surrounding microcellular environment.

Nonetheless, abnormalities in the mechanotransduction cascade have long been implicated in clinical diseases (Ingber 2003). Although diseases associated with mechanotransduction abnormalities include most branches of medicine (Table 2), it is important to note that the mechanism or etiology of the disease had been difficult to envision. Studying these diseases in attempt to determine if they are caused by changes in cell mechanics, alterations in tissue structures, or deregulation of mechanochemical conversions, has been extremely challenging.

Table 2. Mechanotransduction diseases

Medical branches	Examples	References
Cardiology	atherosclerosis	(8)
Dermatology	Ehlers-Danlos syndrome	(112)
Gastroenterology	heartburn	(27)
Nephrology	glomerulosclerosis	(172)
Neurology	migrane	(153)
Oncology	metastasis	(132)
Ophthalmology	glaucoma	(72)
Orthopedics	rheumatoid arthritis	(143)
Pediatrics	congenital deafness	(184)
Pulmonary medicine	emphysema	(154)
Reproductive medicine	pre-eclampsia	(68)
Urology	urinary incontinence	(60)

Identification of primary cilia as sensory organelles has been accomplished by Nauli along with others, thus making the association between mechanical property and its relevance to disease much easier to be studied. Genetically identifying, proteomic finding and localizing many proteins to cilia have demonstrated the mechanosensory role of primary cilia in many vestibular organs. Various organs depend on the mechanosensory characteristic of cilia to sense and transmit extracellular signals into intracellular biochemical responses. Cilia possess the ability to sense a variety of fluid movements in the body, including blood in the vasculature (AbouAlaiwi et al. 2009, Nauli et al. 2008), urine in kidney nephrons (Nauli et al. 2006, Nauli et al. 2003), interstitial fluid in the bone matrix (Whitfield 2008), bile in the hepatic biliary system (Masyuk et al. 2006), pancreatic juice in the pancreatic duct (Rydholm et al. 2010), cerebral spinal fluid in the neuronal tube (Narita et al. 2010), fluid pressure in the inner ears (Lepelletier et al. 2013, Kim et al. 2003), and so on.

The inability to sense fluid-shear stress in these vestibular organs can be a factor which contributes to multiple organ pathogenesis (e.g. hypertension to hydrocephalus or deafness to cystic organ formation). Consequently, abnormal primary cilia function and/or ciliary proteins are now linked to various developmental disorders known as ciliopathies. These include left-right asymmetry defect, nephronophthisis, Bardet Biedl Syndrome, Oral Facial Syndrome, polycystic kidney disease, obesity, hypertension and aneurysm among others.



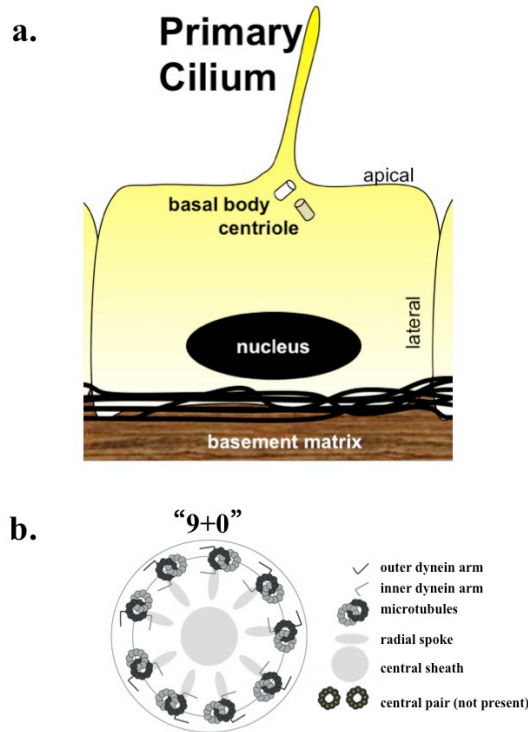


Figure 1. Primary cilium as a sensory organelle. (a) A side-view of primary cilium which acts as a cellular organelle. A primary cilium is projected at the apical membrane of many cell types. The cilium is extended from a mother centriole, also known as a basal body. (b) Based on the central pair of the microtubules in the axoneme seen from the cross-section, a primary cilium is generally categorized into a “9+0” structure. It was once thought that a cilium with “9+0” axoneme was always immotile. Classification of cilia becomes more complex, because some of “9+0” primary cilia are known to be motile.

### Primary cilia as biomechanics

Primary cilia have garnered much interest over the last few years, although it was once thought to be a dormant vestigial organelle with no known function. A primary cilium is a microtubule-based, antenna-like structure and is found in a single copy on the apical surface of fully differentiated mammalian cells (Figure 1). The diameter of a cilium is approximately 0.25  $\mu\text{m}$ , and its length can vary from 2 to 50  $\mu\text{m}$ .

Mechanosensory studies on primary cilia in different organ systems have confirmed that cilia are responsive to fluid-shear stress. Activation of cilia can be accomplished by bending with either suction through a micropipette (Praetorius and Spring 2001), apical fluid perfusion through changing the flow rate (Prasad, Jin, and Nauli 2014) or twisting using magnetic beads (Nauli et al. 2013). Cilia act as micro-sensory compartments, and their role depends on mechano-proteins such as polycystin-1 (Nauli et al. 2008, Nauli et al. 2003), polycystin-2 (AbouAlaiwi et al. 2009), fibrocystin (Wang et al. 2007), transient receptor potential-4 (Kottgen et al. 2008) and many others that have been recently discovered (Table 3). Thus, the overall functions of the sensory cilia compartments depend on the proper localization of cilia's functional proteins (Figure 2). A partial list of ciliary proteins in addition to their specific localizations is summarized in the table below (Table 3).

Table 3. Ciliary proteins and their subcellular localization.

<b>Ciliary tip</b>	<b>Reference</b>	<b>Ciliary soluble compartment</b>	<b>Reference</b>
EB1	(128, 146)	14-3-3	(32)
Gli	(42, 76)	Adenylyl cyclase	(16, 92)
KIF7	(29, 76)	Arl13b	(19, 46)
Smo	(20, 42, 76)	Arl211	(155)
Sufu	(55)	ATP synthase	(49)
		$\beta$ -arrestin-2	(92)
		CaM Kinase II	(92)
		CAML	(101)
		CRB1	(32)
		CRB3	(31, 32, 117)
		Cystin	(47, 178)
		GRK3	(92)
		GSK3 $\beta$	(30, 161)
		Importin	(31)
		Mek1/2	(145)
		OSEG family	(7)
		Par3	(32, 110, 148)
		Par6	(32)
		Phosphodiesterase	(92)
		PKC	(30, 32)
		pVHL	(79, 113, 161)
		STAT6	(81)
		Tubby	(87, 96)
		TULP2	(152)
<b>Ciliary axoneme</b>	<b>Reference</b>		
DNAH11	(12)		
DNAH5	(51)		
DNAH7	(180)		
DNAI1	(130)		
Dyf-1	(21, 122)		
Dyf-3	(98, 123)		
DYNC2H1	(91)		
DYNC2LI1	(138)		
Hydin	(23, 125)		
IFT140	(162)		
IFT172	(38, 50, 83, 129, 155)		
IFT20	(35, 58)		
IFT46	(39)		
IFT52	(78, 162)		
IFT57/curly	(70, 83)		
IFT57/hippi	(48, 162)		

IFT80	(13)		
IFT81	(82, 155)		
IFT88	(43, 99, 126, 137, 179)	<b>Ciliary membrane</b>	<b>Reference</b>
Kif17	(54)	EGFR	(84)
Kif3A/B	(77, 88, 89, 156)	Fibrocystin	(166, 167)
MDHC7	(108, 164)	Mchr1	(14)
PACRG	(24, 80)	PDGFR $\alpha$	(145)
PF13	(118)	Polycystin-1	(11, 178)
PF16	(142, 181)	Polycystin-2	(11, 127, 178)
PF2	(140)	Somatostatin-3 receptor	(147)
PF20	(182)	Serotonin-6 receptor	(18)
Tektin	(158)	Tie-1, Tie-2 receptors	(160)
		TRPN1	(62, 149)
		TRPV4	(136, 159)
<b>Ciliary base (centrosome)</b>	<b>Reference</b>	<b>Ciliary base (centrosome)</b>	<b>Reference</b>
ALMS1	(41, 44, 74, 93)	Nek1	(86, 170)
BBS1	(22, 111, 115)	Nek2	(9)
BBS2	(100, 109, 111)	Nek7	(66, 177)
BBS3	(33)	Nek8	(86, 121)
BBS4	(36, 64, 111)	NPHP-1	(120, 173)
BBS5	(75, 176)	NPHP-2	(120)
BBS6	(65)	NPHP-3	(15, 114)
BBS7	(17, 115)	NPHP-4	(94, 173)
BBS8	(5, 17)	NPHP-5	(119)
CC2D2A	(37)	NPHP-6	(144)
Cep164	(41)	ODF2	(26, 53)
CEP290	(37, 63)	OFD1	(34, 139)
EBI	(6, 131, 146)	p-150	(6)
Fa2p	(85)	PCM-1	(41, 63, 64, 93)
FAPP2	(165)	Pericentrin	(41, 59, 93)
Finl	(40)	POC12/MKS1	(25, 71, 169)
Fleer	(124)	Rab8	(63)
Joubertin	(28)	Rootletin	(9, 174, 175)
MKS-1	(25, 71)	RPGR	(150)
MKS-3	(25, 151, 157)	Seahorse	(67, 95)
		UNC	(10)

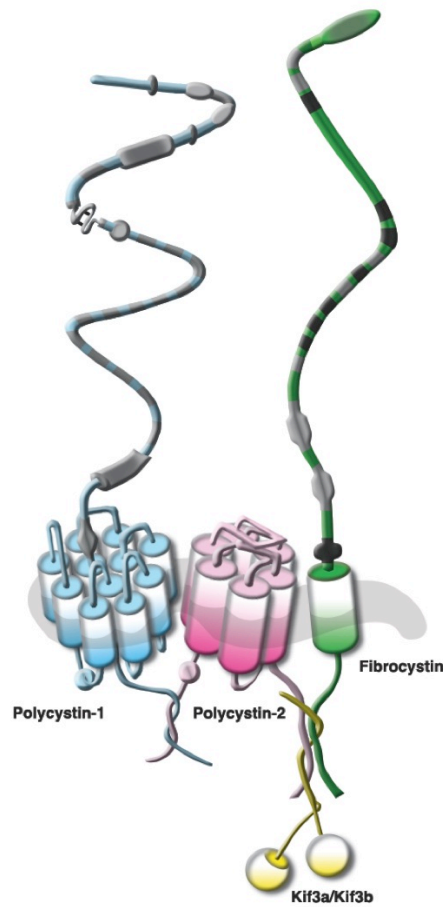


Figure 2. Mechanosensory primary cilia are dependent on functional sensory proteins. Polycystin-1, polycystin-2 and fibrocystin form a mechanosensory complex protein in the cilium to sense fluid-shear stress. Polycystin-1 and polycystin-2 interact with each other at their COOH termini forming a polycystin complex. It is predicted that fibrocystin interacts with this complex through polycystin-2 with kif acting as an adaptor protein.

Cells that no longer possess functional cilia show a loss in response to intracellular calcium after fluid-flow is induced. The primary cilium is able to respond to bending by the use of calcium entry through mechanically sensitive channels (Jin, Muntean, et al. 2014). The initial calcium influx into the cilia results in the gradual development of calcium-induced calcium-release mechanisms from intracellular stores (Jin, Mohieldin, et al. 2014). Large increases in the calcium levels of a cell may activate calcium-sensitive channels or calcium-dependent processes ranging from cell proliferation to cell death. Observation of the flow induced calcium response

in cells lacking cilia, demonstrated that without structural cilia, a cellular response to fluid flow was not detected, although all sensory machineries were still present (Aboualaiwi et al. 2014).

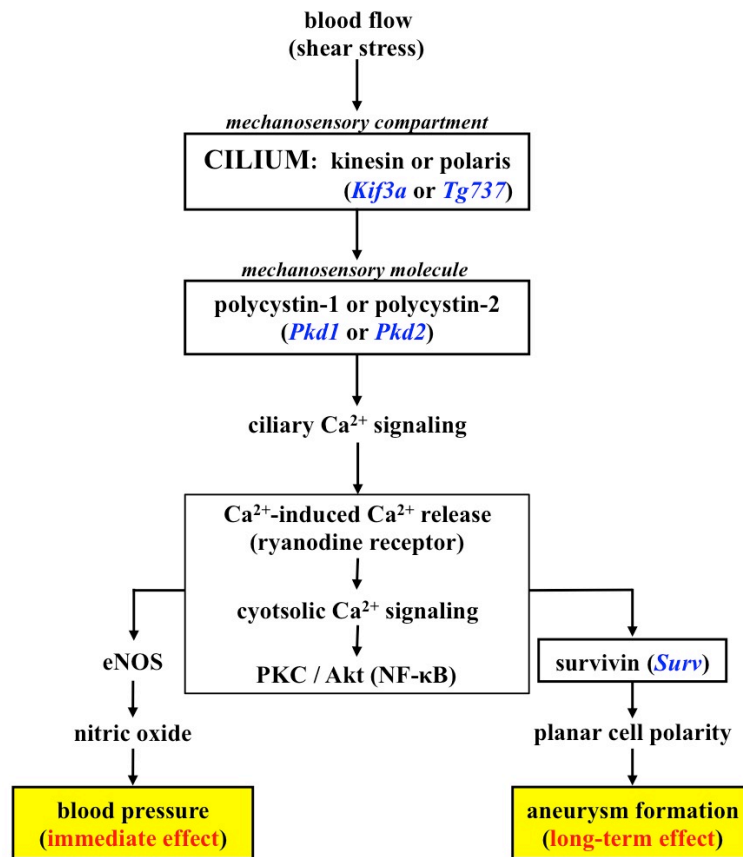


Figure 3. Intracellular signaling pathways are involved in transducing mechanosensory function of primary cilia. Mechanistic divergence pathways initiated from primary cilia are responsible for blood pressure maintenance and aneurysm formation. Abnormal primary cilia would induce high blood pressure earlier than aneurysm formation. However, abnormal survivin function is sufficient to form an aneurysm without altering blood pressure. Blue texts indicate the genes responsible for the mechanotransduction pathway of primary cilia.

### Modulating mechanobiology pathways

Studies on cilia biology have shown that primary cilia are coordinators involved in signaling pathways during development and tissue homeostasis. Cilia are composed of receptors, ion channels, and various transporter proteins. This composition enables primary cilia to play a critical role in several transduction pathways such as Hedgehog (Hh), Wnt, planar cell polarity

and platelet-derived growth factor (PDGF) (Muntean et al. 2014, Zilber et al. 2013, Schneider et al. 2005, Corbit et al. 2005). Mechanosensory pathways have also been probed, and any abnormalities in these pathways could result in hypertension and/or aneurysm formation (Figure 3).

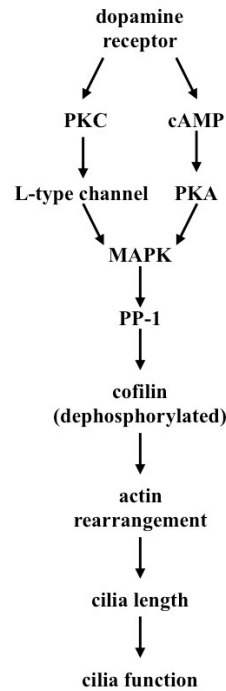


Figure 4. Ciliary dopamine receptor can regulate cilia length and function through a complex cellular pathway. Both calcium- and cAMP-dependent protein kinases (PKC and PKA) are involved in regulating cilia length through MAP kinase (MAPK) and protein phosphatase-1 (PP-1). PP-1 plays an important role in actin rearrangement, which is a requirement for cilia length regulation. As cilia length optimally increases, the cilia function will become more sensitive in response to fluid-shear stress.

### Potential intervention for cilio-therapy

Both ciliary length and function are tightly regulated (Abdul-Majeed, Moloney, and Nauli 2012). Longer cilia tend to have a greater sensitivity in response to fluid-shear stress (Upadhyay et al. 2014). Activation of the ciliary dopamine receptor (DR) will increase cilia length. More

specifically, dopamine receptor-type 5 (DR5) is localized to primary cilia. As such, DR5-specific agonist is among the few stimuli that require cilia for ciliary and intracellular signal transductions (Abdul-Majeed and Nauli 2011). DR5 activation increases cilia length through cofilin and actin polymerization (Figure 4).

The idea that pharmacological DR5 activation could be used as cilio-therapy is evident through *in vitro* studies involving the termination of mechano-ciliary function through silencing DR5 expression (Abdul-Majeed and Nauli 2011). DR5 activation also restores cilia function in the mechano-insensitive cells. Because the chemo-sensory function of cilia via DR5 can alter the mechano-sensory function through changes in sensitivity to fluid-shear stress, it has been proposed that DR5 has functional chemo- and mechano-sensory roles in primary cilia (Abdul-Majeed and Nauli 2011).

### **Potential mechano-therapy**

Patients with polycystic kidney disease (PKD) suffer from uncontrolled hypertension. It has been shown that vascular endothelia in PKD patients are mechanically compensated with abnormal primary cilia function (AbouAlaiwi et al. 2009). Activating DR5 can be used as a potential mechano-therapy by altering the mechanosensory function of primary cilia. This type of therapy is also known as cilio-therapy (Kathem et al. 2014). The initial drug screening indicated that activation of ciliary DR5 in addition to the DR5-specific agonist (fenoldopam), increases nitric oxide (NO) biosynthesis in response to fluid-shear stress in vascular endothelia. DR5 activation increases cilia length, and it also rescues mechanosensitivity of PKD endothelial cells from fluid-shear stress. This, in turn, decreases the overall blood pressure in the PKD mouse model (Kathem et al. 2014). In the clinical study, hypertensive PKD patients have a significantly lower baseline level of NO compared to hypertensive-only patients. DR5 activation decreases blood pressure in PKD patients (Kathem et al. 2014).

The baseline level of asymmetric dimethylarginine (ADMA), an endogenous inhibitor for eNOS and a marker for endothelial dysfunction, is significantly higher in the PKD group of patients compared to the hypertensive-only group of patients (Kathem et al. 2014). ADMA is a

physiological inhibitor of NO biosynthesis and is commonly used as a marker for assessing endothelial function in the clinical setting. Consistent with this idea, plasma ADMA levels are highly correlated with the severity of endothelial dysfunction, and high ADMA levels further impairs blood flow and accelerates endothelial dysfunction in PKD patients. Compared to the hypertensive-only patients, the PKD patients have an abnormality in regulating NO biosynthesis. This is consistent with a previous study indicating that vascular-lining endothelia from patients with PKD are dysfunctional due to their non-sensitivity to flow-induced NO biosynthesis (AbouAlaiwi et al. 2009).

Results from a less complex *in vivo* rodent system with endothelial cilia dysfunction also supports the idea that a DR5-cilia-NO axis plays an important role in regulating blood pressure in PKD (Kathem et al. 2014). In a more complex clinical setting, dopaminergic receptor activation showed a potential therapeutic benefit on overall arterial blood pressure. Together, these studies serve as a proof of principle for targeted-clinical therapy on primary cilia as a novel mechanism to modulate the progression of a ciliopathy and biomechanics-related diseases in general.

Although it was previously proposed that peripheral dopaminergic activation increases renal blood flow (Olsen 1998), we postulate that this vasodilation effect of dopamine on renal arteries acts by sensitizing primary cilia function. Without a doubt, a specific targeted therapy is more suitable for therapeutic management of different mechanical diseases. Future studies are warranted. Nonetheless, recent clinical studies shed light on the possibility for cilia-targeted therapy in PKD patients and hypertensive patients with mechanical-sensing dysfunction.

## Summary

Our knowledge of mechanotransduction has been advanced in the past decades. This includes the recognition of primary cilia, which function as mechanosensory organelles. The importance of sensory cilia in different organ systems has also been confirmed, and many more cilia-related diseases are still to be identified. There is no doubt that the biomedical approach to target mechanosensory primary cilia will continue to be debated in the years to come.



## References

1. Abdul-Majeed, S., B. C. Moloney, and S. M. Nauli. 2012. "Mechanisms regulating cilia growth and cilia function in endothelial cells." *Cell Mol Life Sci* 69 (1):165-73. doi: 10.1007/s00018-011-0744-0.
2. Abdul-Majeed, S., and S. M. Nauli. 2011. "Dopamine receptor type 5 in the primary cilia has dual chemo- and mechano-sensory roles." *Hypertension* 58 (2):325-31. doi: 10.1161/HYPERTENSIONAHA.111.172080.
3. Aboualaiwi, W. A., B. S. Muntean, S. Ratnam, B. Joe, L. Liu, R. L. Booth, I. Rodriguez, B. S. Herbert, R. L. Bacallao, M. Fruttiger, T. W. Mak, J. Zhou, and S. M. Nauli. 2014. "Survivin-induced abnormal ploidy contributes to cystic kidney and aneurysm formation." *Circulation* 129 (6):660-72. doi: 10.1161/CIRCULATIONAHA.113.005746.
4. AbouAlaiwi, W. A., M. Takahashi, B. R. Mell, T. J. Jones, S. Ratnam, R. J. Kolb, and S. M. Nauli. 2009. "Ciliary polycystin-2 is a mechanosensitive calcium channel involved in nitric oxide signaling cascades." *Circ Res* 104 (7):860-9. doi: 10.1161/CIRCRESAHA.108.192765.
5. Corbit, K. C., P. Aanstad, V. Singla, A. R. Norman, D. Y. Stainier, and J. F. Reiter. 2005. "Vertebrate Smoothed functions at the primary cilium." *Nature* 437 (7061):1018-21. doi: 10.1038/nature04117.
6. Hildebrandt, F., T. Benzing, and N. Katsanis. 2011. "Ciliopathies." *N Engl J Med* 364 (16):1533-43. doi: 10.1056/NEJMra1010172.
7. Ingber, D. E. 2003. "Mechanobiology and diseases of mechanotransduction." *Ann Med* 35 (8):564-77.
8. Jin, X., A. M. Mohieldin, B. S. Muntean, J. A. Green, J. V. Shah, K. Mykytyn, and S. M. Nauli. 2014. "Cilioplasm is a cellular compartment for calcium signaling in response to mechanical and chemical stimuli." *Cell Mol Life Sci* 71 (11):2165-78. doi: 10.1007/s00018-013-1483-1.
9. Jin, X., B. S. Muntean, M. S. Aal-Aaboda, Q. Duan, J. Zhou, and S. M. Nauli. 2014. "L-type calcium channel modulates cystic kidney phenotype." *Biochim Biophys Acta* 1842 (9):1518-26. doi: 10.1016/j.bbadis.2014.06.001.
10. Kathem, S. H., A. M. Mohieldin, S. Abdul-Majeed, S. H. Ismail, Q. H. Altaei, I. K. Alshimmari, M. M. Alsaïdi, H. Khammas, A. M. Nauli, B. Joe, and S. M. Nauli. 2014. "Ciliotherapy: a novel intervention in polycystic kidney disease." *J Geriatr Cardiol* 11 (1):63-73. doi: 10.3969/j.issn.1671-5411.2014.01.001.
11. Kim, J., Y. D. Chung, D. Y. Park, S. Choi, D. W. Shin, H. Soh, H. W. Lee, W. Son, J. Yim, C. S. Park, M. J. Kernan, and C. Kim. 2003. "A TRPV family ion channel required for hearing in *Drosophila*." *Nature* 424 (6944):81-4. doi: 10.1038/nature01733.
12. Kottgen, M., B. Buchholz, M. A. Garcia-Gonzalez, F. Kotsis, X. Fu, M. Doerken, C. Boehlke, D. Steffl, R. Tauber, T. Wegierski, R. Nitschke, M. Suzuki, A. Kramer-Zucker, G. G. Germino, T. Watnick, J. Prenen, B. Nilius, E. W. Kuehn, and G. Walz. 2008. "TRPP2 and TRPV4 form a polymodal sensory channel complex." *J Cell Biol* 182 (3):437-47. doi: 10.1083/jcb.200805124.
13. Lepelletier, L., J. B. de Monvel, J. Buisson, C. Desdouets, and C. Petit. 2013. "Auditory hair cell centrioles undergo confined Brownian motion throughout the developmental migration of the kinocilium." *Biophys J* 105 (1):48-58. doi: 10.1016/j.bpj.2013.05.009.
14. Masyuk, A. I., T. V. Masyuk, P. L. Splinter, B. Q. Huang, A. J. Stroope, and N. F. LaRusso. 2006. "Cholangiocyte cilia detect changes in luminal fluid flow and transmit them into intracellular Ca<sup>2+</sup> and cAMP signaling." *Gastroenterology* 131 (3):911-20. doi: 10.1053/j.gastro.2006.07.003.
15. Muntean, B. S., X. Jin, F. E. Williams, and S. M. Nauli. 2014. "Primary cilium regulates CaV1.2 expression through Wnt signaling." *J Cell Physiol* 229 (12):1926-34. doi: 10.1002/jcp.24642.

16. Narita, K., T. Kawate, N. Kakinuma, and S. Takeda. 2010. "Multiple primary cilia modulate the fluid transcytosis in choroid plexus epithelium." *Traffic* 11 (2):287-301. doi: 10.1111/j.1600-0854.2009.01016.x.
17. Nauli, S. M., F. J. Alenghat, Y. Luo, E. Williams, P. Vassilev, X. Li, A. E. Elia, W. Lu, E. M. Brown, S. J. Quinn, D. E. Ingber, and J. Zhou. 2003. "Polycystins 1 and 2 mediate mechanosensation in the primary cilium of kidney cells." *Nat Genet* 33 (2):129-37. doi: 10.1038/ng1076.
18. Nauli, S. M., X. Jin, W. A. AbouAlaiwi, W. El-Jouni, X. Su, and J. Zhou. 2013. "Non-motile primary cilia as fluid shear stress mechanosensors." *Methods Enzymol* 525:1-20. doi: 10.1016/B978-0-12-397944-5.00001-8.
19. Nauli, S. M., X. Jin, and B. P. Hierck. 2011. "The mechanosensory role of primary cilia in vascular hypertension." *Int J Vasc Med* 2011:376281. doi: 10.1155/2011/376281.
20. Nauli, S. M., Y. Kawanabe, J. J. Kaminski, W. J. Pearce, D. E. Ingber, and J. Zhou. 2008. "Endothelial cilia are fluid shear sensors that regulate calcium signaling and nitric oxide production through polycystin-1." *Circulation* 117 (9):1161-71. doi: 10.1161/CIRCULATIONAHA.107.710111.
21. Nauli, S. M., S. Rossetti, R. J. Kolb, F. J. Alenghat, M. B. Consugar, P. C. Harris, D. E. Ingber, M. Loghman-Adham, and J. Zhou. 2006. "Loss of polycystin-1 in human cyst-lining epithelia leads to ciliary dysfunction." *J Am Soc Nephrol* 17 (4):1015-25. doi: 10.1681/ASN.2005080830.
22. Olsen, N. V. 1998. "Effects of dopamine on renal haemodynamics tubular function and sodium excretion in normal humans." *Dan Med Bull* 45 (3):282-97.
23. Praetorius, H. A., and K. R. Spring. 2001. "Bending the MDCK cell primary cilium increases intracellular calcium." *J Membr Biol* 184 (1):71-9.
24. Prasad, R. M., X. Jin, W. A. Aboualaiwi, and S. M. Nauli. 2014. "Real-time vascular mechanosensation through ex vivo artery perfusion." *Biol Proced Online* 16 (1):6. doi: 10.1186/1480-9222-16-6.
25. Prasad, R. M., X. Jin, and S. M. Nauli. 2014. "Sensing a Sensor: Identifying the Mechanosensory Function of Primary Cilia." *Biosensors (Basel)* 4 (1):47-62. doi: 10.3390/bios4010047.
26. Rydholm, S., G. Zwartz, J. M. Kowalewski, P. Kamali-Zare, T. Frisk, and H. Brismar. 2010. "Mechanical properties of primary cilia regulate the response to fluid flow." *Am J Physiol Renal Physiol* 298 (5):F1096-102. doi: 10.1152/ajprenal.00657.2009.
27. Schneider, L., C. A. Clement, S. C. Teilmann, G. J. Pazour, E. K. Hoffmann, P. Satir, and S. T. Christensen. 2005. "PDGFRalpha signaling is regulated through the primary cilium in fibroblasts." *Curr Biol* 15 (20):1861-6. doi: 10.1016/j.cub.2005.09.012.
28. Upadhyay, V. S., B. S. Muntean, S. H. Kathem, J. J. Hwang, W. A. Aboualaiwi, and S. M. Nauli. 2014. "Roles of dopamine receptor on chemosensory and mechanosensory primary cilia in renal epithelial cells." *Front Physiol* 5:72. doi: 10.3389/fphys.2014.00072.
29. Wang, S., J. Zhang, S. M. Nauli, X. Li, P. G. Starremans, Y. Luo, K. A. Roberts, and J. Zhou. 2007. "Fibrocystin/polyductin, found in the same protein complex with polycystin-2, regulates calcium responses in kidney epithelia." *Mol Cell Biol* 27 (8):3241-52. doi: 10.1128/MCB.00072-07.
30. Waters, A. M., and P. L. Beales. 2011. "Ciliopathies: an expanding disease spectrum." *Pediatr Nephrol* 26 (7):1039-56. doi: 10.1007/s00467-010-1731-7.
31. Whitfield, J. F. 2008. "The solitary (primary) cilium--a mechanosensory toggle switch in bone and cartilage cells." *Cell Signal* 20 (6):1019-24. doi: 10.1016/j.cellsig.2007.12.001.
32. Zilber, Y., S. Babayeva, J. H. Seo, J. J. Liu, S. Mootin, and E. Torban. 2013. "The PCP effector Fuzzy controls ciliary assembly and signaling by recruiting Rab8 and Dishevelled to the primary cilium." *Mol Biol Cell* 24 (5):555-65. doi: 10.1091/mbc.E12-06-0437.

### Chapter 3. Measurement of cytoplasmic and cilioplasmic calcium in a single living cell.\*

#### Abstract

Cellular signaling represents an evolution of biological systems to sense external stimuli and communicate extracellular microenvironment to the intracellular compartments. The processes underlying molecular signaling have been widely studied due to their important cellular functions. There are numerous techniques available to quantitate the different molecules involved in cellular processes. Among them, calcium is a ubiquitous signaling molecule involved in many biological pathways. Over time the methods to measure intracellular calcium has advanced to better understand its role as a second messenger. In this chapter, we introduce a method to study a single cilium, a mechanosensor that elicits a calcium signaling cascade. To successfully observe the calcium changes in this thin cylindrical-like projection from the cell surface, we utilize a genetically encoded sensor with a high spatial and temporal resolution. In addition, the probe must be localized to the ciliary compartment in order to observe the intraciliary calcium signaling dynamics. To this end, a cilium targeting genetically encoded indicator is used to observe calcium fluxes in both cytoplasm and cilioplasm.

Keywords: Calcium ( $\text{Ca}^{2+}$ ), Cilia, Calcium Sensor, G-GECO1.0, Fluorescent imaging, Live cell imaging

---

\* Sherpa RT, Pala R, Mohieldin AM, Nauli SM. Measurement of cytoplasmic and cilioplasmic calcium in a single living cell. *Methods Cell Biol.* 2019 Apr 17.

## Introduction

Calcium ions ( $\text{Ca}^{2+}$ ) are essential in biological systems. They play important roles as a secondary messenger in regulating vascular tone (Falcone, Kuo, & Meininger, 1993; Johns et al., 1987), neurotransmitter release (Kerr et al., 2000; Sabatini, Oertner, & Svoboda, 2002), muscle contraction (Ebashi & Endo, 1968; Forder, Scriabine, & Rasmussen, 1985; Wier, Cannell, Berlin, Marban, & Lederer, 1987) and immune responses (Ebashi & Endo, 1968; Forder et al., 1985; Wier et al., 1987) among many others. Even the beginning of life requires the spark of  $\text{Ca}^{2+}$  during fertilization (Ebashi & Endo, 1968; Forder et al., 1985; Wier et al., 1987).  $\text{Ca}^{2+}$  signaling affects every aspect of a cell's life and death. Just as  $\text{Ca}^{2+}$  signaling has been conserved throughout evolution, the primary cilium has also been conserved from our primitive ancestors. Cilia are slender microtubule-based organelles that protrude from the apical membrane in most adherent cells (S. Sorokin, 1962; S. P. Sorokin, 1968). However, these non-motile cilia were once thought to be a vestigial cell appendage without any apparent function. That was the consensus until studies looking into a possible mechanosensory function of the primary cilium proved it to be an essential cellular organelle (Malone et al., 2007; Masyuk et al., 2006; Nauli et al., 2003, 2013, 2008, Praetorius & Spring, 2001, 2003). Praetorius and Spring used a setup of differential interference contrast (DIC) and fluorescent microscopy to observe MDCK (Madin-Darby Canine Kidney) cells incubated with Fluo-4, a fluorescent calcium indicator. Then micropipette suction was applied in order to bend the cilia and detect flow-induced  $\text{Ca}^{2+}$  changes. (Praetorius & Spring, 2001, 2003).

The fluid flow-induced cilium bending initiates an intracellular  $\text{Ca}^{2+}$  influx followed by global  $\text{Ca}^{2+}$  increase and sustained membrane hyperpolarization (Praetorius & Spring, 2001, 2003). Since then, other studies have found a mechanosensory complex of polycystins 1 & 2 (PC 1 and PC 2) in the ciliary membrane of the renal epithelia which mediate flow sensation (Jin et al., 2014; Nauli et al., 2003, 2008). The bending of the primary cilium causes conformational change in the PC 1 and the associated PC 2, a transient receptor potential  $\text{Ca}^{2+}$  channel, is then activated causing an influx of extracellular  $\text{Ca}^{2+}$  (Delmas et al., 2002; Hanaoka et al., 2000; Nauli et al., 2003; Nauli, Pala, & Kleene, 2016). The influx then triggers the release of  $\text{Ca}^{2+}$  from the intracellular stores through the stimulation of ryanodine receptors (Nauli et al., 2003; Xu et al., 2006). Other studies have found that the cilia are enriched with critical proteins in signaling

pathways like Hedgehog, Wnt and Notch as well as membranous GPCRs (Haycraft et al., 2005; Huang & Schier, 2009; Ishikawa, Thompson, Yates, Marshall, & Marshall, 2012; Gregory J Pazour, Agrin, Leszyk, & Witman, 2005; Schou, Pedersen, & Christensen, 2015). All these proteins are synthesized in the cytosol and eventually transported to the cilia by intraflagellar transport (IFT) apparatus (Liem et al., 2012; Mukhopadhyay et al., 2010; G J Pazour, Dickert, & Witman, 1999).

With the function of collecting mechanical and chemical cues from the environmental milieu, the importance and the wide functional coverage of the primary cilia becomes even more apparent when the cilia are defective (Christensen, Clement, Satir, & Pedersen, 2012; Singla & Reiter, 2006). The range of diseases affecting multiple systems in the body that arise from dysfunctional cilia is called ciliopathies (Kathem et al., 2014; Nauli, Sherpa, Reese, & Nauli, 2016; Pala et al., 2018). As the flow-mediated  $Ca^{2+}$  influx can be a functional readout of physiologically relevant cilia function, technologies to study and measure  $Ca^{2+}$  changes within the cilia and the cytoplasm are needed.

The challenge of observing live  $Ca^{2+}$  levels in the cilia arise due to the size of primary cilia. With a diameter around 200 nm and a perpendicular orientation in relation to the cell monolayer, it requires specific setup to visualize the cilium together with the cytoplasm since they are at different planes of view (Jin et al., 2014; Su et al., 2013). In addition to these difficulties, traditional  $Ca^{2+}$  indicators also fail to reach the cilioplasm requiring modification of sensors to target the cilia. The exclusion of most cellular components and exogenous compounds, unless specifically designated for the cilia, happens due to a diffusion barrier at the base of the cilia (Breslow, Koslover, Seydel, Spakowitz, & Nachury, 2013; Hu et al., 2010; Satir, 2017). The presence of a barrier between the cytoplasm and cilioplasm was first observed using freeze-fracture electron microscopy by Gilula and Satir in the form of a “ciliary necklace” (Gilula & Satir, 1972). This detailed molecular composition of this transition zone at the base of cilia remains to be established. Nonetheless it is interesting to find that mutated proteins involved in ciliopathies localize to the ciliary transition zone and might be necessary for shuttling biomolecules (Delous et al., 2007; Fliegauf et al., 2006; Mollet et al., 2005; Otto et al., 2005, 2003; Valente et al., 2010; C. L. Williams, Masyukova, & Yoder, 2010; Corey L. Williams,

Winkelbauer, Schafer, Michaud, & Yoder, 2008). The consensus is that while some small cytosolic proteins might freely diffuse into the cilia larger molecules or complexes will require a favorable interaction with the transition zone before entering the cilioplasm. To overcome this challenge, researchers have added targeting modules intended to transport the attached cargo into the cilia. Relying on the same strategy, we outline a method of single-cell imaging technique to distinctively visualize  $\text{Ca}^{2+}$  signaling in the intraciliary compartment and cytosol of a live cell.

## 1. Choosing $\text{Ca}^{2+}$ indicators

Detecting calcium fluxes in cells are best studied using  $\text{Ca}^{2+}$  indicators. With the backing of years of research, there are now a collection of indicators that can be used to examine  $\text{Ca}^{2+}$  dynamics. There are two main categories of  $\text{Ca}^{2+}$  indicators; 1) small molecule and 2) genetically encoded calcium indicators (GECIs) (Brini et al., 1994; Cobbold & Rink, 1987; Mank et al., 2008; Miyawaki et al., 1997; Nagai, Sawano, Park, & Miyawaki, 2001; Nakai, Ohkura, & Imoto, 2001; Amy E. Palmer et al., 2006; Romoser, Hinkle, & Persechini, 1997). Small molecule indicators have superior dynamic range, higher sensitivity and rapid response kinetics (Pérez Koldenkova & Nagai, 2013; Rudolf, Mongillo, Rizzuto, & Pozzan, 2003).

Small molecule indicators like Fura-2 acetoxymethyl ester (Fura-2AM) are robust, allowing ratiometric measurements that can be easily interpreted and less prone to experimental artifacts (D. A. Williams, Fogarty, Tsien, & Fay, 1985). Another key point to consider is to ensure that the affinity for  $\text{Ca}^{2+}$  ( $K_d$ ), which can vary among the indicators, is suitable to measure the local  $\text{Ca}^{2+}$  concentration in the region of interest. Nonetheless, all these depend on the availability of a microscope with the proper setup of emission channels, acquisition features, and motorized filter wheels if ratiometric indicators are used. Even with their advantages, small molecule indicators cannot be used for applications that focus on delineating organelle specific  $\text{Ca}^{2+}$  changes. Cell-permeant indicators, like Fura-2AM, or ones that require more invasive methods are assumed to be homogeneously distributed in the cytosol after loading. But these indicators face the possibility of being either included or excluded from membrane-enclosed structures in the cell. Since signaling depends on spatial origin and compartmentalization, indicators that can segregate into target organelles are valuable to appreciate the different spatial compartments of signaling.



The other class of indicators is GECI, which are constructed with a  $\text{Ca}^{2+}$  binding module and one or more fluorophores (Figure 5). As a general mechanism, in most GECIs  $\text{Ca}^{2+}$  interacts with the binding domain, conformational changes are transferred to the fluorophores affecting the fluorescence intensity. GECIs require gene transfer, i.e., insertion of the nucleic acid sequence coding for the sensor into the cell line of interest. There are a variety of transduction/transfection methods that can be used for transformation. Once expressed in the cells, the indicator is incorporated in the cellular milieu. This is an advantage over small molecule indicators which require repetitive dye incubation for every experiment, suffer from dye leakage and prone cellular toxicity during extended time-lapse experiments.

To address the lack of cellular localization ability of small molecule indicators, an addition of targeting sequence to the GECI can be done. There are GECIs that have been targeted to organelles like mitochondria (Filippin et al., 2005; Amy E. Palmer et al., 2006), golgi (Griesbeck, Baird, Campbell, Zacharias, & Tsien, 2001), endoplasmic reticulum (Miyawaki et al., 1997; A. E. Palmer, Jin, Reed, & Tsien, 2004) and nucleus (Miyawaki et al., 1997). Choosing indicators is strictly determined by the needs of the researcher, and the key characteristics to consider include the dynamic range, affinity ( $K_d$ ) of the indicator for  $\text{Ca}^{2+}$ , response kinetics and targeting ability.

In our experiments, we are interested in the primary cilia, which is a cellular projection arising from the cell and plays a sensory role in a variety of specialized cells (Malone et al., 2007; Masyuk et al., 2006; Nauli et al., 2003, 2008). For our purpose, we utilize 5HT6-mCherry-G-GECO1.0 (Figure 5c, Addgene, Cat. 47500) developed by Su et al. which contains a cilium-targeting sequence (CTS) derived from 5HT6, a serotonin receptor (Berbari, Johnson, Lewis, Askwith, & Mykytyn, 2008), a mCherry marker and the  $\text{Ca}^{2+}$  sensor G-GECO1 (Zhao et al., 2011). G-GECO1 is a single fluorescent sensor based on G-CaMP3, an iteration of the original G-CaMP. A few G-CaMP3 iterations and their cilia targeting fusions are outlined in Figure 4. Like the original G-CaMP, G-GECO1 still retains the circularly permuted enhanced green fluorescent protein (EGFP), calmodulin (CaM) in the C terminal, and myosin light chain (M13 peptide sequence) (Nakai et al., 2001; Tian et al., 2009). When  $\text{Ca}^{2+}$  binds to the CaM domain, conformational changes due to the  $\text{Ca}^{2+}$ -CaM-M13 interaction induces a subsequent

conformational change in EGFP and a change in fluorescent intensity (Akerboom et al., 2012, 2009; Nakai et al., 2001). This changes the fluorescence intensity of EGFP which can be correlated to  $Ca^{2+}$  levels. Like other  $Ca^{2+}$  indicators, G-CaMP3 by itself fails to penetrate into the cilioplasm and in order to overcome this challenge a CTS derived from ciliary protein can be used. This strategy allows the cellular transportation machinery to move the CTS-attached sensor to the cilia. Like 5HT6, the intracellular C-tail of fibrocystin (Pkh1 C1-68) (Follit, Li, Vucica, & Pazour, 2010) and the third cytoplasmic loop of SSTR3 (Berbari et al., 2008) are also CTSs among others used to deliver sensors to the cilia (Follit et al., 2010; Jin et al., 2014). The  $Ca^{2+}$  sensor, G-GECO1 has double the dynamic range of G-CaMP3, due to substitutions (K119I, L173Q, S404G, and E430V) in the original G-CaMP3. The increased dynamic range is advantageous for observing ciliary  $Ca^{2+}$  with a baseline  $Ca^{2+}$  as high as 742 nM (DeCaen, Delling, Vien, & Clapham, 2013). The other advantage of 5HT6-mCherry-G-GECO1.0 is the presence of constant mCherry fluorescent marker independent of  $Ca^{2+}$  flux. The mCherry aids in visualization of ciliary movement, correction of artifacts and ratiometric analysis of the data.



Name	DR <sup>1</sup>	K <sub>d</sub> (Ca <sup>2+</sup> )	Comments	References
<b>General cytosolic GECl</b>				
G-CaMPs	23X	144 nM	10x higher sensitivity and increased dynamic range than G-CaMP3.	Chen, T.-W., Wardill, T. J., Sun, Y., Pulver, S. R., Renninger, S. L., Baohan, A., ... Kim, D. S. 2013. <i>Nature</i>
G-CaMP	4.3X	235 nM	Weak fluorescence at physiological temperatures compared to its base, EGFP.	Souslova, E. A., Belousov, V. V., Lock, J. G., Strömblad, S., Kasparov, S., Bolshakov, A. P., ... Chudakov, D. M. 2007. <i>BMC Biotechnology</i> .
G-CaMP3	12X	540 nM	1.3x higher affinity to Ca <sup>2+</sup> and 3x more dynamic range compared to G-CaMP.	Nakai, J., Ohkura, M., & Imoto, K. 2001. <i>Nature Biotechnology</i> .
G-GECCO1.0	25X	750 nM	2X higher dynamic range compared to G-CaMP3.	Zhao, Y., Araki, S., Wu, J., Teramoto, T., Chang, Y. F., Nakano, M., ... Campbell, R. E. 2011. <i>Science</i>
G-GECCO1.2	23X	1150 nM	Sensitive to a range of 1-10 μM Ca <sup>2+</sup> .	Zhao, Y., Araki, S., Wu, J., Teramoto, T., Chang, Y. F., Nakano, M., ... Campbell, R. E. 2011. <i>Science Nano Letters</i> .
<b>Cilia Targeting GECl</b>				
Arl13b-G-CaMP6	23X	144 nM	Another available CTS, Arl13b, used to localize G-CaMP6 to the cilium.	Yuan S, Zhao L, Sun Z. 2015. <i>Curr. Biol.</i>
ALC (Arl13b fused to YC3.6)	5.6X	250 nM	FRET-based sensor with ECFP & cpYenus (donor-acceptor)	Chen, T.-W., Wardill, T. J., Sun, Y., Pulver, S. R., Renninger, S. L., Baohan, A., ... Kim, D. S. 2013. <i>Nature</i>
Arl13b-mCherry-GECCO1.2	8X	450 nM	Reaches saturation at a 800 nM Ca <sup>2+</sup>	Lee, K. L., Guevarra, M. D., Nguyen, A. M., Chua, M. C., Wang, Y., & Jacobs, C. R. 2015. <i>Cilia</i> .
CTS-G-CaMP3	12X	542 nM	Contains the intracellular C-tail of fibrocytin, Pkh1 (C1-68) for ciliary localization of the sensor.	Nagai, T., Yamada, S., Tomimaga, T., Ichikawa, M., & Miyawaki, A. 2004. <i>Proc Natl Acad Sci U S A</i> .
SHT6-mCherry-G-GECCO1.0	25X	750 nM	mCherry allows constant cilia fluorescence and ratiometric analysis.	Deiling M., Indzhykulia A. A., Liu X., Liul Y., Xie T., Corey D. P., Clapham D. E., 2016. <i>Nature</i> .

<sup>1</sup> Dynamic Range (DR) is defined as the ratio of emission intensities (AF/F<sub>0</sub>) for intensiometric GECCOs and the ratio of emission ratios (ΔEGFP/EGFP<sub>0</sub>)/ΔmCherry/mCherry<sub>0</sub> for Arl13b-mCherry-GECCO1.2 & SHT6-mCherry-G-GECCO1.0. For ALC, the dynamic range is derived from (E<sub>max</sub> - E<sub>min</sub>)/E<sub>min</sub>, where E is FRET efficiency.

Table 4. Properties of some G-CaMP based sensors and their cilia targeting derivatives.

## 2. Experimental Setup

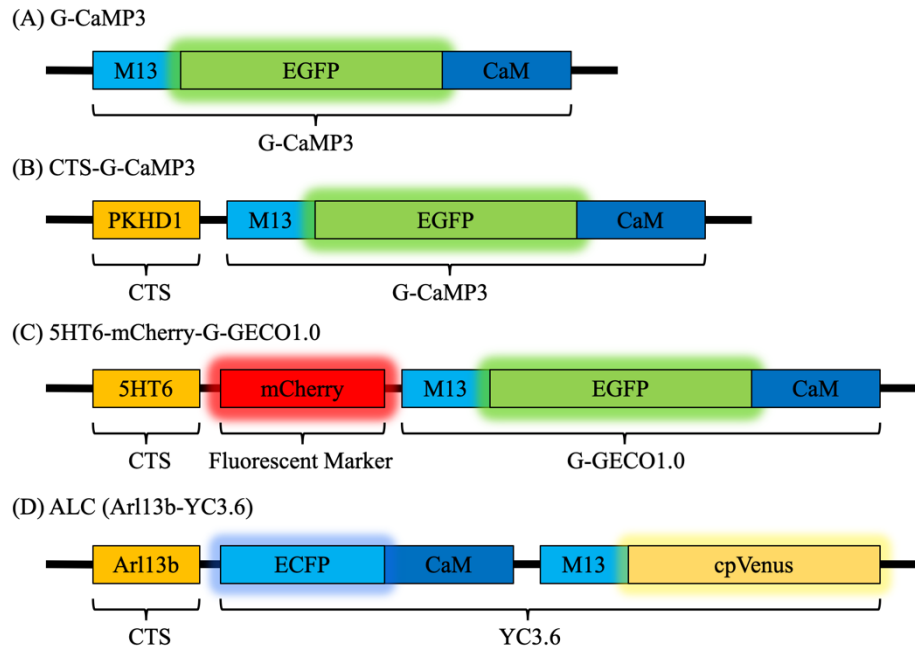


Figure 5. Schematic representation of GECI construct. (a) G-CaMP3 is a single fluorescent  $\text{Ca}^{2+}$  sensor and after fusion with CTS such as the cytoplasmic tail of PKHD1 in (b) CTS-G-CaMP3, the sensor localizes to the cilioplasm. (c) In 5HT6-mCherry-G-GECO1.0 the  $\text{Ca}^{2+}$  sensor, G-GECO1.0 is attached to a CTS derived from 5HT6 and mCherry, a stable fluorescence marker to track ciliary movement. (d) ALC is another GECI based on FRET for  $\text{Ca}^{2+}$  quantification, fused with the CTS Arl13b for cilia localization.

### 2.1. Expression of genetically encoded cilia targeting sensor

5HT6-mCherry-G-GECO1.0 plasmid construction has been outlined by Su et al., 2013. Porcine kidney epithelial cells (LLC-PK1, ATCC CL-101) derived from proximal tubules is grown at  $37^{\circ}\text{C}$  in Dulbecco's modified Eagle's medium containing 10% fetal bovine serum (FBS) and 1% penicillin-streptomycin hence referred as growth media. After reaching a confluence of 60-70%, the cells are transfected with the 5HT6-mCherry-G-GECO1.0 construct using Jetprime transfection reagent (Polyplus Transfection, Ref. 114-15) according to the manufacturer's instructions and selected using G418 at a concentration of  $500 \mu\text{g/ml}$ .

## 2.2. Cell growth on microwire

After selecting cells that express 5HT6-mCherry-G-GECO1.0, the transfected cells can now be grown on a precision tungsten microwire. Tungsten microwire can be obtained through Luma Metall AB, Sweden. We recommend a high purity wire (Wire quality #823) and straightened electrolytically etched with a final diameter of less than 100  $\mu\text{m}$  (Surface finish #42) for the experiment. The preparation of the precision microwire requires coating with type I collagen (50  $\mu\text{g}/\text{mL}$  in 0.02N acetic acid) to provide a conducive surface for cell attachment and growth. The microwires are then UV sterilized for 30 minutes and mounted on the imaging chamber before seeding cells. Continue to monitor cell growth for 1-2 days and when the confluency reached  $\sim 95\text{-}98\%$  add low serum media (2% FBS) to promote ciliation of the cells. If needed the microwire can be gently rotated to observe the confluency of the cells around the microwire.

## 3. Fluorescence Microscopy

### 3.1. Overview

Microscopy has permitted an appreciation of molecular level activities in cells. Starting from a simple setup of optical lenses used by pioneer scientists to view simple structures, the microscope has evolved into sophisticated digital imaging systems with increased spatial and temporal resolution for specialized procedures in scientific research. The concurrent development of molecular techniques, innovative approaches and iterative progression of fluorescent proteins have contributed to the breakthrough in our understanding of cellular functions.

Fluorescence is the phenomenon of absorption of electromagnetic radiation and the subsequent release of radiation by a fluorophore. A basic fluorescence microscope functions to irradiate the specimen with a desired and specific band of wavelengths. An illumination source produces a specific wavelength band and passes it through a selective excitation filter. The excitation light then reflects off from a dichroic mirror to the sample. If the specimen fluoresces, the illumination is then emitted back, albeit at a lower energy level in a phenomenon called Stokes shift. The emission is gathered by the objective and passed back through the dichroic mirror into the

emission filter, which blocks the unwanted excitation wavelengths. Building on these basic principles, innovative indicator design using molecular approaches have significantly advanced the use of fluorescence microscopy to study cell processes. So, in addition to a suitable fluorescent indicator for experimental needs, a basic prerequisite is the microscope system which should have the capabilities to support required specifications.

### 3.2. Experimental setup

Our experimental setup consists of two main components

- i) Flow equipment that includes imaging dishes which are standard 35 mm plates with a custom-made glass coverslip bottom. For the imaging dishes, a hole is cut out from the bottom of the plate and using a silicone-based glue (Loctite® Clear Silicone Waterproof Sealant; Item#908570) a glass coverslip is attached to the plate. We also have a perfusion pump with variable flow settings and inlet/outlet tubing to allow fluid flow over the microwire (Figure 6a).
- ii) Imaging equipment, which in our case is an inverted fluorescent microscope with accessories for rapid imaging. We use a Nikon Ti-Eclipse outfitted with excitation and emission filter wheels, controlled by a Lambda 10-3 filter changer. In addition, the DG-5 Plus module high-speed wavelength switcher for rapid imaging of two signals, EGFP and mCherry. The software package is NIS-elements and used to interface with the microscope, filter changer and camera as well as conduct data analysis. The setup can capture DIC and fluorescence images. With the okoLab incubator module, the cells can be sustained in a controlled environment of 37°C, 5% CO<sub>2</sub> and appropriate humidity for long periods if needed. The 5HT6-mCherry-G-GECO1.0 has EGFP with excitation and emission wavelengths of 495 and 515 nm, respectively. The mCherry has excitation and emission wavelengths of 587 and 610 nm, respectively. The user must adjust the excitation and emission setup to successfully view the signals. Exposure will also need to be adjusted around 200-600 ms for rapid imaging while also maintaining satisfactory baseline signal of the EGFP and mCherry.

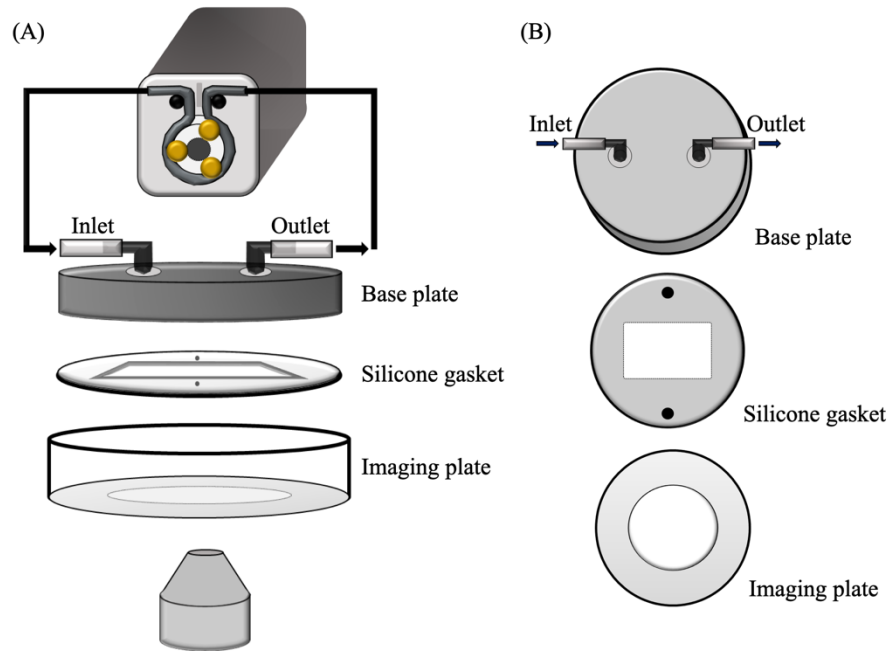


Figure 6. Flow equipment setup for live cell and cilia imaging. (a) The flow setup uses a peristaltic pump in a closed loop system. The perfusion chamber consists of a top base plate with inlet and outlet connected to the pump. Then we have a silicone gasket to form a channel for laminar flow and finally, a glass bottom imaging plate. (b) Top view of each perfusion chamber component.

### 3.2.1. Flow equipment setup

In our experiment, we use an Instech P720 peristaltic pump in a closed perfusion system with inlet and outlet to the perfusion chamber (Brown & Larson, 2001; Jin et al., 2014; Nauli et al., 2013). The flow chamber from GlycoTech (Cat. 31–001) is arranged as follows from top to bottom (Figure 6b)

1. base plate with an inlet and outlet port for perfusate flow.
2. silicone gasket that defines the geometry of the flow region to achieve non-turbulence, laminar flow and seals the chamber from potential fluid leakage.
3. glass bottom plate on which the microwire is to be placed.

The components are set up to minimize the use of excessive long tubing; the volume of perfusate is determined empirically; the pump is primed with perfusate before each experiment. Once the transfected cells expressing 5HT6-mCherry-G-GECO1.0 are fully confluent on the microwire,

they are placed on the imaging dish. The assembly is then put together as mentioned above providing an inlet and outlet of fluid (Figure 6). A range of shear-stress from 0.1 to 50 dyne/cm<sup>2</sup> can be used to induce bending of cilia. Assuming the GlycoTech perfusion chamber to be shaped as a cuboid based on the dimensions of the gasket, the flow rate can be adjusted to obtain the desired shear stress using the following formula.

$$\tau_w = \frac{6Q\eta}{a^2b}$$

Where:

- $\tau_w$  = Wall shear stress (dyne/cm<sup>2</sup>)
- $Q$  = Volumetric flow rate in (mL/s)
- $\eta$  = Apparent fluid viscosity in (dyne.s/cm<sup>2</sup>)
- $a$  = Chamber height / Gasket thickness (cm)
- $b$  = Chamber / Gasket width (cm)

As a note, at 33-39 °C, Dulbecco's Modified Eagle Medium or HEPES has a calculated viscosity of ~ 0.0076 dyne.s/cm<sup>2</sup> (Nauli et al., 2013).

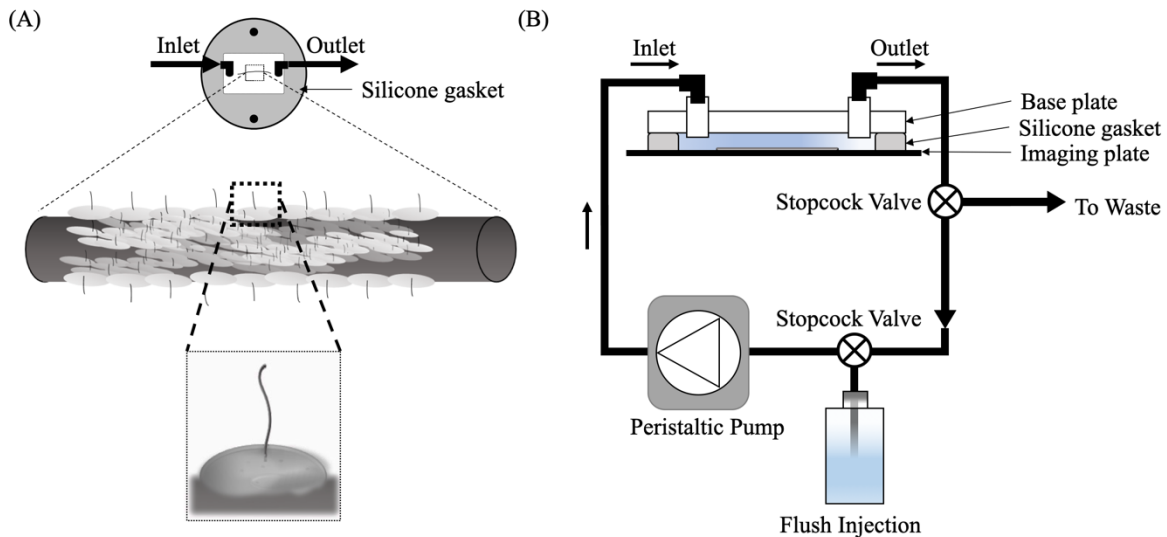


Figure 7. Microwire with cells in a perfusion chamber. (a) In the diagram, the gasket is placed on the imaging dish in a manner to orient the microwire parallel to laminar flow. At a higher magnification, the cilium protruding outward should become even clearer. We will focus on a



single cell and capture  $\text{Ca}^{2+}$  data in response to fluid flow. (b) Schematic of the experimental setup with stopcock valves to load and unload buffers into circulation.

### 3.2.2. Monitoring experiment

After assembling flow chamber with the microwire inside, place the plate onto the stage. Join the fluid channels to the pump. Eliminate air bubbles and equilibrate the cells for 15-20 minutes. Use brightfield illumination to focus on the edge to the precision microwire at a lower magnification. Switch to a 100X objective to find a cell with cilia. At a 100X objective and correct positioning, side-view imaging should show both the cilium and the cell body at the same time (Figure 7a). One can switch directly to the fluorescence illumination, using the mCherry signal to find cilia that should possess the 5HT6-mCherry-G-GECO1.0 sensor. As a note, even the cell body will fluoresce because the sensor is produced in the cytosol before being trafficked into the cilioplasm. Due to the random probability of orientation and mostly due to the  $\sim 200$  nm size of the cilium, finding one may remain elusive and might take a while to find a field that captures both the cilioplasm in its full length and the cytoplasm in focus.

After confirming the fluorescence localization and checking to see proper cell morphology, we can start the experiment. To measure the resting  $\text{Ca}^{2+}$ , start the data acquisition and collect images every  $\sim 1-10$  s for 5 minutes. The pump can be turned on after collecting baseline data. At this time, data can be collected continuously; i.e., no delay data acquisition to view rapid fluxes in  $\text{Ca}^{2+}$ . The introduction of flow might lead to small movement initially, but that can be resolved with a focal or stage adjustment to ensure the cilium remains visible and in-focus. After the fluid flow data capture, buffer can be exchanged using stopcock valves to introduce new perfusate and simultaneously eliminate the initial circulating buffer (Figure 7b). To obtain the minimum fluorescence the buffer is replaced with  $\text{Ca}^{2+}$ -free solution containing 2 mM EGTA and 10  $\mu\text{M}$  ionomycin. Using tubing with an inner diameter of 0.02 inches (0.5 mm) and length of 8 inches (20 cm), we get a dead volume of 39  $\text{mm}^3$  or 39  $\mu\text{L}$ . Complete media exchange in the flow chamber takes about a minute and the same applies to the time for diverting the  $\text{Ca}^{2+}$  solution to the waste container. After the minimum signal is determined, the cell is challenged with  $\text{Ca}^{2+}$  (10 mM) to obtain a maximum signal. This is to ensure that 1) the system

is responding accordingly to the ambient  $\text{Ca}^{2+}$  concentration and 2) the dynamic range (or  $K_d$ ) of the  $\text{Ca}^{2+}$  indicator is within the expected target.

### 3.2.3. Data analysis

For analysis, a region of interest (ROI) is generated around the cilium using the ROI tool, and a duplicate ROI is placed adjacent to the cilium for background measurement. A separate ROI is created for the cell body as well. The ROI can be adjusted at various time points after fluid flow to account for the cilium bending. The fluorescence signal intensity data from the ROI can be subtracted from the background fluorescence and two steps of normalization i) against the mCherry and ii) basal signal intensities applied to the data. EGFP/mCherry images can be generated by taking the ratio of EGFP and mCherry signal intensities and pseudo-colored for viewing (Figure 8).

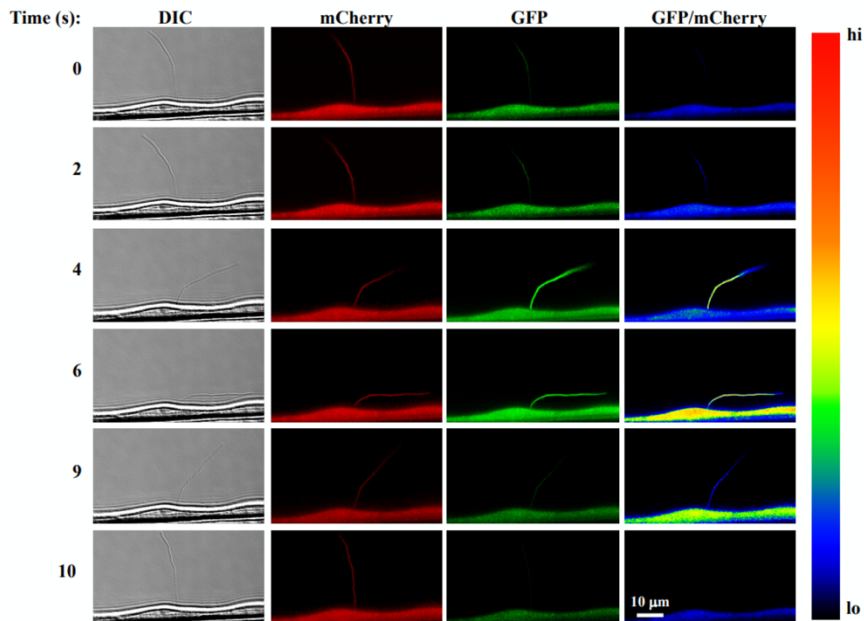


Figure 8. Single-live cell and cilia imaging with 5HT6-mCherry-G-GECO1.0. The images show (from left to right column) DIC used for tracking a cilium, mCherry fluorescent ciliary marker, the  $\text{Ca}^{2+}$  sensitive GECO1.0 and an EGFP/mCherry ratio pseudocolored to show  $\text{Ca}^{2+}$  levels. When fluid flow is applied (time series from top to bottom), the cilium bends inducing a  $\text{Ca}^{2+}$  increase in both the cytoplasm and cilioplasm. Adapted with permission from Pala, R., Mohieldin, A. M., Shamloo, K., Sherpa, R. T., Kathem, S. H., Zhou, J., ... Nauli, S. M. Personalized Nanotherapy by Specifically Targeting Cell Organelles To Improve Vascular Hypertension. *Nano Letters* Copyright 2018 American Chemical Society.



For quantification, this process is done for all time points in the time series file and exported to a suitable format for statistical analysis. Multiple experiments will confirm the response seen during stimulation with fluid flow. There might be cases with movement artifacts or fluorescent aggregates, appearing in the field of view after flow initiation. These might introduce significant deviations, but with the help of mCherry, we can evaluate the  $\text{Ca}^{2+}$ -independent signal deviations and determine the viability of the data.

## Conclusion

A typical experimental result will provide EGFP and mCherry intensities for the cilioplasm and cytoplasm in response to fluid flow over time which can be presented as a time series plot or a comparative bar graph showing  $\text{Ca}^{2+}$  levels. A plot of the EGFP as a function of time will show an expected increase in signal intensity upon addition of fluid flow. Upon cessation of fluid flow, the increase in EGFP returns to baseline. The treatment with ionomycin/EGTA causes a transient increase due to the extracellular  $\text{Ca}^{2+}$  entry from the ionomycin-induced pore formation followed by a slow decline in  $\text{Ca}^{2+}$  signal due to the  $\text{Ca}^{2+}$  chelator EGTA. Subsequent treatment with higher  $\text{Ca}^{2+}$  should increase the signal intensity to a level higher than that observed with fluid flow. The presence of mCherry provides the opportunity to apply ratiometric analysis and elimination of  $\text{Ca}^{2+}$  related artifacts. Moreover, the time-lapse images can be compiled into a movie to observe  $\text{Ca}^{2+}$  increases in the cilioplasm and cytoplasm.

## References

1. Akerboom, J., Chen, T.-W., Wardill, T. J., Tian, L., Marvin, J. S., Mutlu, S., ... Looger, L. L. (2012). Optimization of a GCaMP calcium indicator for neural activity imaging. *The Journal of Neuroscience : The Official Journal of the Society for Neuroscience*, 32(40), 13819–13840. <https://doi.org/10.1523/JNEUROSCI.2601-12.2012>
2. Akerboom, J., Rivera, J. D. V., Guilbe, M. M. R., Malavé, E. C. A., Hernandez, H. H., Tian, L., ... Schreiter, E. R. (2009). Crystal structures of the GCaMP calcium sensor reveal the mechanism of fluorescence signal change and aid rational design. *The Journal of Biological Chemistry*, 284(10), 6455–6464. <https://doi.org/10.1074/jbc.M807657200>
3. Berbari, N. F., Johnson, A. D., Lewis, J. S., Askwith, C. C., & Mykytyn, K. (2008). Identification of Ciliary Localization Sequences within the Third Intracellular Loop of G Protein-coupled Receptors. *Molecular Biology of the Cell*. <https://doi.org/10.1091/mbc.E07-09-0942>
4. Breslow, D. K., Koslover, E. F., Seydel, F., Spakowitz, A. J., & Nachury, M. V. (2013). An in vitro assay for entry into cilia reveals unique properties of the soluble diffusion barrier. *The Journal of Cell Biology*, 203(1), 129–147. <https://doi.org/10.1083/jcb.201212024>
5. Brini, M., Pasti, L., Bastianutto, C., Murgia, M., Pozzan, T., & Rizzuto, R. (1994). Targeting of aequorin for calcium monitoring in intracellular compartments. *Journal of Bioluminescence and Chemiluminescence*, 9(3), 177–184. <https://doi.org/10.1002/bio.1170090312>
6. Brown, D. C., & Larson, R. S. (2001). Improvements to parallel plate flow chambers to reduce reagent and cellular requirements. *BMC Immunology*. <https://doi.org/10.1186/1471-2172-2-9>
7. Chen, T.-W., Wardill, T. J., Sun, Y., Pulver, S. R., Renninger, S. L., Baohan, A., ... Kim, D. S. (2013). Ultrasensitive fluorescent proteins for imaging neuronal activity. *Nature*, 499(7458), 295–300. <https://doi.org/10.1038/nature12354>
8. Christensen, S. T., Clement, C. A., Satir, P., & Pedersen, L. B. (2012). Primary cilia and coordination of receptor tyrosine kinase (RTK) signalling. *The Journal of Pathology*, 226(2), 172–184. <https://doi.org/10.1002/path.3004>
9. Cobbold, P. H., & Rink, T. J. (1987). Fluorescence and bioluminescence measurement of cytoplasmic free calcium. *The Biochemical Journal*, 248(2), 313–328. Retrieved from <http://www.ncbi.nlm.nih.gov/pubmed/3325037>
10. DeCaen, P. G., Dellinger, M., Vien, T. N., & Clapham, D. E. (2013). Direct recording and molecular identification of the calcium channel of primary cilia. *Nature*, 504(7479), 315–318. <https://doi.org/10.1038/nature12832>
11. Delmas, P., Nomura, H., Li, X., Lakkis, M., Luo, Y., Segal, Y., ... Zhou, J. (2002). Constitutive activation of G-proteins by polycystin-1 is antagonized by polycystin-2. *Journal of Biological Chemistry*. <https://doi.org/10.1074/jbc.M110483200>
12. Delous, M., Baala, L., Salomon, R., Laclef, C., Vierkotten, J., Tory, K., ... Saunier, S. (2007). The ciliary gene RPGRIP1L is mutated in cerebello-oculo-renal syndrome (Joubert syndrome type B) and Meckel syndrome. *Nature Genetics*, 39(7), 875–881. <https://doi.org/10.1038/ng2039>
13. Ebashi, S., & Endo, M. (1968). Calcium ion and muscle contraction. *Progress in Biophysics and Molecular Biology*, 18, 123–183. Retrieved from <http://www.ncbi.nlm.nih.gov/pubmed/4894870>
14. Falcone, J. C., Kuo, L., & Meininger, G. A. (1993). Endothelial cell calcium increases during flow-induced dilation in isolated arterioles. *The American Journal of Physiology*, 264(2 Pt 2), H653-9. <https://doi.org/10.1152/ajpheart.1993.264.2.H653>
15. Filippin, L., Abad, M. C., Gastaldello, S., Magalhães, P. J., Sandonà, D., & Pozzan, T. (2005). Improved strategies for the delivery of GFP-based Ca<sup>2+</sup> sensors into the mitochondrial matrix. *Cell Calcium*, 37(2), 129–136. <https://doi.org/10.1016/j.ceca.2004.08.002>
16. Fliegau, M., Horvath, J., von Schnakenburg, C., Olbrich, H., Müller, D., Thumfart, J., ... Omran, H. (2006). Nephrocystin Specifically Localizes to the Transition Zone of Renal and Respiratory Cilia and Photoreceptor Connecting Cilia. *Journal of the American Society of Nephrology*, 17(9),

- 2424–2433. <https://doi.org/10.1681/ASN.2005121351>
17. Follit, J. A., Li, L., Vucica, Y., & Pazour, G. J. (2010). The cytoplasmic tail of fibrocystin contains a ciliary targeting sequence. *The Journal of Cell Biology*, *188*(1), 21–28. <https://doi.org/10.1083/jcb.200910096>
  18. Forder, J., Scriabine, A., & Rasmussen, H. (1985). Plasma membrane calcium flux, protein kinase C activation and smooth muscle contraction. *The Journal of Pharmacology and Experimental Therapeutics*, *235*(2), 267–273. Retrieved from <http://www.ncbi.nlm.nih.gov/pubmed/2414429>
  19. Gilula, N. B., & Satir, P. (1972). The ciliary necklace. A ciliary membrane specialization. *The Journal of Cell Biology*, *53*(2), 494–509. Retrieved from <http://www.pubmedcentral.nih.gov/articlerender.fcgi?artid=2108734&tool=pmcentrez&rendertype=abstract>
  20. Griesbeck, O., Baird, G. S., Campbell, R. E., Zacharias, D. A., & Tsien, R. Y. (2001). Reducing the environmental sensitivity of yellow fluorescent protein. Mechanism and applications. *Journal of Biological Chemistry*. <https://doi.org/10.1074/jbc.M102815200>
  21. Hanaoka, K., Qian, F., Boletta, A., Bhunia, A. K., Piontek, K., Tsiokas, L., ... Germino, G. G. (2000). Co-assembly of polycystin-1 and -2 produces unique cation-permeable currents. *Nature*, *408*(6815), 990–994. <https://doi.org/10.1038/35050128>
  22. Haycraft, C. J., Banizs, B., Aydin-Son, Y., Zhang, Q., Michaud, E. J., & Yoder, B. K. (2005). Gli2 and Gli3 localize to cilia and require the intraflagellar transport protein polaris for processing and function. *PLoS Genetics*, *1*(4), e53. <https://doi.org/10.1371/journal.pgen.0010053>
  23. Hu, Q., Milenkovic, L., Jin, H., Scott, M. P., Nachury, M. V., Spiliotis, E. T., & Nelson, W. J. (2010). A septin diffusion barrier at the base of the primary cilium maintains ciliary membrane protein distribution. *Science*. <https://doi.org/10.1126/science.1191054>
  24. Huang, P., & Schier, A. F. (2009). Dampened Hedgehog signaling but normal Wnt signaling in zebrafish without cilia. *Development*, *136*(18), 3089–3098. <https://doi.org/10.1242/dev.041343>
  25. Ishikawa, H., Thompson, J., Yates, J. R., Marshall, W. F., & Marshall, W. F. (2012). Proteomic analysis of mammalian primary cilia. *Current Biology : CB*, *22*(5), 414–419. <https://doi.org/10.1016/j.cub.2012.01.031>
  26. Jin, X., Mohieldin, A. M., Muntean, B. S., Green, J. A., Shah, J. V., Mykytyn, K., & Nauli, S. M. (2014). Cilioplasm is a cellular compartment for calcium signaling in response to mechanical and chemical stimuli. *Cellular and Molecular Life Sciences : CMLS*, *71*(11), 2165–2178. <https://doi.org/10.1007/s00018-013-1483-1>
  27. Johns, A., Lategan, T. W., Lodge, N. J., Ryan, U. S., Van Breemen, C., & Adams, D. J. (1987). Calcium entry through receptor-operated channels in bovine pulmonary artery endothelial cells. *Tissue and Cell*, *19*(6), 733–745. [https://doi.org/10.1016/0040-8166\(87\)90015-2](https://doi.org/10.1016/0040-8166(87)90015-2)
  28. Kathem, S. H., Mohieldin, A. M., Abdul-Majeed, S., Ismail, S. H., Altaei, Q. H., Alshimmari, I. K., ... Nauli, S. M. (2014). Ciliotherapy: a novel intervention in polycystic kidney disease. *Journal of Geriatric Cardiology : JGC*, *11*(1), 63–73. <https://doi.org/10.3969/j.issn.1671-5411.2014.01.001>
  29. Kerr, R., Lev-Ram, V., Baird, G., Vincent, P., Tsien, R. Y., & Schafer, W. R. (2000). Optical imaging of calcium transients in neurons and pharyngeal muscle of *C. elegans*. *Neuron*. [https://doi.org/10.1016/S0896-6273\(00\)81196-4](https://doi.org/10.1016/S0896-6273(00)81196-4)
  30. Lee, K. L., Guevarra, M. D., Nguyen, A. M., Chua, M. C., Wang, Y., & Jacobs, C. R. (2015). The primary cilium functions as a mechanical and calcium signaling nexus. *Cilia*, *4*, 7. <https://doi.org/10.1186/s13630-015-0016-y>
  31. Liem, K. F., Ashe, A., He, M., Satir, P., Moran, J., Beier, D., ... Anderson, K. V. (2012). The IFT-A complex regulates Shh signaling through cilia structure and membrane protein trafficking. *The Journal of Cell Biology*, *197*(6), 789–800. <https://doi.org/10.1083/jcb.201110049>
  32. Malone, A. M. D., Anderson, C. T., Tummala, P., Kwon, R. Y., Johnston, T. R., Stearns, T., & Jacobs, C. R. (2007). Primary cilia mediate mechanosensing in bone cells by a calcium-independent mechanism. *Proceedings of the National Academy of Sciences of the United States of*

- America*, 104(33), 13325–13330. <https://doi.org/10.1073/pnas.0700636104>
33. Mank, M., Santos, A. F., Dierenberger, S., Mrcic-Flogel, T. D., Hofer, S. B., Stein, V., ... Griesbeck, O. (2008). A genetically encoded calcium indicator for chronic in vivo two-photon imaging. *Nature Methods*. <https://doi.org/10.1038/nmeth.1243>
  34. Masyuk, A. I., Masyuk, T. V., Splinter, P. L., Huang, B. Q., Stroope, A. J., & LaRusso, N. F. (2006). Cholangiocyte cilia detect changes in luminal fluid flow and transmit them into intracellular Ca<sup>2+</sup> and cAMP signaling. *Gastroenterology*, 131(3), 911–920. <https://doi.org/10.1053/j.gastro.2006.07.003>
  35. Miyawaki, A., Llopis, J., Heim, R., Michael McCaffery, J., Adams, J. A., Ikura, M., & Tsien, R. Y. (1997). Fluorescent indicators for Ca<sup>2+</sup> based on green fluorescent proteins and calmodulin. *Nature*. <https://doi.org/10.1038/42264>
  36. Mollet, G., Silbermann, F., Delous, M., Salomon, R., Antignac, C., & Saunier, S. (2005). Characterization of the nephrocystin/nephrocystin-4 complex and subcellular localization of nephrocystin-4 to primary cilia and centrosomes. *Human Molecular Genetics*, 14(5), 645–656. <https://doi.org/10.1093/hmg/ddi061>
  37. Mukhopadhyay, S., Wen, X., Chih, B., Nelson, C. D., Lane, W. S., Scales, S. J., & Jackson, P. K. (2010). TULP3 bridges the IFT-A complex and membrane phosphoinositides to promote trafficking of G protein-coupled receptors into primary cilia. *Genes & Development*, 24(19), 2180–2193. <https://doi.org/10.1101/gad.1966210>
  38. Nagai, T., Sawano, A., Park, E. S., & Miyawaki, A. (2001). Circularly permuted green fluorescent proteins engineered to sense Ca<sup>2+</sup>. *Proceedings of the National Academy of Sciences*. <https://doi.org/10.1073/pnas.051636098>
  39. Nagai, T., Yamada, S., Tominaga, T., Ichikawa, M., & Miyawaki, A. (2004). Expanded dynamic range of fluorescent indicators for Ca<sup>2+</sup> by circularly permuted yellow fluorescent proteins. *Proceedings of the National Academy of Sciences*. <https://doi.org/10.1073/pnas.0400417101>
  40. Nakai, J., Ohkura, M., & Imoto, K. (2001). A high signal-to-noise Ca<sup>2+</sup> probe composed of a single green fluorescent protein. *Nature Biotechnology*, 19(2), 137–141. <https://doi.org/10.1038/84397>
  41. Nauli, S. M., Alenghat, F. J., Luo, Y., Williams, E., Vassilev, P., Li, X., ... Zhou, J. (2003). Polycystins 1 and 2 mediate mechanosensation in the primary cilium of kidney cells. *Nature Genetics*, 33(2), 129–137. <https://doi.org/10.1038/ng1076>
  42. Nauli, S. M., Jin, X., AbouAlaiwi, W. A., El-Jouni, W., Su, X., & Zhou, J. (2013). Non-Motile Primary Cilia as Fluid Shear Stress Mechanosensors. In *Methods in enzymology* (Vol. 525, pp. 1–20). <https://doi.org/10.1016/B978-0-12-397944-5.00001-8>
  43. Nauli, S. M., Kawanabe, Y., Kaminski, J. J., Pearce, W. J., Ingber, D. E., & Zhou, J. (2008). Endothelial Cilia Are Fluid Shear Sensors That Regulate Calcium Signaling and Nitric Oxide Production Through Polycystin-1. *Circulation*, 117(9), 1161–1171. <https://doi.org/10.1161/CIRCULATIONAHA.107.710111>
  44. Nauli, S. M., Pala, R., & Kleene, S. J. (2016). Calcium channels in primary cilia. *Current Opinion in Nephrology and Hypertension*, 25(5), 452–458. <https://doi.org/10.1097/MNH.0000000000000251>
  45. Nauli, S. M., Sherpa, R. T., Reese, C. J., & Nauli, A. M. (2016). Mechanosensory and Chemosensory Primary Cilia in Ciliopathy and Ciliotherapy. In *Mechanobiology* (pp. 75–99). Hoboken, NJ, USA: John Wiley & Sons, Inc. <https://doi.org/10.1002/9781118966174.ch5>
  46. Otto, E. A., Loeys, B., Khanna, H., Hellems, J., Sudbrak, R., Fan, S., ... Hildebrandt, F. (2005). Nephrocystin-5, a ciliary IQ domain protein, is mutated in Senior-Loken syndrome and interacts with RPGR and calmodulin. *Nature Genetics*, 37(3), 282–288. <https://doi.org/10.1038/ng1520>
  47. Otto, E. A., Schermer, B., Obara, T., O'Toole, J. F., Hiller, K. S., Mueller, A. M., ... Hildebrandt, F. (2003). Mutations in INVS encoding inversin cause nephronophthisis type 2, linking renal cystic disease to the function of primary cilia and left-right axis determination. *Nature Genetics*,

- 34(4), 413–420. <https://doi.org/10.1038/ng1217>
48. Pala, R., Mohieldin, A. M., Shamloo, K., Sherpa, R. T., Kathem, S. H., Zhou, J., ... Nauli, S. M. (2018). Personalized Nanotherapy by Specifically Targeting Cell Organelles To Improve Vascular Hypertension. *Nano Letters*, *acs.nanolett.8b04138*. <https://doi.org/10.1021/acs.nanolett.8b04138>
  49. Palmer, A. E., Giacomello, M., Kortemme, T., Hires, S. A., Lev-Ram, V., Baker, D., & Tsien, R. Y. (2006). Ca<sup>2+</sup> Indicators Based on Computationally Redesigned Calmodulin-Peptide Pairs. *Chemistry and Biology*. <https://doi.org/10.1016/j.chembiol.2006.03.007>
  50. Palmer, A. E., Jin, C., Reed, J. C., & Tsien, R. Y. (2004). Bcl-2-mediated alterations in endoplasmic reticulum Ca<sup>2+</sup> analyzed with an improved genetically encoded fluorescent sensor. *Proceedings of the National Academy of Sciences*. <https://doi.org/10.1073/pnas.0408030101>
  51. Pazour, G. J., Agrin, N., Leszyk, J., & Witman, G. B. (2005). Proteomic analysis of a eukaryotic cilium. *The Journal of Cell Biology*, *170*(1), 103–113. <https://doi.org/10.1083/jcb.200504008>
  52. Pazour, G. J., Dickert, B. L., & Witman, G. B. (1999). The DHC1b (DHC2) isoform of cytoplasmic dynein is required for flagellar assembly. *The Journal of Cell Biology*, *144*(3), 473–481. Retrieved from <http://www.ncbi.nlm.nih.gov/pubmed/9971742>
  53. Pérez Koldenkova, V., & Nagai, T. (2013). Genetically encoded Ca<sup>2+</sup> indicators: Properties and evaluation. *Biochimica et Biophysica Acta - Molecular Cell Research*. <https://doi.org/10.1016/j.bbamcr.2013.01.011>
  54. Praetorius, H. A., & Spring, K. R. (2001). Bending the MDCK cell primary cilium increases intracellular calcium. *The Journal of Membrane Biology*, *184*(1), 71–79. <https://doi.org/10.1007/s00232-001-0075-4>
  55. Praetorius, H. A., & Spring, K. R. (2003). Removal of the MDCK Cell Primary Cilium Abolishes Flow Sensing. *Journal of Membrane Biology*, *191*(1), 69–76. <https://doi.org/10.1007/s00232-002-1042-4>
  56. Romoser, V. A., Hinkle, P. M., & Persechini, A. (1997). Detection in living cells of Ca<sup>2+</sup>-dependent changes in the fluorescence emission of an indicator composed of two green fluorescent protein variants linked by a calmodulin-binding sequence. A new class of fluorescent indicators. *The Journal of Biological Chemistry*, *272*(20), 13270–13274. Retrieved from <http://www.ncbi.nlm.nih.gov/pubmed/9148946>
  57. Rudolf, R., Mongillo, M., Rizzuto, R., & Pozzan, T. (2003). Looking forward to seeing calcium. *Nature Reviews Molecular Cell Biology*, *4*(7), 579–586. <https://doi.org/10.1038/nrml153>
  58. Sabatini, B. L., Oertner, T. G., & Svoboda, K. (2002). The life cycle of Ca<sup>2+</sup> ions in dendritic spines. *Neuron*. [https://doi.org/10.1016/S0896-6273\(02\)00573-1](https://doi.org/10.1016/S0896-6273(02)00573-1)
  59. Satir, P. (2017). CILIA: before and after. *Cilia*, *6*(1), 1. <https://doi.org/10.1186/s13630-017-0046-8>
  60. Schou, K. B., Pedersen, L. B., & Christensen, S. T. (2015). Ins and outs of GPCR signaling in primary cilia. *EMBO Reports*, *16*(9), 1099–1113. <https://doi.org/10.15252/embr.201540530>
  61. Singla, V., & Reiter, J. F. (2006). The primary cilium as the cell's antenna: signaling at a sensory organelle. *Science (New York, N.Y.)*, *313*(5787), 629–633. <https://doi.org/10.1126/science.1124534>
  62. Sorokin, S. (1962). Centrioles and the formation of rudimentary cilia by fibroblasts and smooth muscle cells. *The Journal of Cell Biology*, *15*(2), 363–377. <https://doi.org/10.1083/jcb.15.2.363>
  63. Sorokin, S. P. (1968). Reconstructions of centriole formation and ciliogenesis in mammalian lungs. *Journal of Cell Science*, *3*(2), 207–230. Retrieved from <http://www.ncbi.nlm.nih.gov/pubmed/5661997>
  64. Souslova, E. A., Belousov, V. V., Lock, J. G., Strömblad, S., Kasparov, S., Bolshakov, A. P., ... Chudakov, D. M. (2007). Single fluorescent protein-based Ca<sup>2+</sup> sensors with increased dynamic range. *BMC Biotechnology*, *7*(1), 37. <https://doi.org/10.1186/1472-6750-7-37>
  65. Su, S., Phua, S. C., Derosé, R., Chiba, S., Narita, K., Kalugin, P. N., ... Inoue, T. (2013). Genetically encoded calcium indicator illuminates calcium dynamics in primary cilia. *Nature*



- Methods*. <https://doi.org/10.1038/nmeth.2647>
66. Tian, L., Hires, S. A., Mao, T., Huber, D., Chiappe, M. E., Chalasani, S. H., ... Looger, L. L. (2009). Imaging neural activity in worms, flies and mice with improved GCaMP calcium indicators. *Nature Methods*, 6(12), 875–881. <https://doi.org/10.1038/nmeth.1398>
  67. Valente, E. M., Logan, C. V., Mougou-Zerelli, S., Lee, J. H., Silhavy, J. L., Brancati, F., ... Gleeson, J. G. (2010). Mutations in TMEM216 perturb ciliogenesis and cause Joubert, Meckel and related syndromes. *Nature Genetics*, 42(7), 619–625. <https://doi.org/10.1038/ng.594>
  68. Wier, W., Cannell, M., Berlin, M., Marban, E., & Lederer, W. (1987). Cellular and subcellular heterogeneity of  $[Ca^{2+}]_i$  in single heart cells revealed by fura-2. *Science*, 235(4786), 325–328. <https://doi.org/10.1126/science.3798114>
  69. Williams, C. L., Masyukova, S. V., & Yoder, B. K. (2010). Normal Ciliogenesis Requires Synergy between the Cystic Kidney Disease Genes MKS-3 and NPHP-4. *Journal of the American Society of Nephrology*, 21(5), 782–793. <https://doi.org/10.1681/ASN.2009060597>
  70. Williams, C. L., Winkelbauer, M. E., Schafer, J. C., Michaud, E. J., & Yoder, B. K. (2008). Functional Redundancy of the B9 Proteins and Nephrocystins in *Caenorhabditis elegans* Ciliogenesis. *Molecular Biology of the Cell*, 19(5), 2154–2168. <https://doi.org/10.1091/mbc.e07-10-1070>
  71. Williams, D. A., Fogarty, K. E., Tsien, R. Y., & Fay, F. S. (1985). Calcium gradients in single smooth muscle cells revealed by the digital imaging microscope using Fura-2. *Nature*, 318(6046), 558–561. <https://doi.org/10.1038/318558a0>
  72. Xu, C., Rossetti, S., Jiang, L., Harris, P. C., Brown-Glaberman, U., Wandinger-Ness, A., ... Alper, S. L. (2006). Human ADPKD primary cyst epithelial cells with a novel, single codon deletion in the PKD1 gene exhibit defective ciliary polycystin localization and loss of flow-induced  $Ca^{2+}$  signaling. *AJP: Renal Physiology*, 292(3), F930–F945. <https://doi.org/10.1155/2013/715848>
  73. Yuan, S., Zhao, L., Brueckner, M., & Sun, Z. (2015). Intraciliary Calcium Oscillations Initiate Vertebrate Left-Right Asymmetry. *Current Biology*, 25(5), 556–567. <https://doi.org/10.1016/j.cub.2014.12.051>
  74. Zhao, Y., Araki, S., Wu, J., Teramoto, T., Chang, Y. F., Nakano, M., ... Campbell, R. E. (2011). An expanded palette of genetically encoded  $Ca^{2+}$  indicators. *Science*. <https://doi.org/10.1126/science.1208592>

## Chapter 4. The Role of the Primary Cilium in Sensing Extracellular pH.\*

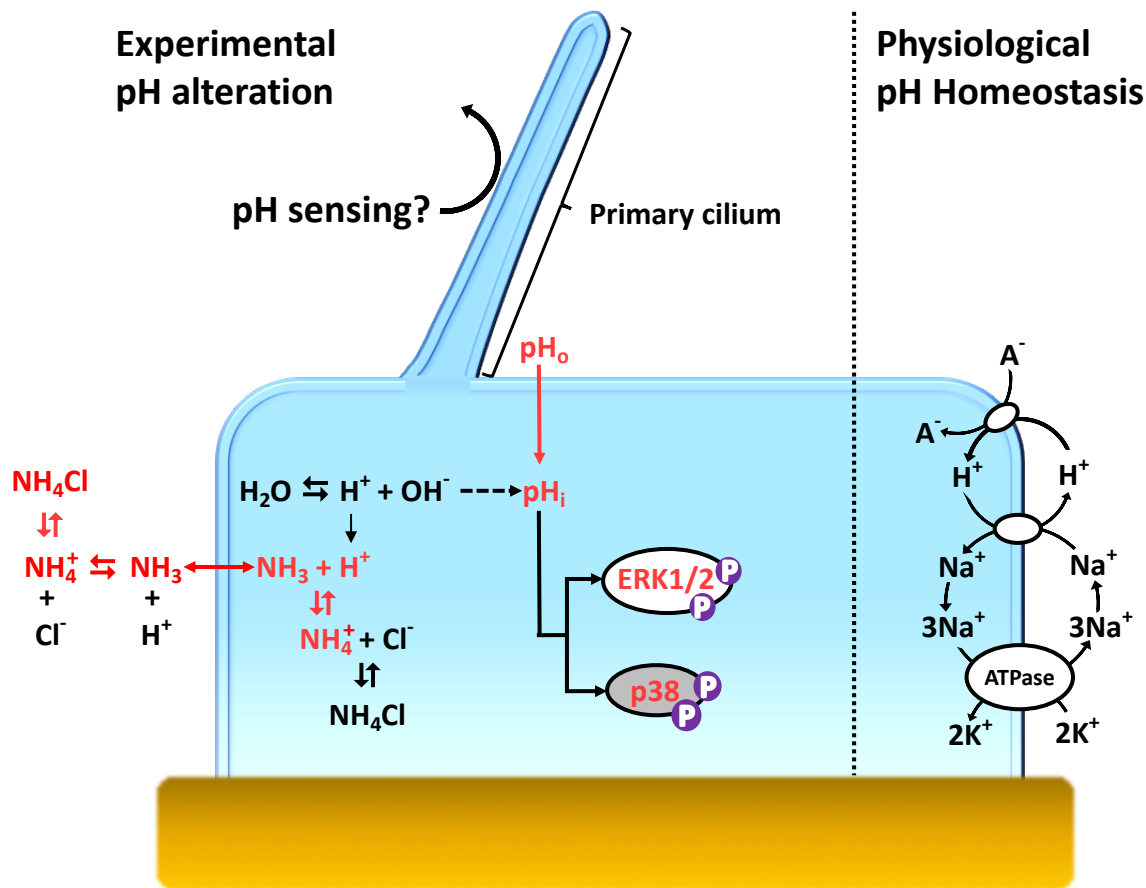
### Abstract

Biosensors on the membrane of the vascular endothelium are responsible for sensing mechanical and chemical signals in the blood. Transduction of these stimuli into intracellular signaling cascades regulate cellular processes including ion transport, gene expression, cell proliferation, and/or cell death. The primary cilium is a well-known biosensor of shear stress but its role in sensing extracellular pH change has never been examined. As a cellular extension into the immediate microenvironment, the cilium could be a prospective sensor for changes in pH and regulator of acid response in cells. We aim to test our hypothesis that the primary cilium plays the role of an acid sensor in cells using vascular endothelial and embryonic fibroblast cells as in vitro models. We measure changes in cellular pH using pH-sensitive 2',7'-biscarboxyethyl-5,6-carboxyfluorescein acetoxymethyl ester (BCECF) fluorescence and mitogen-activated protein kinase (MAPK) activity to quantify responses to both extracellular pH ( $\text{pH}_o$ ) and intracellular pH ( $\text{pH}_i$ ) changes. Our studies show that changes in  $\text{pH}_o$  affect  $\text{pH}_i$  in both wild-type and cilia-less *Tg737* cells and that the kinetics of the  $\text{pH}_i$  response are similar in both cells. Acidic  $\text{pH}_o$  or  $\text{pH}_i$  was observed to change the length of primary cilia in wild-type cells while the cilia in *Tg737* remained absent. Vascular endothelial cells respond to acidic pH through activation of ERK1/2 and p38-mediated signaling pathways. The cilia-less *Tg737* cells exhibit delayed responsiveness to  $\text{pH}_o$  dependent and independent  $\text{pH}_i$  acidification as depicted in the phosphorylation profile of ERK1/2 and p38. Otherwise, intracellular pH homeostatic response to acidic  $\text{pH}_o$  is similar between wild-type and *Tg737* cells, indicating that the primary cilia may not be the sole sensor for physiological pH changes. These endothelial cells respond to pH changes with a predominantly  $\text{K}^+$ -dependent  $\text{pH}_i$  recovery mechanism, regardless of ciliary presence or absence.

---

\* Atkinson KF, Sherpa RT, Nauli SM. The Role of the Primary Cilium in Sensing Extracellular pH. *Cells*. 2019 Jul 11;8(7):704. doi: 10.3390/cells8070704.

Figure 9. We adopt two ways to alter intracellular pH ( $pH_i$ ); (1) Extracellular pH mediated  $pH_i$  change and (2) ammonium pre-pulse mediated  $pH_i$  change. These methods will be used to test our hypothesis that the primary cilium acts as a pH sensor. The ammonium pre-pulse acidification technique selectively lowers intracellular pH. Addition of ammonium chloride ( $NH_4Cl$ ) to the media produces ammonia ( $NH_3$ ) and  $H^+$ . There is an influx of  $NH_3$  into the cytoplasm which combines with intracellular  $H^+$ , resulting in  $pH_i$  alkalization. Removal of external  $NH_4Cl$  causes an efflux of intracellular  $NH_3$ , leaving  $H^+$  ions behind in the cytoplasm and causing  $pH_i$  acidification. Typical homeostatic  $pH_i$  recovery involves acid extrusion mechanisms, including anion/ $H^+$  symporters and  $Na^+/H^+$  exchanger which is coupled with  $Na^+/K^+$ -ATPase. Changes to  $pH_i$  are also observed through activation of mitogen-activated protein kinases, such as extracellular signal-related kinase (ERK1/2) and p38.



## 1. Introduction

The normal blood pH level is tightly maintained between 7.35 and 7.45 by the renal and respiratory systems along with buffering mediators in the blood. Lowering of blood  $pH < 7.35$  or acidosis causes several symptoms such as drowsiness, exhaustion, and arrhythmia depending on the type of acidosis. More dramatic changes in pH will induce cytotoxicity and neuronal cell



death. The vascular endothelium, which also regulates physical dynamics of blood such as local blood flow and pressure, is best suited to measure local circulating blood pH. Any pH sensor in the body needs to be responsive to extracellular pH fluctuations and regulate downstream mechanisms for homeostatic adaptation. Such adaptation mechanisms include local activation of ion transporters and modulation of channel activity to balance the intracellular ionic gradient, while global regulation is achieved by adjusting the ventilation or renal excretion.

Several studies have shown that mitogen-activated protein kinases (MAPKs) are activated by changes in pH [1,2]. The three known MAPKs, extracellular signal-regulated kinase (ERK1/2 aka p32/p44), p38, and JNK1/2, respond to a variety of environmental stimuli to mediate gene expression, ion transport, cell proliferation, and/or apoptosis [3]. ERK1/2 phosphorylation regulates acid-stimulated vacuolar H<sup>+</sup>-ATPase and Na<sup>+</sup>/H<sup>+</sup> exchanger (NHE) activation [1,4]. When intracellular pH becomes acidic, ERK1/2 activation acts in parallel with Pyk2 kinase to increase NHE3 activity [5,6]. The MAPK, p38 is activated by various extracellular stress stimuli such as UV light, heat, inflammatory cytokines, and pH changes. Depending on the initial stimuli, substrates of activated p38 include transcription factors and the MAP kinase-activated protein kinase 2 (MK2). MK2 subsequently activates various small heat shock protein 27 (HSP27), lymphocyte-specific protein 1 (LSP1), cAMP response element-binding protein (CREB) among others [7,8].

In the present study, we explore if the primary cilia, distinct from motile cilia in the brain ventricles or Hensen's node, have a role in acid pH sensation in endothelial cells. Our interest arises from the fact that the primary cilium, a solitary extension of the cell, has been implicated in the sensation of mechanical forces and chemical cues [9–12]. With the localization of various ion channels, G protein-coupled receptors and receptor-cytoskeletal proteins in the ciliary membrane, the primary cilium is a candidate biosensor that responds to a variety of stimuli [13]. Numerous studies have shown that cilia regulate cytosolic calcium influx and intracellular calcium release upon application of shear stress [12,14–16]. The response to blood flow-induced shear stress is very important in the regulation of blood pressure, vascular tone, and vasodilation [13]. As a cellular structure that protrudes out to the vascular lumen and remains in contact with the extracellular milieu, the cilia are poised to be a sensory extension. A recent study on

Zebrafish showed localization of acid-sensing ion channels (ASICs), which are proton-gated cation channels, in the cilia of the non-sensory olfactory cell [17]. ASICs are Na<sup>+</sup> channels activated by external protons and exhibit a rapid response to reduction in extracellular pH (pH<sub>o</sub>) below pH 6.9 [18]. Another Na<sup>+</sup> channel, the alpha-epithelial sodium channel, has been immunodetected in the cilia and are regulated by flow as well as acidic pH<sub>o</sub> through Na<sup>+</sup> gating phenomenon of self-inhibition [19–21].

A study by Banizs et al. on cilia-less *Tg737* mice shows that *Tg737* mice have lower intrinsic buffering power when challenged with a weak acid NH<sub>4</sub><sup>+</sup> compared to wild-type mice [22]. This indicates that primary cilia might be involved in either sensing pH<sub>o</sub> change or regulating intracellular pH (pH<sub>i</sub>) in response to pH<sub>o</sub> changes through ciliary ion transport activity. With the evidence that pH sensitive channels are selectively localized in the cilia of the non-sensory olfactory epithelium [17] and the cilium is known as a sensory organelle of the extracellular milieu [9,12,23,24], we hypothesize that primary cilia could function as pH sensors. We, therefore, examine the role of the primary cilia in acid-activation of MAPK signaling pathways in endothelial cells. We compare the acid response of cilia-less *Tg737* endothelial cells to their wild-type counterparts to examine a possible pH sensing role of the primary cilia.

## 2. Materials and Methods

### 2.1. Cell Culture

Previously isolated and characterized vascular endothelial cells (*Tg737*<sup>+/+</sup> and *Tg737*<sup>-/-</sup>) were used for the study [23,25]. These cell lines were generated from the same littermates of *Tg737*<sup>+/-</sup> mice with Balb/C background. The *Tg737* gene encodes for polaris, a structural protein for cilia [26]. These endothelial cells were also immortalized from mice carrying the simian virus-40 (SV40) gene. The promoter of SV40 is regulated by temperature and IFN- $\gamma$ . As such, cells were grown under permissive conditions in the presence of 0.75  $\mu$ g/L IFN- $\gamma$  at 33 °C express SV40 large T antigen regardless of the status of their confluence. The permissive conditions allow cells to hyper-proliferate. When switched to non-permissive conditions in the absence of IFN- $\gamma$  at 37 °C, the endothelial cells completely shut down the *SV40* gene. Cells under the non-permissive conditions are readily differentiated [23,25].

These cells express common markers for endothelial cells, including eNOS, ICAM-2 (CD102), PECAM-1 (CD31), VE-cadherin (CD144), readily responding to acetylcholine, forming endothelial barrier integrity and having functional intracellular calcium signaling, focal adhesion kinase, calmodulin, Akt/PKB, protein kinase C and eNOS activity [23,25,27]. Aside from abnormal mechanosensory function due to lacking primary cilia, the *Tg737* cilia-less cells also have abnormal cell division [28,29]. Three days prior to experiments, cells were cultured under sterile conditions and maintained at 37 °C in a 5% CO<sub>2</sub> incubator. Cells were kept in Dulbecco's Modification of Eagle's Medium (DMEM), media with 4.5 g/L glucose, L-glutamate, and sodium pyruvate (Corning Cellgro) containing 2% fetal bovine serum (FBS) and 5% penicillin/streptomycin. DMEM with 2% FBS is a low serum condition that promotes ciliation [30]. For NIH3T3 fibroblast cells, growth media consisting of 10% bovine calf serum (BCS) and 5% penicillin/streptomycin in DMEM was used. Cells were grown on poly-L-lysine coated cover glass and incubated with low serum media (2% BCS, 5% penicillin/streptomycin and DMEM) to promote ciliation. To investigate Hedgehog (Hh) signaling in various pH<sub>o</sub>, purmorphamine (Sigma-Aldrich, St. Louis, MO, USA) at a final concentration of 10 μM was used as a positive control. Purmorphamine was added and incubated for 1 h with the cells to induce Hh activation.

## 2.2. Decreased Extracellular pH (pH<sub>o</sub>)

Physiological saline solution (PSS; Table 1) was adjusted to pH<sub>o</sub> 5.5, 6.0, 6.5, and 7.0 from pH 7.4 (control) using 100 mM HCl. For immunoblot, each 35-mm dish was exposed to media of a given pH for 10 min. Control cells underwent similar treatment with vehicle. Cells were trypsinized and 10<sup>6</sup> cells transferred into 100 μL 2× Laemelli Sample Buffer (BioRad, Hercules, CA, USA) containing β-mercaptoethanol. Samples were sonicated and heated at 100 °C for 5 min. For tracings of pH<sub>i</sub> measurement, BCECF-AM-loaded cells were exposed to media of each pH<sub>o</sub>, one at a time for 10 min, sequentially from pH<sub>o</sub> 7.4 to 5.5. In all our experiments, we maintained our solution osmolality between 290–300 mOsm/L.

## 2.3. Decreased Intracellular pH (pH<sub>i</sub>)

The NH<sub>4</sub>Cl pulse was used to alter pH<sub>i</sub> using a series of solutions, as previously described [1] and shown in Table 1. All solutions were adjusted to pH<sub>o</sub> 7.4 and maintained at 37 °C with osmolality between 290–300 mOsm/L. PSS was added to the cells for 5 min, then aspirated. The

NH<sub>4</sub>Cl solution (20 mM NH<sub>4</sub>Cl) was then added to cells until intracellular pH stabilized, then aspirated. The cells were immediately incubated in 0K<sup>+</sup>/0Na<sup>+</sup> solution, causing dissociation of intracellular NH<sub>4</sub>, releasing protons into the cytosol, thus decreasing pH<sub>i</sub>. pH<sub>i</sub> recovery was accomplished by adding 5K<sup>+</sup>/0Na<sup>+</sup> solution (5 mM KCl) to the cells and incubation in PSS.

Table 5. Composition of solutions used in the NH<sub>4</sub>Cl pre-pulse. Solution names are listed along the first row, and the composition of each is shown in each column. Components of each solution are in mM. HEPES = (4-(2-hydroxyethyl)-1-piperazineethanesulfonic acid); NMDG = N-methyl-D-glucamine.

Solution	PSS	NH <sub>4</sub> Cl	0K <sup>+</sup> /0Na <sup>+</sup>	5K <sup>+</sup> /0Na <sup>+</sup>
CaCl <sub>2</sub>	1.8	1.8	1.8	1.8
MgSO <sub>4</sub>	0.8	0.8	0.8	0.8
Glucose	5.5	5.5	5.5	5.5
HEPES	10	10	10	10
NaCl	135	0	0	0
KCl	5	0	0	5
NH <sub>4</sub> Cl	0	20	0	0
NMDG	0	120	140	135

#### 2.4. Intracellular pH Measurement

Intracellular pH was measured with 2',7'-biscarboxyethyl-5,6-carboxyfluorescein acetoxymethylester (BCECF-AM; Molecular Probes, #B1150, Invitrogen, Eugene, OR, USA). Wild-type and *Tg737* cells were incubated with 5 μM BCECF-AM for 15 min at 37 °C. Images were acquired with a Nikon Eclipse Ti-E inverted microscope using 40× objective and NIS-Elements imaging software (version 4.30, Melville, NY, USA, 2016). Intracellular pH measurements were recorded with emission intensity at wavelength 535 nm. The ratio of emission intensity was determined through excitation wavelengths of pH-dependent 490 nm and an isosbestic point 440 nm. BCECF fluorescence ratio intensity was calibrated to represent intracellular pH using H<sup>+</sup> ionophore nigericin-containing solutions (Sigma-Aldrich, #N7143). This calibration was performed at the end of each experiment. 20 μM nigericin was used to equilibrate pH<sub>o</sub> and pH<sub>i</sub> to pH values of 5.5, 6.0, 6.5, 7.0 and 7.4. Once the 490/440 ratio for each calibration pH value was obtained, the ratio values were fitted to a sigmoidal plot. Subsequent experimental ratios were converted to the pH values.

## 2.5. Immunoblot

All extracellular and intracellular pH manipulations were performed in the same manner for both pH measurement and Western blot analysis. 35 mm dishes were each lysed at different steps of decreased pH<sub>o</sub> or pH<sub>i</sub> with NH<sub>4</sub>Cl pre-pulse. Control cells underwent similar treatment with vehicle. Immunoblot of the lysates was used to analyze the phosphorylation of p38 and ERK1/2 in response to decreased pH<sub>o</sub> or during the different steps of the NH<sub>4</sub>Cl pre-pulse. Blots were probed for  $\beta$ -actin to confirm equal protein loading. Membranes were blocked for 1 h then incubated with primary antibody for 2 h. Primary antibodies include: anti-ERK1/2 (Cell Signaling, #9101), anti-phospho-ERK1/2 (Cell Signaling, #9102), anti-p38 (Abcam, #ab7952), anti-phospho-p38 (Abcam, #ab45381), or anti- $\beta$ -actin (CellBioLabs, #AKR-002). Cells were rinsed 3 $\times$  for 10 min then incubated in secondary antibody for 1 h. Secondary antibodies include anti-mouse IgG, HRP-linked (Cell Signaling Technologies, #7076) or anti-rabbit IgG, HRP-linked (Cell Signaling Technologies, #7074). After rinsing three times for 10 min each, membranes were visualized using SuperSignaling West Pico Luminol Enhancers solution (Thermo Scientific, #1859675) and detected with the ChemiDoc from BioRad. Images were acquired and analyzed using ImageLab3.0 software.

## 2.6. Primary Cilia Immunostaining

Cells were grown to confluence on coverslips according to the cell culture conditions mentioned above. The cells were then exposed to media with pH of 5.5, 6.0, 6.5, 7.0 and 7.4 (control) for 5 min. The cells were fixed using 4% paraformaldehyde and 2% sucrose in PBS for 10 min and permeabilized for 5 min in 10% Triton X-100. The cells were incubated with Gli antibody (1:200 dilution in PBS, Abcam, Cambridge, MA, USA) for 16 h at 4 °C, acetylated- $\alpha$ -tubulin (1:10,000 dilution in PBS, Sigma Aldrich, St. Louis, MO, USA) for 1 h at 27 °C followed by fluorescein isothiocyanate (FITC)-conjugated anti-mouse antibody then Texas-red conjugated anti-rabbit antibody (1:1000 dilution in PBS, Vector Labs Burlingame, CA) for 1 h at 27 °C. Slides were mounted with DAPI hard set mounting media (Southern Biotech, Birmingham, AL, USA) Images were acquired using a Nikon Eclipse Ti-E inverted microscope with the NIS-Elements imaging software (version 4.30) in 100 $\times$  magnification fields with z-stack slices of 0.25  $\mu$ m. Flat cilia defined by consistent length in four z-slices were measured [31]. The majority of our cilia

were flattened on the slide surface, and cilia were measured in three-dimensionally (3D). We used Nikon NIS-Elements for Advanced Research software to capture and measure all cilia length in 3D. This software package included pre-programmed length analysis through iterations of automatic object recognition followed by image scanning and segmentation, optical flow and 3D object reconstruction. The single-particle tracking was activated only when cilia length was less than 1  $\mu\text{m}$ , especially in *Tg737* cells. In such cases (wild-type and *Tg737* cells), cells with less than 1  $\mu\text{m}$  length of cilia were denoted as non-ciliated cells.

Length measurements of 150 primary cilia was randomly selected using NIS-Elements. To obtain number of cells possessing cilia, six random 100 $\times$  fields were scanned and a maximum intensity projection created for each field. The total number of cilia and nuclei, as a representation of cell number, was used to calculate ciliated cell percentage. Statistical analysis was performed on Prism GraphPad 8.1.2 software (GraphPad, San Diego, CA, USA).

## 2.7. Scanning Electron Microscopy

Cells were fixed with 2.5% paraformaldehyde/glutaraldehyde in sodium cacodylate buffer for 1 h at 27 °C. Samples were post-fixed with 1% aqueous osmium tetroxide solution. Dehydration was done using ethanol solutions. Samples were further dried with a 2-h incubation in 50% hexamethyldisilazane (HMDS)-ethyl alcohol mixture, followed by two 30-min incubations in 100% HMDS. Micrographs were obtained and analyzed using a Hitachi HD-2300 scanning electron microscope (SEM) [24].

## 2.8. Data Analysis

The rate of  $\text{pH}_i$  changes is denoted as a rate constant of  $\Delta\text{pH}_i$  and expressed as  $\text{dpH}/\text{dt}$  ( $\Delta\text{pH}_i$  units/min). Because the  $\Delta\text{pH}_i$  is defined as rate constant of  $\text{pH}_i$  decreased with respect to time, this  $\text{pH}_i$  was not necessarily decreased at a constant speed. In other words, the changes in  $\text{pH}_i$  could speed up and slow down during the period of measurement. We, therefore, looked at a second order kinetics of these acceleration and deceleration events. The second order kinetics were determined through the tangential rates in the changes of rate constant of  $\Delta\text{pH}_i$  using Microsoft Excel software (version 15.32). The mathematical expression to calculate the change of function  $f$  at the time  $t_1$  is as follows:

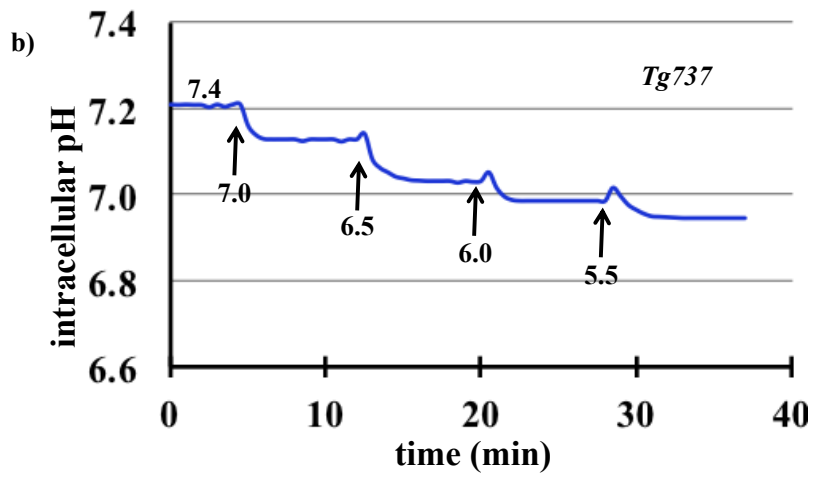
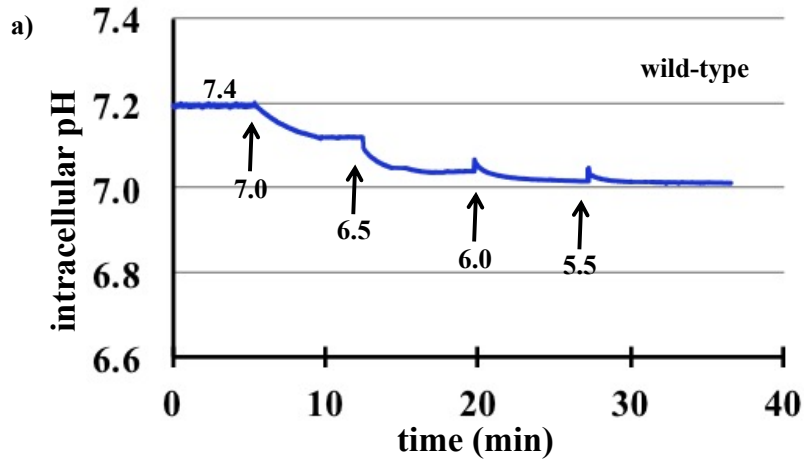
$$\text{Changes in Rate Constant of } \Delta\text{pH}_i = f'(t_1) = \lim_{t_2 \rightarrow t_1} \frac{f(t_2) - f(t_1)}{t_2 - t_1}$$

All the data shown are mean  $\pm$  SEM from at least three independent experiments. Data was analyzed using ANOVA test followed by Tukey post-hoc test for multiple groups with  $p < 0.05$  being considered as significant. Analysis of data was performed with Prism GraphPad 7 software.

### 3. Results

#### 3.1. Intracellular Acidosis in Response to Decreasing $pH_o$ in Wild-Type and *Tg737* Cells

Incubation of cells in PSS of decreasing extracellular pH ( $pH_o$ ) from 7.4 to 5.5 acidified the intracellular environment in both wild-type (Figure 10a) and cilia-less *Tg737* cells (Figure 10b). The acidic  $pH_o$  mediated decrease in  $pH_i$  was similar in both wild-type and *Tg737* cells (Figure 10c). The rate of  $pH_i$  changes ( $\Delta pH_i$ ) was not significantly different between wild-type and *Tg737* cells (Figure 10d). The negative values of  $\Delta pH_i$  indicated that the  $pH_i$  was decreased in acidified media. There was no significant different between wild-type and *Tg737* cells in the uniformity of or changes in  $\Delta pH_i$  ( $\Delta \Delta pH_i$ ; Figure 10e). The positive values of  $\Delta \Delta pH_i$  indicated that the  $\Delta pH_i$  was predominantly involved in acceleration to decrease  $pH_i$ .





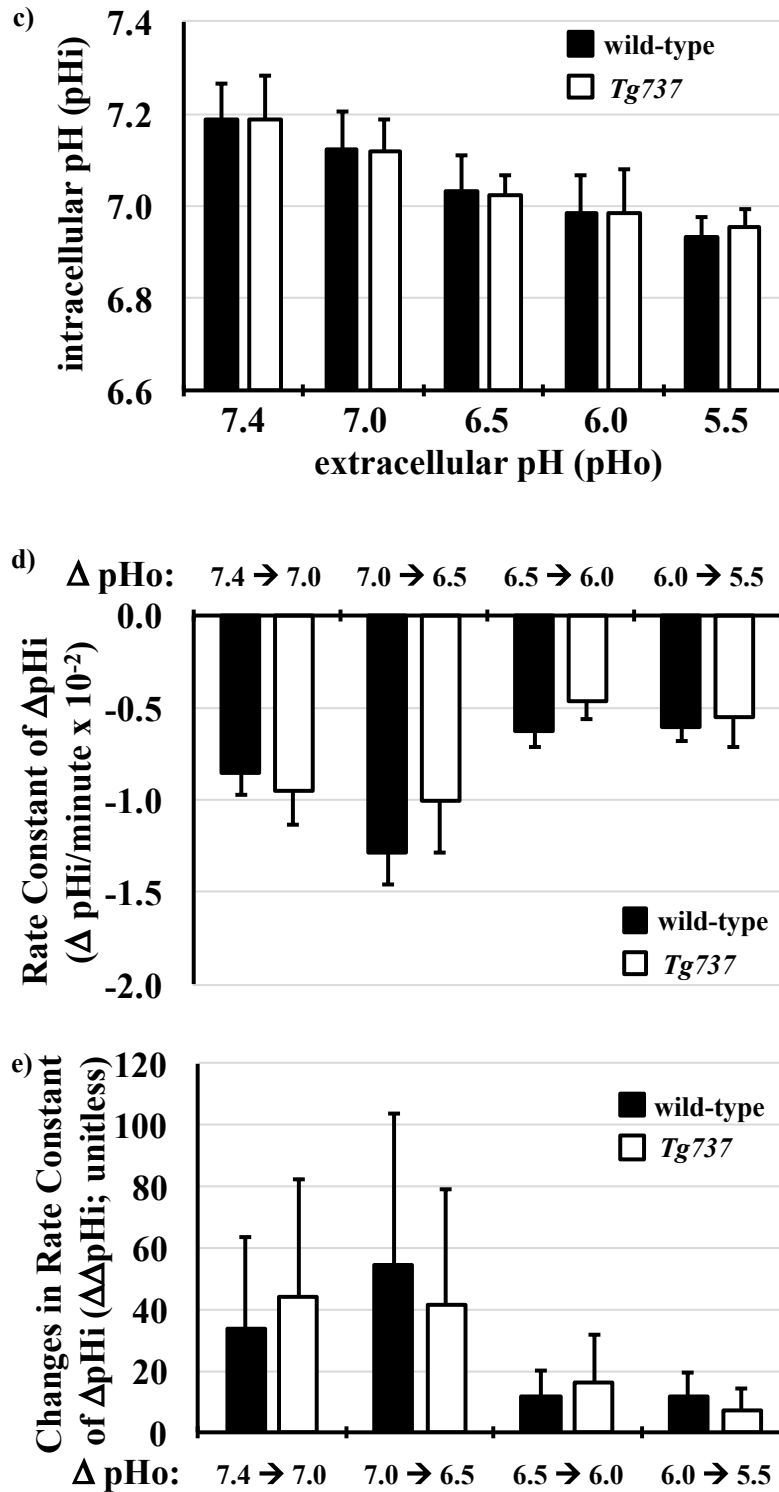
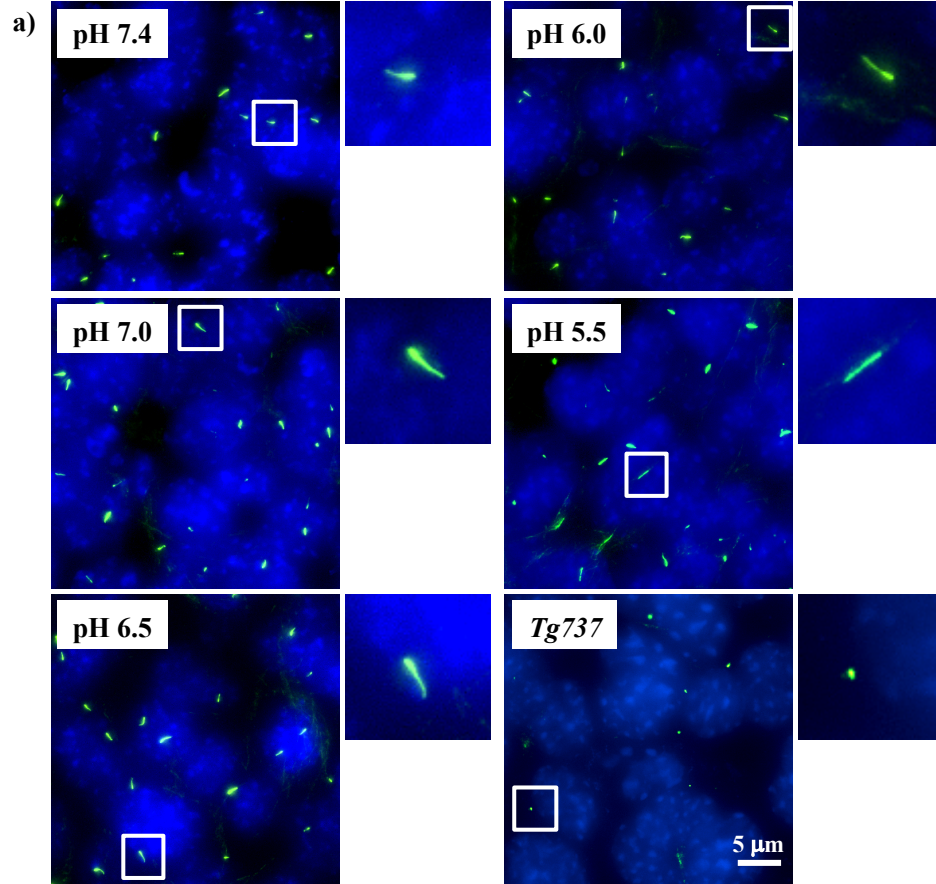


Figure 10. Decreased intracellular pH in response to acidic extracellular pH in wild-type and *Tg737* cells. (a,b) Representative tracings of changes in intracellular pH<sub>i</sub> when wild-type and *Tg737* cells are exposed to media of decreasing extracellular pH (pH<sub>o</sub>) from 7.4 to 5.5. (c) As the

pH<sub>o</sub> is decreased, both cell lines show a similar decrease in their pH<sub>i</sub>. (d) The rate constant pH<sub>i</sub> changes ( $\Delta\text{pH}_i$ ) in response step changes in pH<sub>o</sub> are also similar in both cell lines. A negative value indicates a decrease in pH<sub>i</sub>. (e) Changes in  $\Delta\text{pH}_i$  ( $\Delta\Delta\text{pH}_i$ ) are normalized to identify variability within  $\Delta\text{pH}_i$  in response to step changes in pH<sub>o</sub>. No variation is observed if there is no acceleration or deceleration (first order kinetic or  $\Delta\Delta\text{pH}_i = 0$ ). Highest variation ( $\Delta\Delta\text{pH}_i = 100$ ) indicates that an alternate acceleration-deceleration pattern occurred (if acceleration = deceleration, then  $\Delta\text{pH}_i = 0$ ).

To validate that primary cilia remained intact and structurally stable in acidified media, endothelial cilia were examined with ciliary marker acetylated- $\alpha$ -tubulin (Figure 11a). To examine the effect of extracellular pH on the length of primary cilia, the distribution of cilia length as well as ciliation frequency is tabulated in the bar graph (Figure 11b). Compared to control at pH 7.4, a small but significant increase in cilia length was observed at pH<sub>o</sub> of 7.0, 6.5 and 5.5 while there were no significant differences observed in ciliation frequency (Figure 11c). There were no apparent differences in the cilia formation at different extracellular pH levels. Approximately 80–85% of wild-type cells were ciliated in acidified media, as well as at pH 7.4. For cilia-less *Tg737* cells, the only representative image at pH 7.4 is shown with no further apparent differences in acidified media. There were no cilia length increase in *Tg737* cells at various pH<sub>i</sub>.

Most importantly, the data shows that wild-type cells continued to possess primary cilia without any structural aberrations in an acidic environment. Further validation with another ciliated cell line, NIH3T3, was conducted to observe changes in ciliary length or ciliation frequency when challenged with acidified media (Figure 12–14). Lower acidic media was able to significantly increase ciliary length at pH<sub>o</sub> of 6.5 and 5.5 while ciliation frequency remained unchanged at lower pH<sub>o</sub>. Among the many signaling activities related to the primary cilia, Hedgehog signaling (Hh) is unique in translocating activated receptors and proteins to the cilia [32]. To observe changes in functional role of the primary cilia under our experimental conditions, we used purmophamine to activate the Hh pathway. After observing no effect of Hh activation on ciliary length or ciliation frequency of the cells, we studied if acidified media induced Hh signaling, as shown by Gli translocation to the ciliary tip in NIH3T3 cells (Figure 14). There is also no apparent structural defect in cilia following a decrease in intracellular pH (Figure 15).



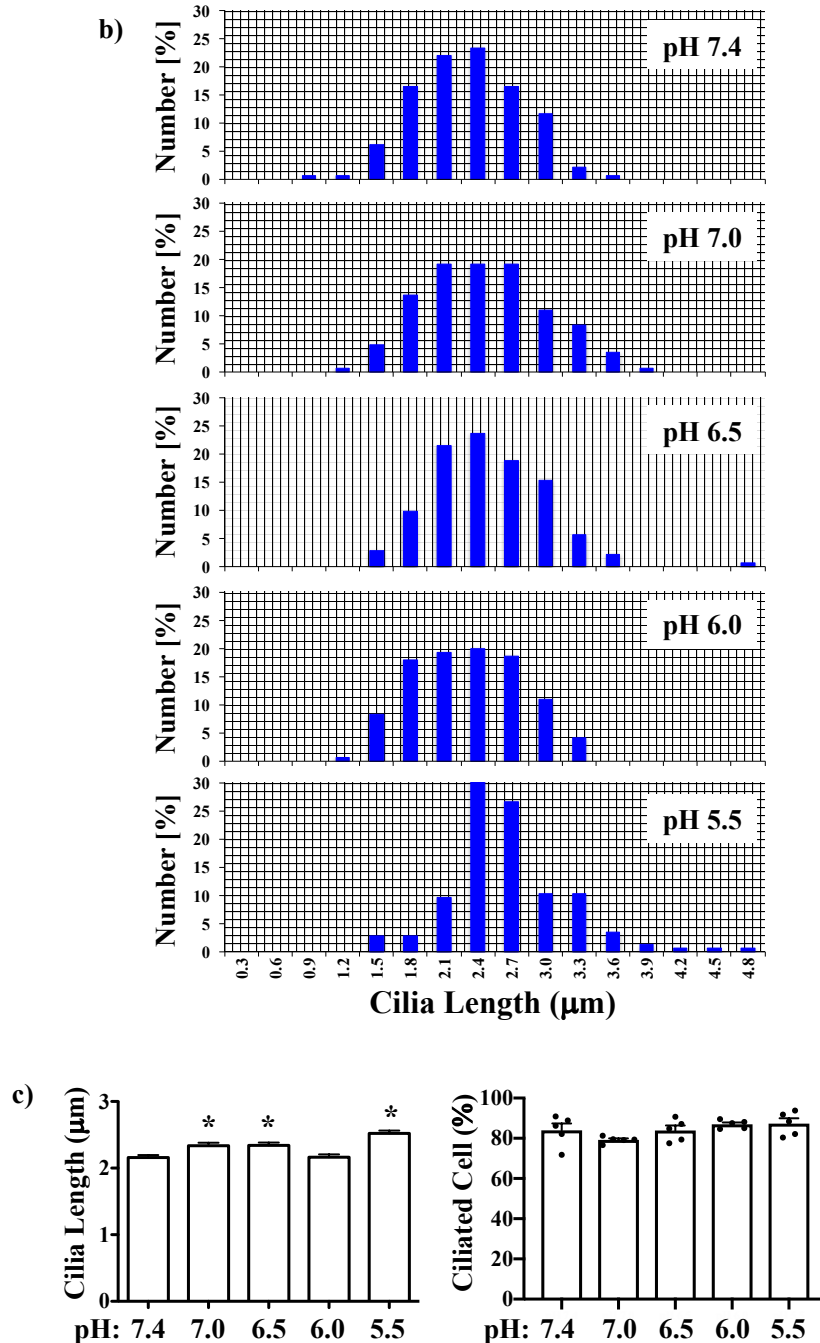


Figure 11. Immunofluorescence staining to study effects of pHo on primary cilia. (a) Cells (wild-type and Tg737) were stained with ciliary marker (acetylated- $\alpha$ -tubulin; green) and nucleus marker (DAPI; blue). Representative images are shown for wild-type cells at different pHo and Tg737 at pHo 7.4. White boxes show enlargement of the images to depict the presence of primary cilia. (b) The lengths of primary cilia from 50 cells were measured from each preparation (N = 3) and illustrated in the bar graph to depict length distribution within each pHo. (c) Cilia length was averaged from 150 cells (N = 3; each with 50 randomly selected cells) and

the number of cells possessing cilia represented as a percentage with each point representing a individual experimental data. \* indicates a significant difference to control pHo 7.4.

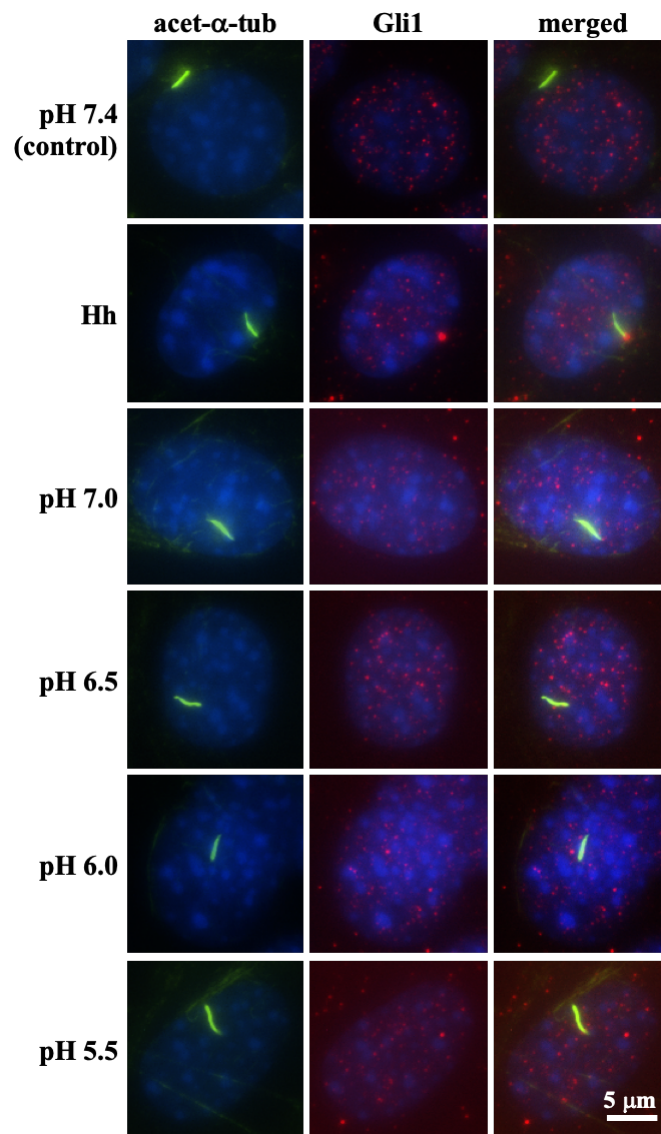


Figure 12. NIH3T3 were stained with ciliary marker (acetylated- $\alpha$ -tubulin; green), Gli (red) and nucleus marker (DAPI; blue).

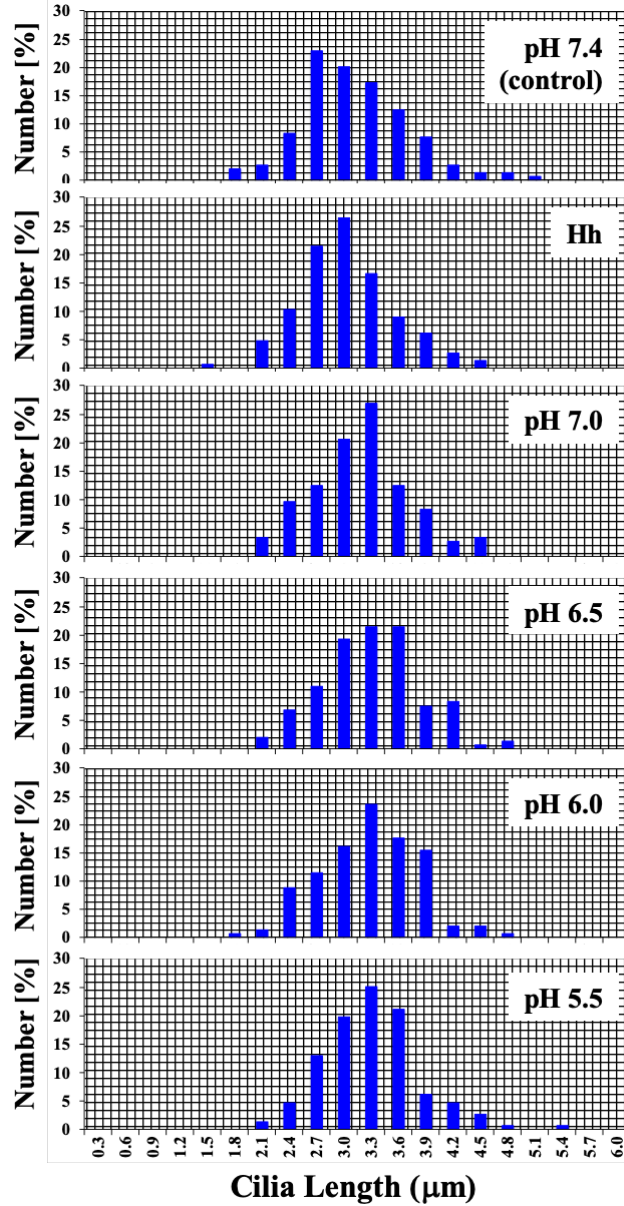


Figure 13. The lengths of primary cilia from 150 NIH3T3 cells were measured from each preparation (N = 3; each 50 randomly selected cilia).

### 3.2. MAPK Activation in Response to Decreasing pH<sub>o</sub> in Wild-Type and Tg737 Cells

Both wild-type and *Tg737* cells exhibited MAPK phosphorylation in response to decreased pH<sub>o</sub>. Significant increase of ERK1/2 phosphorylation occurred at pH<sub>o</sub> 6.5 in wild-type cells (178% increase versus control pH<sub>o</sub> 7.4) and persisted at pH<sub>o</sub> 6.0 and pH<sub>o</sub> 5.5 (227% and 189% increase in ERK1/2 phosphorylation, respectively versus control pH<sub>o</sub> 7.4) (Figure 16a). ERK1/2 phosphorylation occurred at pH<sub>o</sub> 6.0 in *Tg737* cells (140% increase versus control pH<sub>o</sub> 7.4) (Figure 16b). Another MAPK, p38 was phosphorylated at pH<sub>o</sub> 7.0 in wild-type cells (242% increase versus control pH<sub>o</sub> 7.4) and persisted at pH<sub>o</sub> 6.0 and pH<sub>o</sub> 5.5 (227% and 189% increase in p38 phosphorylation, respectively versus control pH<sub>o</sub> 7.4) (Figure 17a). p38 phosphorylation occurred at pH<sub>o</sub> 6.5 in *Tg737* cells (393% increase versus control pH<sub>o</sub> 7.4) and persisted through pH<sub>o</sub> 5.5 (321% and 360% increase in p38 phosphorylation at pH<sub>o</sub> 6.0 and 5.5, respectively, versus control pH<sub>o</sub> 7.4) (Figure 17b). *Tg737* cells required higher acidic conditions to increase MAPK phosphorylation than the wild-type cells. There did not seem to be a significant impairment in cilia-less *Tg737* cells' ability to sense and respond to decreased pH<sub>o</sub>, but we find a lower pH threshold for activation of MAPK in *Tg737* compared to wild-type cells.

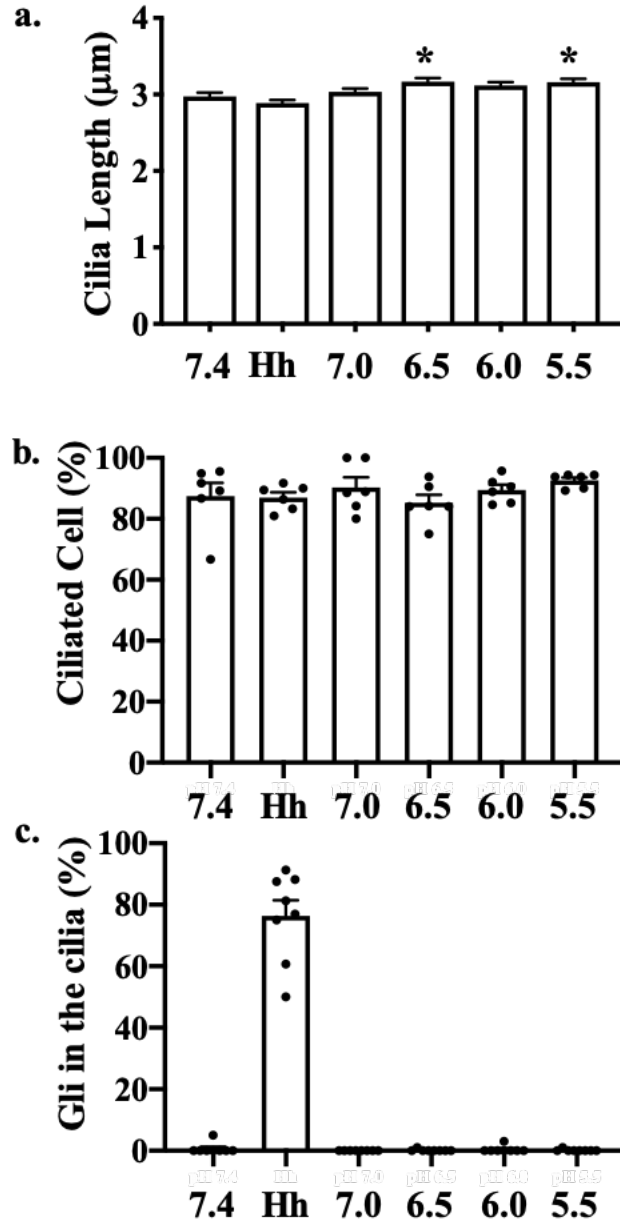


Figure 14. (a) Cilium length of NIH3T3 cells before and after Hh activation or different acidic  $\text{pH}_o$  exposures was averaged. (b) The percentage of cells with cilia is shown. (c) The percentage of cells is shown with Gli localization to the cilia.



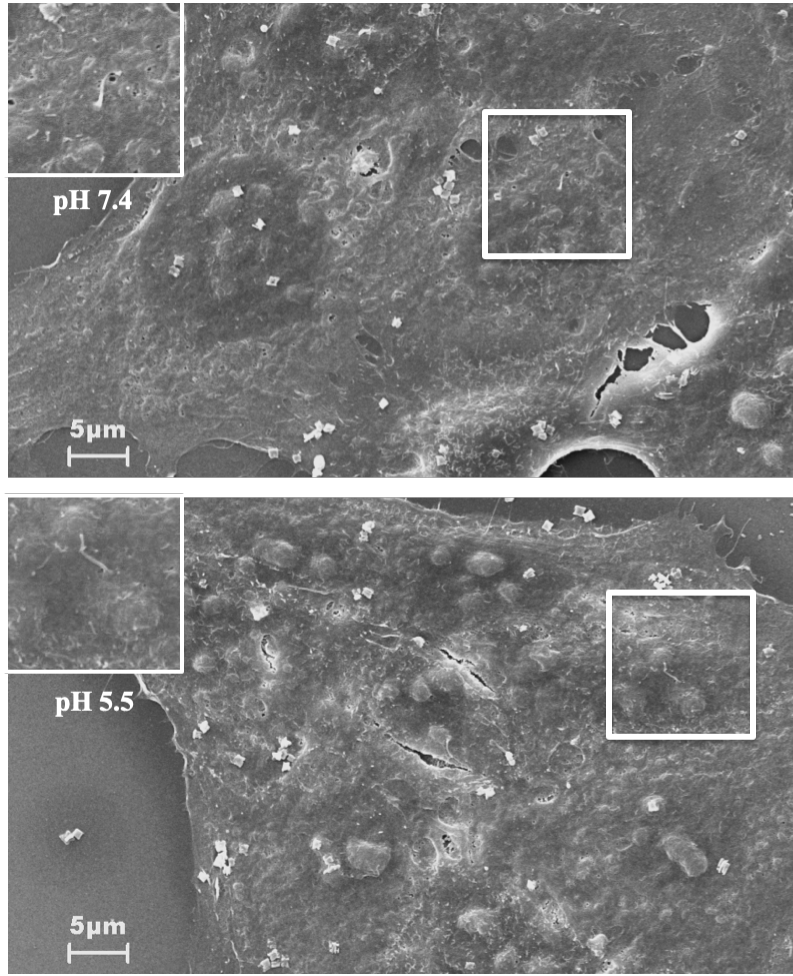


Figure 15. Electron micrographs of endothelial cells at pH 7.4 (top) and pH 5.5 (bottom).

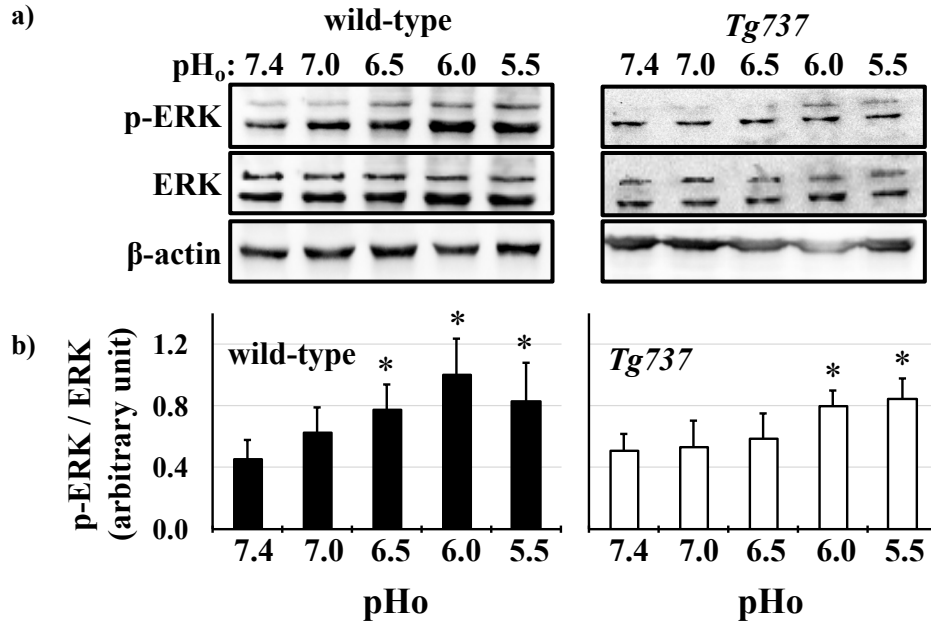


Figure 16. Decreasing extracellular pH increases ERK1/2 phosphorylation in wild-type and *Tg737* cells. (a) Representative immunoblots show ERK1/2 phosphorylation in wild-type and *Tg737* cells as they are exposed to media of decreasing extracellular pH ( $pH_o$ ) from 7.4 to 5.5 for 5 minutes. (b) Bar graph shows the mean p-ERK/ERK, where wild-type cells phosphorylate ERK1/2 at pH of 6.5 while the same level of phosphorylation occurs at a lower pH of 6.0. \* denotes  $p < 0.05$  as compared to control  $pH_o$  7.4; N = 10 for wild-type cells and N = 10 for *Tg737* cells.

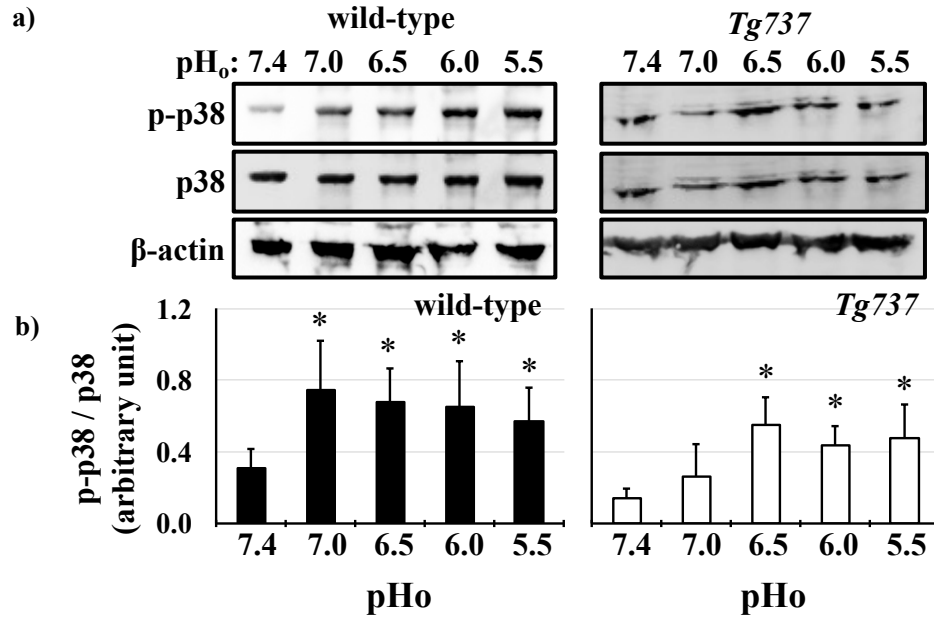


Figure 17. p38 phosphorylation by decreased extracellular pH in wild-type and *Tg737* cells. (a) Representative immunoblots show p38 phosphorylation in wild-type and *Tg737* cells as they are exposed to media of decreasing extracellular pH (pH<sub>o</sub>) from 7.4 to 5.5 for 5 minutes. (b) Bar graph shows mean p-p38/p38. Significant increase in p-38 phosphorylation occurs when pH changes from 7.4 to 7.0. But in *Tg737* cells the pH had to drop to 6.5 before significant changes in p38 phosphorylation was observed. \* =  $p < 0.05$  as compared to control pH<sub>o</sub> 7.4; N = 8 for wild-type cells and N = 8 for *Tg737* cells.

### 3.3. NH<sub>4</sub>Cl Pre-Pulse Induces Intracellular Acidosis in Wild-Type and *Tg737* Cells

To eliminate the effect of pH<sub>o</sub> and observe intracellularly restricted pH acidosis NH<sub>4</sub>Cl pre-pulse was used to lower pH<sub>i</sub>. Changes in pH<sub>i</sub> during the NH<sub>4</sub>Cl pre-pulse using Na<sup>+</sup>- and K<sup>+</sup>-containing PSS for pH<sub>i</sub> recovery are depicted in representative tracings (Figure 18a and 13b of wild-type and *Tg737* cells, respectively) and data is summarized in Figure 18c. In wild-type cells, NH<sub>4</sub>Cl caused an increase in intracellular pH ( $0.014 \pm 0.002$  pH units/min); in *Tg737* cells, NH<sub>4</sub>Cl also increased the pH<sub>i</sub> ( $0.019 \pm 0.003$  pH units/min). In the absence of sodium and potassium, the pH<sub>i</sub> decreased in both cell types ( $0.028 \pm 0.004$  pH units/min in wild-type cells and  $0.020 \pm 0.003$  pH units/min in *Tg737* cells, from NH<sub>4</sub>Cl conditions). pH<sub>i</sub> recovery occurred upon addition of the Na<sup>+</sup>- and K<sup>+</sup>-containing PSS solution, at a rate of  $0.006 \pm 0.0001$  pH units/min in wild-type cells, and more significantly in *Tg737* cells at a rate of  $0.031 \pm 0.003$  pH units/min, from 0K<sup>+</sup>/0Na<sup>+</sup> conditions. Because rates did not increase during incubation in the 0K<sup>+</sup>/0Na<sup>+</sup> solution, Na<sup>+</sup>- or

$K^+$ -dependent transport is likely responsible for endothelial cells' recovery from decreased  $pH_i$ . Another inference is that  $Na^+$ - and  $K^+$ -independent transport may not be present or activated by intracellular acidosis, in vascular endothelial cells.

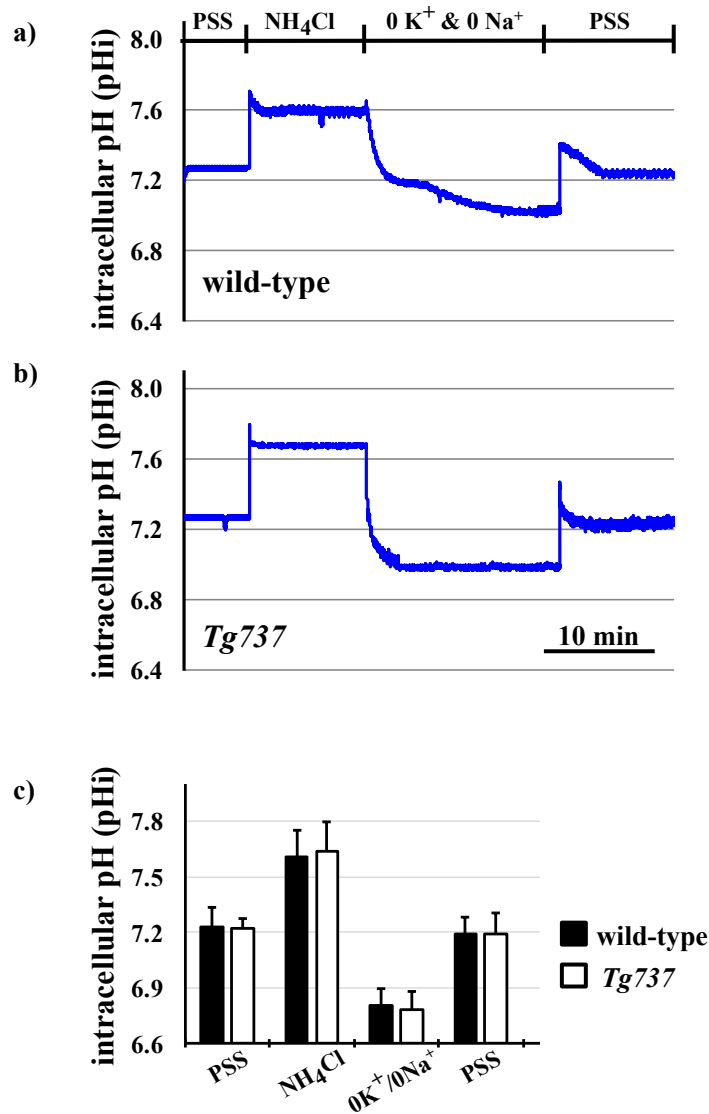


Figure 18. Changes in  $pH_i$  during the  $NH_4Cl$  pre-pulse in wild-type and  $Tg737$  cells. (a,b) Representative tracings of changes in intracellular pH when wild-type and  $Tg737$  cells are exposed to solutions of the  $NH_4Cl$  pre-pulse in  $Na^+$ - and  $K^+$ -devoid solution for  $pH_i$  recovery. (c) Bar graph shows the summary of mean changes in  $pH_i$  recovery in wild-type and  $Tg737$  cells.

To validate that primary cilia remained intact and structurally stable after intracellular acidification independent of  $pH_o$ , endothelial cilia were examined with ciliary marker acetylated- $\alpha$ -tubulin (Figure 19). To examine the effect of  $pH_i$  acidification on the length of primary cilia, the distribution of cilia length as well as ciliation frequency is tabulated in the bar graph (Figure 20). Compared to control at  $pH_i$  7.4, a small but significant decrease in cilia length was observed at  $pH_i$  of 7.0 while there were no significant differences observed in ciliation frequency. There were no apparent differences in the cilia formation between  $pH_i$  7.4 and 7.0. Approximately 80–85% of wild-type cells were ciliated. There were no cilia length recovery in *Tg737* cells at  $pH_i$  of 7.0.

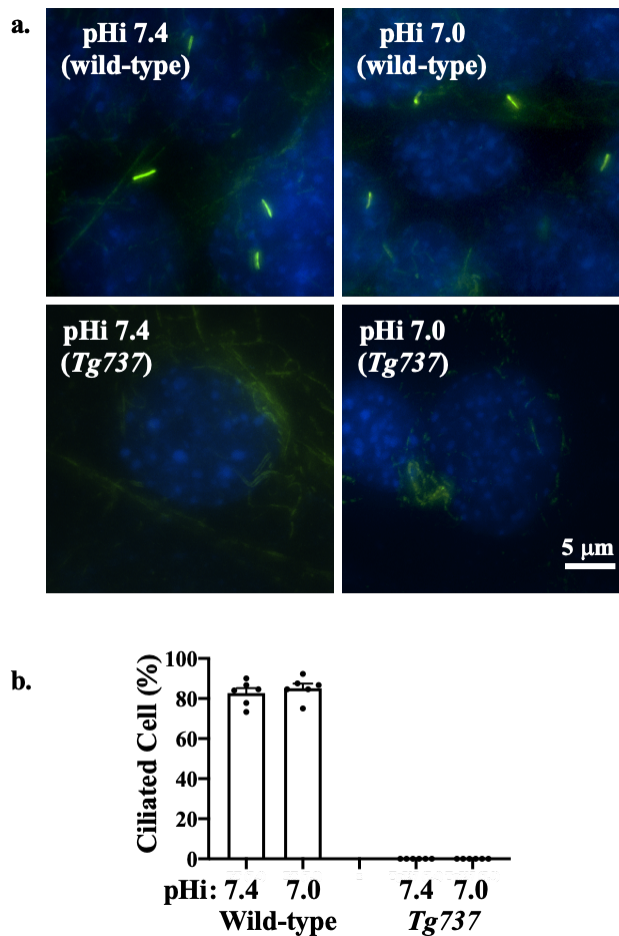


Figure 19. Endothelial cells were stained with ciliary marker (acetylated- $\alpha$ -tubulin; green) and nucleus marker (DAPI; blue).

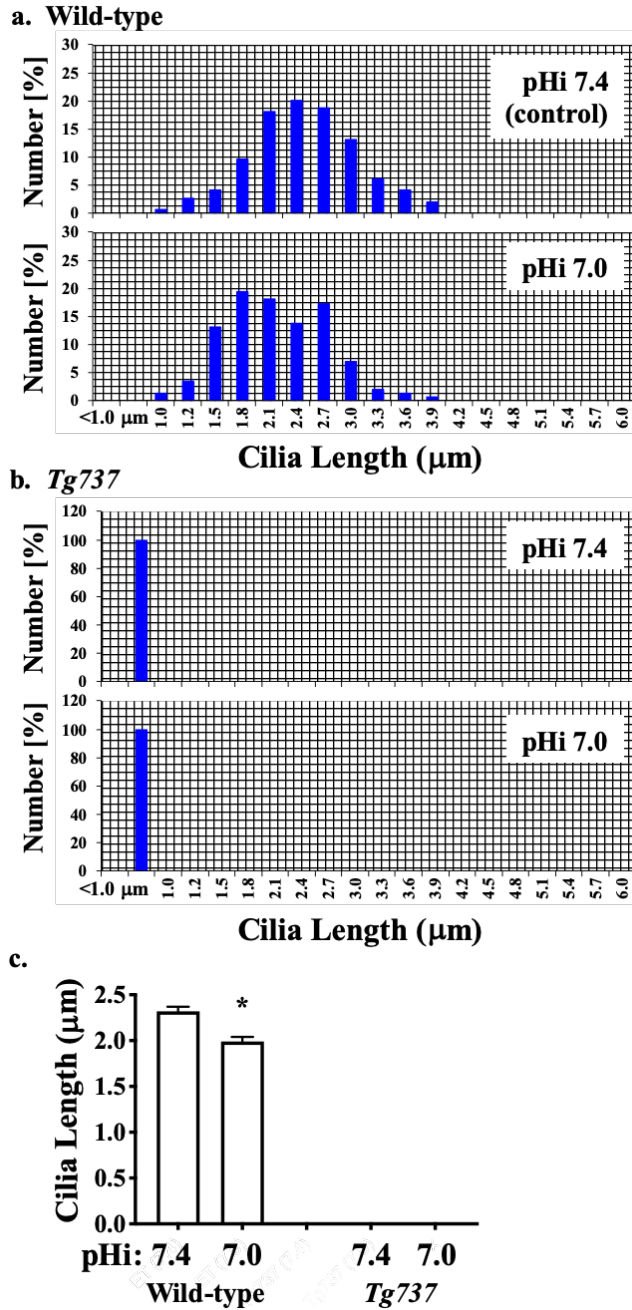


Figure 20. The lengths of primary cilia from 150 endothelial cells were measured from each preparation before and after  $\text{NH}_4\text{Cl}$  pre-pulse in  $0\ \text{Na}^+/\text{K}^+$  solution ( $N = 3$ ; each 50 randomly selected cilia).

### 3.4. Intracellular Acidosis Activates MAPK Signaling Pathways

MAPK phosphorylation during the  $\text{NH}_4\text{Cl}$  pre-pulse was similar in both cell types, with slight variations (Figure 21a). ERK1/2 phosphorylation at acid  $\text{pH}_i$  during the  $0\text{K}^+/0\text{Na}^+$  step of the  $\text{NH}_4\text{Cl}$  pre-pulse occurred in only wild-type cells (3.7-fold increase in ERK1/2 phosphorylation versus control conditions) (Figure 21b). ERK1/2 phosphorylation was observed during  $\text{pH}_i$  recovery in both wild-type and *Tg737* cells (2.1-fold and 2.3-fold respective increases in phosphorylation versus control conditions). p38 phosphorylation pattern varied between the wild type and cilia-less *Tg737* as well. In wild-type cells, p38 phosphorylation occurred at low  $\text{pH}_i$  during the  $0\text{K}^+/0\text{Na}^+$  step of the  $\text{NH}_4\text{Cl}$  pre-pulse (10-fold increase in phosphorylation versus control conditions); in *Tg737* cells, p38 phosphorylation was dampened, occurring only during  $\text{pH}_i$  recovery (4.0-fold increase in p38 phosphorylation versus control conditions) (Figure 21c).

### 3.5. Effects of $\text{K}^+$ on $\text{pH}_i$ Recovery and on MAPK Phosphorylation during the $\text{NH}_4\text{Cl}$ Pre-Pulse in Wild-Type and *Tg737* Cells

Potassium-containing  $5\text{K}^+/0\text{Na}^+$  solution could be used to study  $\text{K}^+$ -dependent  $\text{pH}_i$  recovery [1]. When the  $\text{NH}_4\text{Cl}$  pre-pulse was expanded to include potassium-containing  $5\text{K}^+/0\text{Na}^+$  solution in between the  $0\text{K}^+/0\text{Na}^+$  and PSS solutions during  $\text{pH}_i$  recovery, the  $\text{pH}_i$  increased very rapidly in wild-type cells and *Tg737* cells, highlighting the importance of  $\text{K}^+$ -dependent transporter activity during  $\text{pH}_i$  recovery in vascular endothelial cells, shown in representative tracings in Figure 22a and 22b, and summarized in Figure 22c. Addition of potassium-containing  $5\text{K}^+/0\text{Na}^+$  solution drove the  $\text{pH}_i$  up in both cell types ( $0.030 \pm 0.003$  pH units/min in wild-type cells and  $0.035 \pm 0.003$  pH units in *Tg737* cells, versus  $0\text{K}^+/0\text{Na}^+$  conditions). Interestingly, addition of PSS at the end of the pulse returned the  $\text{pH}_i$  to a normal level by driving the  $\text{pH}_i$  down at a rate of  $0.036 \pm 0.005$  pH units/min in wild-type cells and  $0.035 \pm 0.006$  pH units/min in *Tg737* cells, from  $5\text{K}^+/0\text{Na}^+$  conditions.

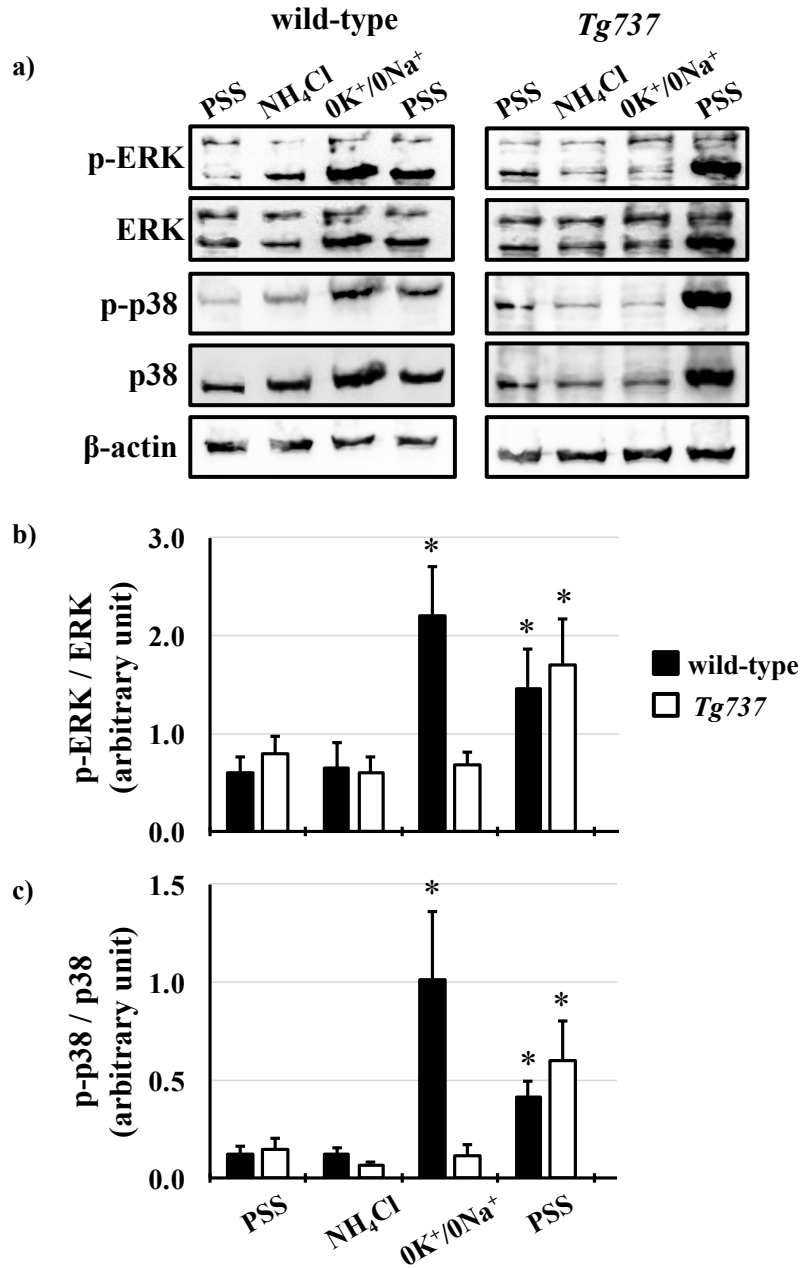


Figure 21. ERK1/2 and p38 phosphorylation during the NH<sub>4</sub>Cl pre-pulse in wild-type and *Tg737* cells. (a) Representative immunoblots show ERK1/2 and p38 phosphorylation in wild-type and *Tg737* cells as they are exposed to different solutions during the NH<sub>4</sub>Cl pre-pulse. (b,c) Bar graphs show mean p-ERK/ERK and p-p38/p38. \* indicates  $p < 0.05$  as compared to control conditions; for ERK1/2 N = 6 for wild-type cells and N = 5 for *Tg737* cells; for p38 N = 5 for wild-type cells and N = 5 for *Tg737* cells.



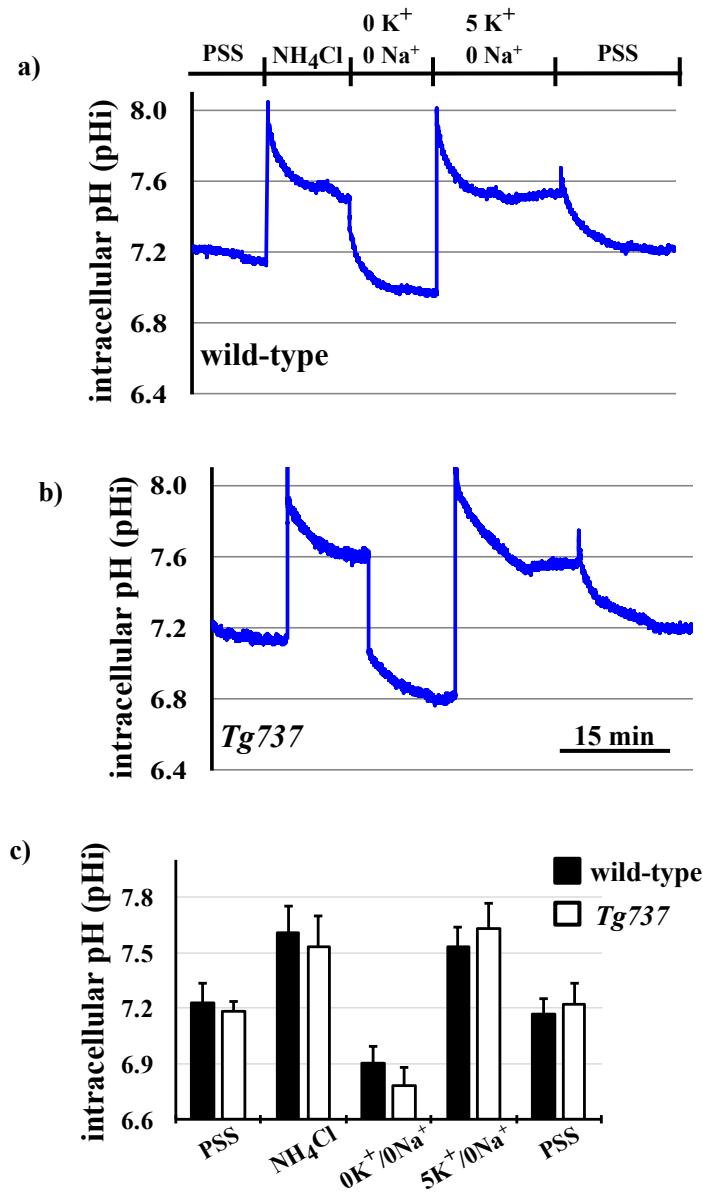


Figure 22. Changes in pHi during the NH<sub>4</sub>Cl pre-pulse in wild-type and *Tg737* cells. (a,b) Representative tracings of changes in intracellular pH when wild-type and *Tg737* cells are exposed to solutions of the NH<sub>4</sub>Cl pre-pulse including the 5 mM K<sup>+</sup> solution during pHi recovery of wild-type and *Tg737* cells. (c) Bar graph shows the summary of pHi recovery data from pre-pulse tracings in wild-type and *Tg737* cells.

Addition of potassium-containing 5K<sup>+</sup>/0Na<sup>+</sup> solution during pHi recovery also influenced MAPK phosphorylation, more specifically p38 phosphorylation (Figure 23). In wild-type cells, p38 phosphorylation coincided with ERK1/2 phosphorylation at acidified pHi, during the 0K<sup>+</sup>/0Na<sup>+</sup>

step of the  $\text{NH}_4\text{Cl}$  pre-pulse (10-fold increase in phosphorylation versus control conditions), and p38 phosphorylation persisted through  $\text{pH}_i$  recovery using the  $5\text{K}^+/\text{0Na}^+$  solution (5.5-fold increase in phosphorylation versus control conditions). In *Tg737* cells, p38 phosphorylation occurred later during  $\text{pH}_i$  recovery with the PSS solution (4.0-fold increase in phosphorylation versus control conditions). Both ERK1/2 and p38 phosphorylation were absent in *Tg737* cells as compared to wild-type cells, where significant increases in MAPK phosphorylation occurred after inducing intracellular acidosis.

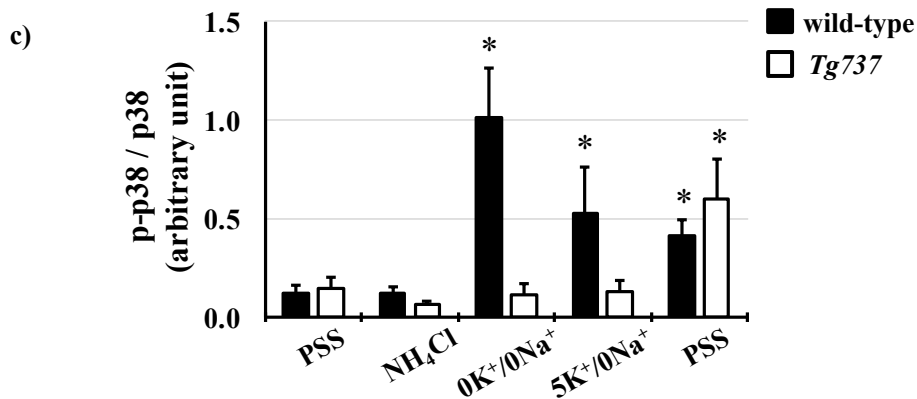
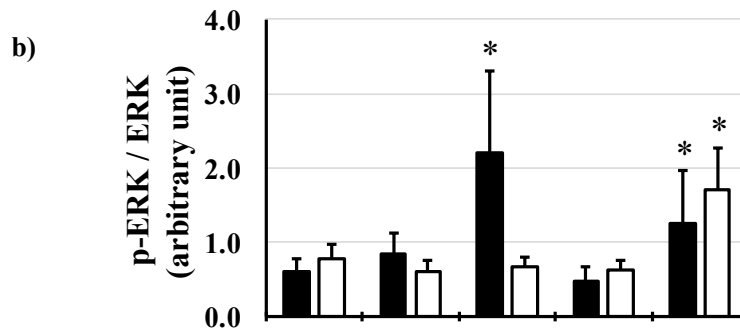
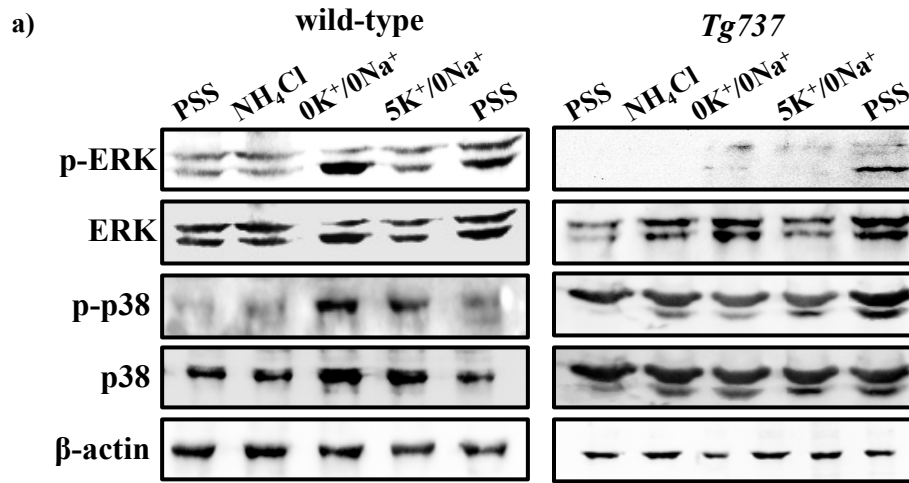


Figure 23. Effect of  $K^+$  on ERK1/2 and p38 phosphorylation during the  $NH_4Cl$  pre-pulse in wild-type and *Tg737* cells. (a) Representative immunoblots show ERK1/2 and p38 phosphorylation in wild-type and *Tg737* cells as they are exposed to different solutions during the  $NH_4Cl$  pre-pulse. (b,c) Bar graphs show mean p-ERK/ERK and p-p38/p38, respectively. \* denotes  $p < 0.05$  as compared to control conditions. For ERK1/2,  $N = 8$  for wild-type cells and  $N = 8$  for *Tg737* cells; for p38,  $N = 7$  for wild-type cells and  $N = 5$  for *Tg737* cells.

#### 4. Discussion

In the present studies, we assessed the role of primary cilia in pH sensing of vascular endothelial cells. We compared intracellular responses in wild-type and cilia-less *Tg737* mutant cells against extracellular pH changes and obtained three main results. First, intracellular pH homeostasis was not significantly different between the wild-type and *Tg737* cells. Second, phosphorylation of two mitogen-activated kinases, p38 and ERK1/2, were increased by lowering extracellular pH in both the wild-type and the *Tg737* cells, but for *Tg737* cells the same extent of phosphorylation needed a stronger acidic condition. Third, when the cells were exposed to  $0K^+/0Na^+$  and  $5K^+/0Na^+$  solutions after the  $NH_4Cl$  solution, the phosphorylation of p38 and ERK1/2 was enhanced only in the wild-type cells.

Wild-type and *Tg737* cells have similar responses to decreased extracellular pH ( $pH_o$ ), including decreased intracellular pH ( $pH_i$ ) relative to drops in  $pH_o$  and acute ERK1/2 and p38 phosphorylation at  $pH_o < 6.0$ . Diminished MAPK phosphorylation was observed in *Tg737* cells compared to wild-type cells at certain  $pH_o$ . A significant finding from these experiments was that MAPK phosphorylation in vascular endothelial cells when exposed to low  $pH_o$  may be associated to the cilia or there could be inherited machinery differences between wild-type and *Tg737* cells in terms of ERK1/2 and p38 phosphorylation.

An acidic environment increased the length of primary cilia in wild-type cells, whereas isolated acidification of intracellular pH decreased cilia length. The *Tg737* cells remained cilia-less under all conditions. Similar to endothelial cells, the NIH3T3 fibroblast cells also presented with longer cilia when challenged with an acidic environment. The physiological significance of this cilia length changes is not clear at present. However, it has been speculated that cilia length could be used as a cellular marker in response to injury or environmental insults [33–35]. SEM

micrographs showed no structural defects in the cilia after exposure to acidified media. With the aim of finding any functional effects of acidified media in the cilium, we looked at possible acidic  $pH_o$  induced Hh signaling but found no unexpected activation of Hh.

The next set of experiments were designed to bypass extracellular pH sensing by lowering intracellular pH only. In terms of  $pH_i$  acidification,  $NH_4Cl$  pre-pulse procedure lowered control and *Tg737* cell  $pH_i$  in the same manner. *Tg737* cells showed no ERK1/2 or p38 phosphorylation in response to decreased intracellular pH, compared to wild-type cells, consistent with a lower pH requirement as seen in  $pH_o$  induced intracellular acidification. Phosphorylation of p38 during  $K^+$ -mediated  $pH_i$  recovery is absent in *Tg737* cells but this does not produce any differences in  $pH_i$  recovery pattern in comparison to wild-type cells. From our findings we conclude that endothelial cilia are unlikely to serve as the only acid sensing organelle but may be involved in buffering capacity of cytosolic pH in vascular endothelial cells. The significance in this could mean that ciliopathy (abnormal cilia) may have very little direct role in the physiological acid-base imbalance.

Acid-induced MAPK activation has been observed in the renal epithelial cells [36]. Our studies show that acid activation of MAPK, p38, is relevant in endothelial cells and may be involved in the regulation of acid-mediated transport. Consistent with our observation, Flacke et al. showed that Wistar rat coronary endothelial cells exposed to acidosis (pH 6.4) led to a transient activation of p38 and Akt kinases, which are essential for protection against apoptosis [37]. The importance of  $K^+$  channels in  $pH_i$  recovery in vascular endothelial cells has been highlighted in this study, with profound increases in intracellular pH upon addition of  $K^+$ -containing solution following intracellular acidosis. Our data on  $K^+$ -dependent  $pH_i$  recovery indicates that  $K^+$ -transporters are primarily activated by low  $pH_i$ , which could include  $K^+$ -channels,  $Na^+/K^+$  pumps, and/or  $Na^+/K^+/2Cl^-$  cotransporters. Studies have shown that ATP-sensitive  $K^+$  channels are activated directly by intracellular but not by extracellular acidosis. This has been established in rat basilar artery where  $pH_i$ -acidification mediated dilation was blocked by glibenclamide, an inhibitor of ATP-sensitive potassium channels [38]. Future studies will be needed to determine the precise potassium channel, pump, or transporter responsible for  $K^+$ -dependent  $pH_i$  recovery in vascular endothelial cells.

A single, universal pH/acid sensor in the cardiovascular and renal systems that regulates MAPK pathways and ion transport has yet to be identified, but there are several possible candidates. These putative pH sensors expressed by vascular endothelial cells will lie upstream of acid-activated ERK1/2 and p38, and may include epidermal growth factor receptor (EGFR) [4], an acid-sensing ion channel (ASIC) [39], or a G-protein coupled receptor. The GPCR GPR4 is known to be acid-activated [40,41] and regulates potassium-driven transport to maintain pH [42]. GPR4-null mice have minor defects in renal acid excretion and mild metabolic acidosis. GPR4 deficiency also affects the quality of small blood vessels during angiogenesis [43]. In vascular endothelial cells, acidosis activation of GPR4 stimulates inflammatory responses [43]. With p38 being the notorious inflammatory MAPK [3] and its activation being clear in response to acid pH, GPR4 would be a promising pH sensor in vascular endothelial cells in the regulation of p38-mediated signaling pathways described here.

Other good candidates for a pH sensor in vascular endothelial cells are acid-sensing ion channels (ASICs), which are ligand-gated and amiloride-sensitive cation channels activated by extracellular  $H^+$  [44]. ASICs are members of the degenerin/epithelial sodium channel (DEG/ENaC) superfamily and contain an acidic pocket responsible for acid-dependent gating of sodium and calcium, albeit to a lesser degree. ASICs are expressed in the central and peripheral nervous system, including afferent tissues such as skin, cardiovascular system, muscle, joint, teeth, vestibular, and visceral cells [45].

With the primary cilium being established as a sensor of different mechanical and biochemical cues, we test whether the primary cilium has a role in sensing and transducing pH changes. We compare acidosis response using vascular endothelial cells as an *in vitro* model compared to cilia-less *Tg737* cells. Our study on non-motile primary cilia may not be extrapolated to the motile cilia in developing nodes or in the brain ventricles. Nonetheless, our data shows that acid-activation of p38- and ERK1/2-mediated signaling pathways regulate ion transport to maintain acid-base homeostasis in endothelia. We showed that  $pH_i$  recovery after an  $NH_4Cl$  pre-pulse in vascular endothelial cells is predominantly a  $K^+$ -dependent process. We also observed that a more acidic  $pH_o$  was needed to induce MAPK phosphorylation in cilia-less *Tg737* cells

compared to wild-type cell.  $\text{NH}_4\text{Cl}$  pre-pulse is a technique used to create  $\text{pH}_o$ -independent  $\text{pH}_i$  acidification, in this scenario  $\text{pH}_i$  recovery was seen to be delayed in *Tg737* cells. Therefore, we conclude that the primary cilium, a known cardiovascular mechanosensor [23,46,47] and chemoreceptor [24,48,49] is not the sole sensor for acid sensation but does influence the pH threshold for MAPK kinase phosphorylation. Future studies to examine the identity of the acid sensors distributed in the cilia might be able to detail the nuanced role of primary cilia or *Tg737* deletion that might affect the buffering capacity of the *Tg737* mice model.

## References

1. Fisher, K.D.; Codina, J.; Petrovic, S.; DuBose, T.D., Jr. Pyk2 regulates H<sup>+</sup>-ATPase-mediated proton secretion in the outer medullary collecting duct via an ERK1/2 signaling pathway. *Am. J. Physiol. Ren. Physiol.* **2012**, *303*, F1353–F1362.
2. Li, S.; Sato, S.; Yang, X.; Preisig, P.A.; Alpern, R.J. Pyk2 activation is integral to acid stimulation of sodium/hydrogen exchanger 3. *J. Clin. Investig.* **2004**, *114*, 1782–1789.
3. Johnson, G.L.; Lapadat, R. Mitogen-activated protein kinase pathways mediated by ERK, JNK, and p38 protein kinases. *Science* **2002**, *298*, 1911–1912.
4. Coaxum, S.D.; Blanton, M.G.; Joyner, A.; Akter, T.; Bell, P.D.; Luttrell, L.M.; Raymond, J.R., Sr.; Lee, M.H.; Blichmann, P.A.; Garnovskaya, M.N.; et al. Epidermal growth factor-induced proliferation of collecting duct cells from oak ridge polycystic kidney mice involves activation of Na<sup>+</sup>/H<sup>+</sup> exchanger. *Am. J. Physiol. Cell Physiol.* **2014**, *307*, C554–C560.
5. Skelton, L.A.; Boron, W.F. Effect of acute acid-base disturbances on the phosphorylation of phospholipase c-gamma1 and ERK1/2 in the renal proximal tubule. *Physiol. Rep.* **2015**, *3*, e12280.
6. Preisig, P.A. The acid-activated signaling pathway: Starting with pyk2 and ending with increased NHE3 activity. *Kidney Int.* **2007**, *72*, 1324–1329.
7. Zarubin, T.; Han, J. Activation and signaling of the p38 map kinase pathway. *Cell Res.* **2005**, *15*, 11–18.
8. Xue, L.; Lucocq, J.M. Low extracellular pH induces activation of ERK 2, JNK, and p38 in a431 and swiss 3t3 cells. *Biochem. Biophys. Res. Commun.* **1997**, *241*, 236–242.
9. Jin, X.; Mohieldin, A.M.; Muntean, B.S.; Green, J.A.; Shah, J.V.; Mykytyn, K.; Nauli, S.M. Cilioplasm is a cellular compartment for calcium signaling in response to mechanical and chemical stimuli. *Cell. Mol. Life Sci. CMLS* **2014**, *71*, 2165–2178.
10. Kwon, R.Y.; Temiyasathit, S.; Tummala, P.; Quah, C.C.; Jacobs, C.R. Primary cilium-dependent mechanosensing is mediated by adenylyl cyclase 6 and cyclic amp in bone cells. *FASEB J. Off. Publ. Fed. Am. Soc. Exp. Biol.* **2010**, *24*, 2859–2868.
11. Lee, K.L.; Guevarra, M.D.; Nguyen, A.M.; Chua, M.C.; Wang, Y.; Jacobs, C.R. The primary cilium functions as a mechanical and calcium signaling nexus. *Cilia* **2015**, *4*, 7.
12. Masyuk, A.I.; Masyuk, T.V.; Splinter, P.L.; Huang, B.Q.; Stroope, A.J.; LaRusso, N.F. Cholangiocyte cilia detect changes in luminal fluid flow and transmit them into intracellular Ca<sup>2+</sup> and camp signaling. *Gastroenterology* **2006**, *131*, 911–920.
13. Yamamoto, K.; Ando, J. New molecular mechanisms for cardiovascular disease: Blood flow sensing mechanism in vascular endothelial cells. *J. Pharm. Sci.* **2011**, *116*, 323–331.
14. Rohatgi, R.; Battini, L.; Kim, P.; Israeli, S.; Wilson, P.D.; Gusella, G.L.; Satlin, L.M. Mechanoregulation of intracellular Ca<sup>2+</sup> in human autosomal recessive polycystic kidney disease cyst-lining renal epithelial cells. *Am. J. Physiol. Ren. Physiol.* **2008**, *294*, F890–F899.
15. Nauli, S.M.; Alenghat, F.J.; Luo, Y.; Williams, E.; Vassilev, P.; Li, X.; Elia, A.E.; Lu, W.; Brown, E.M.; Quinn, S.J.; et al. Polycystins 1 and 2 mediate mechanosensation in the primary cilium of kidney cells. *Nat. Genet.* **2003**, *33*, 129–137.
16. Praetorius, H.A.; Spring, K.R. Bending the mdck cell primary cilium increases intracellular calcium. *J. Membr. Biol.* **2001**, *184*, 71–79.
17. Vina, E.; Parisi, V.; Abbate, F.; Cabo, R.; Guerrera, M.C.; Laura, R.; Quiros, L.M.; Perez-Varela, J.C.; Cobo, T.; Germana, A.; et al. Acid-sensing ion channel 2 (asic2) is selectively localized in the cilia of the non-sensory olfactory epithelium of adult zebrafish. *Histochem. Cell Biol.* **2015**, *143*, 59–68.
18. Waldmann, R.; Champigny, G.; Bassilana, F.; Heurteaux, C.; Lazdunski, M. A proton-gated cation channel involved in acid-sensing. *Nature* **1997**, *386*, 173–177.



19. Collier, D.M.; Snyder, P.M. Extracellular protons regulate human enac by modulating Na<sup>+</sup> self-inhibition. *J. Biol. Chem.* **2009**, *284*, 792–798.
20. Raychowdhury, M.K.; McLaughlin, M.; Ramos, A.J.; Montalbetti, N.; Bouley, R.; Ausiello, D.A.; Cantiello, H.F. Characterization of single channel currents from primary cilia of renal epithelial cells. *J. Biol. Chem. USA* **2005**, *280*, 34718–34722.
21. Satlin, L.M.; Sheng, S.; Woda, C.B.; Kleyman, T.R. Epithelial Na<sup>+</sup> channels are regulated by flow. *Am. J. Physiol. Ren. Physiol.* **2001**, *280*, F1010–F1018.
22. Banizs, B.; Komlosi, P.; Bevensee, M.O.; Schwiebert, E.M.; Bell, P.D.; Yoder, B.K. Altered pH(i) regulation and Na<sup>+</sup>/HCO<sub>3</sub><sup>-</sup> transporter activity in choroid plexus of cilia-defective tg737(ORPK) mutant mouse. *Am. J. Physiol. Cell Physiol.* **2007**, *292*, C1409–C1416.
23. Nauli, S.M.; Kawanabe, Y.; Kaminski, J.J.; Pearce, W.J.; Ingber, D.E.; Zhou, J. Endothelial cilia are fluid shear sensors that regulate calcium signaling and nitric oxide production through polycystin-1. *Circulation* **2008**, *117*, 1161–1171.
24. Abdul-Majeed, S.; Nauli, S.M. Dopamine receptor type 5 in the primary cilia has dual chemo- and mechano-sensory roles. *Hypertension* **2011**, *58*, 325–331.
25. AbouAlaiwi, W.A.; Takahashi, M.; Mell, B.R.; Jones, T.J.; Ratnam, S.; Kolb, R.J.; Nauli, S.M. Ciliary polycystin-2 is a mechanosensitive calcium channel involved in nitric oxide signaling cascades. *Circ. Res.* **2009**, *104*, 860–869.
26. Yoder, B.K.; Tousson, A.; Millican, L.; Wu, J.H.; Bugg, C.E., Jr.; Schafer, J.A.; Balkovetz, D.F. Polaris, a protein disrupted in ORPK mutant mice, is required for assembly of renal cilium. *Am. J. Physiol. Ren. Physiol.* **2002**, *282*, F541–F552.
27. Jones, T.J.; Adapala, R.K.; Geldenhuys, W.J.; Bursley, C.; AbouAlaiwi, W.A.; Nauli, S.M.; Thodeti, C.K. Primary cilia regulates the directional migration and barrier integrity of endothelial cells through the modulation of hsp27 dependent actin cytoskeletal organization. *J. Cell Physiol.* **2012**, *227*, 70–76.
28. Aboualawi, W.A.; Muntean, B.S.; Ratnam, S.; Joe, B.; Liu, L.; Booth, R.L.; Rodriguez, I.; Herbert, B.S.; Bacallao, R.L.; Fruttiger, M.; et al. Survivin-induced abnormal ploidy contributes to cystic kidney and aneurysm formation. *Circulation* **2014**, *129*, 660–672.
29. AbouAlaiwi, W.A.; Ratnam, S.; Booth, R.L.; Shah, J.V.; Nauli, S.M. Endothelial cells from humans and mice with polycystic kidney disease are characterized by polyploidy and chromosome segregation defects through survivin down-regulation. *Hum. Mol. Genet.* **2011**, *20*, 354–367.
30. Nauli, S.M.; Jin, X.; AbouAlaiwi, W.A.; El-Jouni, W.; Su, X.; Zhou, J. Non-motile primary cilia as fluid shear stress mechanosensors. *Methods Enzymol.* **2013**, *525*, 1–20.
31. Dummer, A.; Poelma, C.; DeRuiter, M.C.; Goumans, M.-J.T.H.; Hierck, B.P. Measuring the primary cilium length: Improved method for unbiased high-throughput analysis. *Cilia* **2016**, *5*, 7.
32. Tukachinsky, H.; Lopez, L.V.; Salic, A. A mechanism for vertebrate hedgehog signaling: Recruitment to cilia and dissociation of sufu-gli protein complexes. *J. Cell Biol.* **2010**, *191*, 415–428.
33. Prodromou, N.V.; Thompson, C.L.; Osborn, D.P.; Cogger, K.F.; Ashworth, R.; Knight, M.M.; Beales, P.L.; Chapple, J.P. Heat shock induces rapid resorption of primary cilia. *J. Cell Sci.* **2012**, *125*, 4297–4305.
34. Verghese, E.; Zhuang, J.; Saiti, D.; Ricardo, S.D.; Deane, J.A. In vitro investigation of renal epithelial injury suggests that primary cilium length is regulated by hypoxia-inducible mechanisms. *Cell Biol. Int.* **2011**, *35*, 909–913.
35. Verghese, E.; Weidenfeld, R.; Bertram, J.F.; Ricardo, S.D.; Deane, J.A. Renal cilia display length alterations following tubular injury and are present early in epithelial repair. *Nephrol. Dial. Transpl.* **2008**, *23*, 834–841.
36. Brown, D.; Wagner, C.A. Molecular mechanisms of acid-base sensing by the kidney. *J. Am. Soc. Nephrol.* **2012**, *23*, 774–780.



37. Flacke, J.P.; Kumar, S.; Kostin, S.; Reusch, H.P.; Ladilov, Y. Acidic preconditioning protects endothelial cells against apoptosis through p38- and AKT-dependent bcl-xl overexpression. *Apoptosis* **2009**, *14*, 90–96.
38. Santa, N.; Kitazono, T.; Ago, T.; Ooboshi, H.; Kamouchi, M.; Wakisaka, M.; Ibayashi, S.; Iida, M. ATP-sensitive potassium channels mediate dilatation of basilar artery in response to intracellular acidification in vivo. *Stroke* **2003**, *34*, 1276–1280.
39. Abboud, F.M.; Benson, C.J. Asics and cardiovascular homeostasis. *Neuropharmacology* **2015**, *94*, 87–98.
40. Chen, A.; Dong, L.; Leffler, N.R.; Asch, A.S.; Witte, O.N.; Yang, L.V. Activation of gpr4 by acidosis increases endothelial cell adhesion through the CAMP/EPAC pathway. *PLoS ONE* **2011**, *6*, e27586.
41. Sun, X.; Yang, L.V.; Tiegs, B.C.; Arend, L.J.; McGraw, D.W.; Penn, R.B.; Petrovic, S. Deletion of the pH sensor gpr4 decreases renal acid excretion. *J. Am. Soc. Nephrol.* **2010**, *21*, 1745–1755.
42. Codina, J.; Opyd, T.S.; Powell, Z.B.; Furdui, C.M.; Petrovic, S.; Penn, R.B.; DuBose, T.D., Jr. pH-dependent regulation of the alpha-subunit of H<sup>+</sup>-K<sup>+</sup>-ATPase (HKalpha2). *Am. J. Physiol. Ren. Physiol.* **2011**, *301*, F536–F543.
43. Dong, L.; Li, Z.; Leffler, N.R.; Asch, A.S.; Chi, J.T.; Yang, L.V. Acidosis activation of the proton-sensing GPR4 receptor stimulates vascular endothelial cell inflammatory responses revealed by transcriptome analysis. *PLoS ONE* **2013**, *8*, e61991.
44. Liu, S.; Cheng, X.Y.; Wang, F.; Liu, C.F. Acid-sensing ion channels: Potential therapeutic targets for neurologic diseases. *Transl. Neurodegener.* **2015**, *4*, 10.
45. Chen, C.C.; Wong, C.W. Neurosensory mechanotransduction through acid-sensing ion channels. *J. Cell Mol. Med.* **2013**, *17*, 337–349.
46. Pedrozo, Z.; Criollo, A.; Battiprolu, P.K.; Morales, C.R.; Contreras-Ferrat, A.; Fernandez, C.; Jiang, N.; Luo, X.; Caplan, M.J.; Somlo, S.; et al. Polycystin-1 is a cardiomyocyte mechanosensor that governs l-type Ca<sup>2+</sup> channel protein stability. *Circulation* **2015**, *131*, 2131–2142.
47. Sharif-Naeini, R.; Folgering, J.H.; Bichet, D.; Duprat, F.; Lauritzen, I.; Arhatte, M.; Jodar, M.; Dedman, A.; Chatelain, F.C.; Schulte, U.; et al. Polycystin-1 and -2 dosage regulates pressure sensing. *Cell* **2009**, *139*, 587–596.
48. Kathem, S.H.; Mohieldin, A.M.; Nauli, S.M. The roles of primary cilia in polycystic kidney disease. *AIMS Mol. Sci.* **2014**, *1*, 27–46.
49. Upadhyay, V.S.; Muntean, B.S.; Kathem, S.H.; Hwang, J.J.; Aboualaiwi, W.A.; Nauli, S.M. Roles of dopamine receptor on chemosensory and mechanosensory primary cilia in renal epithelial cells. *Front. Physiol.* **2014**, *5*, 72.

## Chapter 5. Sensory primary cilium is a responsive cAMP microdomain in renal epithelia.\*

### Abstract

Primary cilia are hair-like cellular extensions that sense microenvironmental signals surrounding cells. The role of adenylyl cyclases in ciliary function has been of interest because the product of adenylyl cyclase activity, cAMP, is relevant to cilia-related diseases. In the present study, we show that vasopressin receptor type-2 (V2R) is localized to cilia in kidney epithelial cells. Pharmacologic inhibition of V2R with tolvaptan increases ciliary length and mechanosensory function. Genetic knockdown of V2R, however, does not have any effect on ciliary length, although effect of tolvaptan on ciliary length is dampened. Our study reveals that tolvaptan may have a cilia-specific effect independent of V2R or verapamil-sensitive calcium channels. Live-imaging of single cilia shows that V2R activation increases cilioplasmic and cytoplasmic cAMP levels, whereas tolvaptan mediates cAMP changes only in a cilia-specific manner. Furthermore, fluid-shear stress decreases cilioplasmic, but not cytoplasmic cAMP levels. Our data indicate that cilioplasmic and cytoplasmic cAMP levels are differentially modulated. We propose that the cilium is a critical sensor acting as a responsive cAMP microcompartment during physiologically relevant stimuli.

---

\* Sherpa RT, Mohieldin AM, Pala R, Wachten D, Ostrom RS, Nauli SM. Sensory primary cilium is a responsive cAMP microdomain in renal epithelia. *Sci Rep.* 2019 Dec 25;9(1):6523.

## Introduction

The cilium is a dynamic structure that acts as a mechanosensory appendage of the cell and is involved in the pathogenesis of polycystic kidney disease (PKD)<sup>1-4</sup>. The hair-like cilium extends from epithelial lining cells into the lumen and bends upon fluid shear stress, triggering an influx of calcium<sup>3-7</sup>. It has previously been shown that the functional efficiency of the cilia depends on the length; i.e., longer cilia can detect a lower magnitude of shear stress and elicit a larger increase in calcium influx<sup>8-10</sup>. Structural defects of the cilium, such as in intra-flagellar transport protein 88 (IFT88) deletion resulting in shortened cilia, cause ciliopathy phenotype in PKD mouse models<sup>1</sup>. Likewise, functional defects of the cilium, such as dysfunctional polycystins proteins (PC1 or PC2), cause polycystic kidneys<sup>2-4,11,12</sup>. Both PC1 and PC2 form a mechanosensory complex in the cilium, which upon bending modulates calcium fluxes<sup>13,14</sup>.

Similar to calcium, cyclic adenosine monophosphate (cAMP) is a second messenger involved in different signaling pathways. Studies have shown that increasing cAMP levels in cystic epithelial cells, via either adenylyl cyclase (AC) activation or addition of membrane-permeable cAMP analogs, enhances cyst formation and/or cyst enlargement. The cAMP-mediated cystogenic effect has been observed in *in vitro* cultures obtained from murine models and intact cysts excised from PKD patients<sup>15-17</sup>. Arginine vasopressin (AVP), the endogenous antidiuretic hormone, is also observed to aggravate the cystic phenotype as it raises cAMP levels by vasopressin activating receptor type 2 (V2R), a G protein-coupled receptor (GPCR). Activation of V2R induces an intracellular cAMP increase, leading to the insertion of aquaporin 2 (AQP2) into the apical membrane and regulation of body fluid homeostasis<sup>18,19</sup>. Strategies focusing on blocking vasopressin action have shown reduced cystogenesis in murine models of PKD<sup>20-25</sup>. Polycystic Kidney (PCK) rats develop progressive cystic enlargement of the kidneys and hepatic histologic abnormalities that resemble human autosomal dominant PKD<sup>26</sup>. Using this model, Wang et. al. evaluated renal cyst development in the PCK rats without circulating vasopressin. PCK rats were crossed with Brattleboro (AVP<sup>-/-</sup>) rats and in the resulting PCK AVP<sup>-/-</sup> rats, renal cAMP levels were lowered along with a marked reduction in renal cysts<sup>23,27</sup>. The promising results of preclinical data have spurred interest in pursuing V2R antagonists as a prospective treatment for PKD<sup>23-25</sup>. Clinical trials have shown that tolvaptan, a V2R antagonist, is effective in decreasing cyst growth and in slowing the decline of renal function<sup>28-32</sup>

Cyclic AMP is a ubiquitous second messenger, produced by AC activation upon binding of ligands to GPCR coupled to Gs. Thus, cAMP regulates a wide range of cellular processes, ranging from gene regulation to immune function<sup>33</sup>. Previous studies have demonstrated that increasing intracellular cAMP levels, through the addition of forskolin or a cell-permeable cAMP analog, causes an increase in ciliary length of renal epithelia<sup>34,35</sup>. Consistent with this finding, forskolin or a cell-permeable cAMP analog also increases ciliary length in vascular endothelia<sup>36</sup>. Interestingly, forskolin or a cell-permeable cAMP has a minimal effect in serum-deprived synoviocytes<sup>37</sup>. Furthermore, inhibition of ciliary-localized adenylyl cyclase 3 (AC3) induces primary cilia elongation in synoviocytes<sup>37</sup>. However, the effect of tolvaptan in modulating ciliary length through cAMP has never been evaluated. Moreover, the dynamic level of cilioplasmic and cytoplasmic cAMP has not been previously examined with a targeted sensor. Given the potential treatment of tolvaptan and the role of cilia in PKD, we sought to characterize the effect of tolvaptan on ciliary length and ciliary cAMP signaling.

We show that tolvaptan increases ciliary length and enhances mechanosensitivity in response to shear stress. We also show that V2R and AC3 are localized in renal epithelial cilia. Monitoring cAMP levels in the cilioplasm after stimulation with tolvaptan revealed that the cilium is a distinct cAMP microdomain. Changes in cilioplasmic cAMP levels were found to be distinct and independent from cytoplasmic level of cAMP. Furthermore, shear stress decreased cilioplasmic, but not cytoplasmic cAMP below basal levels. We therefore hypothesize that primary cilia are chemosensitive and mechanosensitive organelles that form dynamic cAMP microdomain distinct from cell body.

## **Materials and Methods:**

### 1. Reagents and antibodies

For cell culture, Dulbecco's Modified Eagle Medium (DMEM), trypsin, penicillin-streptomycin solution, phosphate buffered saline (PBS), Dulbecco's Phosphate-Buffered Saline (DPBS) and were acquired from *Corning* (Manassas, VA). Fetal bovine serum (FBS) was obtained from *Seradigm* and Dulbecco's phosphate buffered saline (DPBS) from *HyClone* (Logan, UT). Sucrose,

Triton-X and Adenosine 5'-triphosphate Disodium (ATP) Salt were purchased from *Fisher Scientific* (Fair Lawn, NJ) and paraformaldehyde (PFA) from *Electron Microscopy Services* (Hatfield, PA). Propidium iodide (PI) from obtained from *Biotium* (Fremont, CA), forskolin from *BioVision* (Milpitas, CA), verapamil (Ver) from *Sigma-Aldrich* (Milwaukee, WI), tolvaptan (Tvp) from *AK Scientific* (Union City, CA) and arginine vasopressin (AVP) was purchased from *Bachem* (Torrance, CA). Laemmli 2X sample buffer was obtained from *BioRad* (Hercules, CA), cOmplete Protease Inhibitor Cocktail from *Roche* (St. Louis, MO) and Western blot visualization kit was obtained from *Thermo Scientific* (Rockford, IL). Nonfat dry milk was purchased from *LabScientific* (Livingston, NJ). Primary antibodies, acetylated- $\alpha$ -tubulin was acquired from *Abcam* (Cambridge, MA),  $\beta$ -actin from *Cell Biolabs* (San Diego, CA) and V2R antibody from *EMD Millipore* (Billerica, MA). Previously validated adenylyl cyclase 2, 3, 4, 5/6, 7, 8 and 9 antibodies were obtained from *Santa Cruz Biotech* (Santa Cruz, CA)<sup>80</sup>. The secondary antibodies, fluorescein anti-mouse, texas-red anti-rabbit and mounting media with DAPI were purchased from *Vector Laboratories* (Burlingame, CA).

## 2. Cell culture

Porcine renal epithelial cells from proximal tubule (LL-CPK1), dog epithelial cells from inner medullary collecting duct (IMCD), and mouse vascular endothelial (ET) cells were cultured to a confluent monolayer in DMEM supplemented with 10% FBS at 37°C in 5% CO<sub>2</sub>. In some experiments, LL-CPK1 cells were also grown on Corning Transwell permeable supports to induce polarization for receptor localization studies and allow antibody access to the basal membrane. ET and LL-CPK1 cells have been previously described in detail<sup>5,81</sup>. Once differentiated, different concentrations of tolvaptan or vasopressin was added to culture plates. Concentration for tolvaptan was determined to be 0.1  $\mu$ M based on the optimal ciliary length increase based on dose-response studies, whereas a vasopressin concentration of 10  $\mu$ M was selected because it maximally increases cAMP levels<sup>82</sup>. Verapamil was added to cells at a final concentration of 2  $\mu$ M for 10 minutes before drug treatment<sup>83</sup>. The drugs were mixed in starvation medium (DMEM with 2% FBS) and cells were incubated for another 20 hours. Vehicle alone (PBS containing 0.0005% DMSO) was used as a control groups to account for the DMSO concentration in both tolvaptan and vasopressin working solutions.

### 3. FACS analysis

Florescent-activated cell sorting (FACS) was used to investigate a possibility of an effect on cell division by tolvaptan (0.1  $\mu\text{M}$ ). Cells were harvested with and without drug treatment. Cells were then fixed using 70% ethanol and incubated with propidium iodide (PI), a DNA-intercalating fluorescent molecule, for 30 minutes at 37°C. Cell division analysis was carried out with flow cytometry BDFacsverse with BD FACsuite software.

### 4. Immunofluorescent staining

Cells were fixed for 10 minutes (4% PFA/2% sucrose in PBS) and permeabilized for 5 minutes (10% Triton X-100). Acetylated  $\alpha$ -tubulin (1:10,000 dilution in PBS) and fluorescein isothiocyanate (FITC)-conjugated secondary (1:1000 dilution in PBS) antibodies were each incubated with the cells for 1 hour at 37°C. For V2R visualization, V2R antibody (1:10,000 dilution in PBS) and texas-red conjugated anti-rabbit antibody were applied for 1 hour each at 37°C. All adenylyl cyclase (AC) antibodies were used at a 1:1,000 dilution, and incubated with appropriate texas-red conjugated secondary antibody for 1 hour each at 37°C. Slides were then mounted with dapi hard set mounting media (*VectorLabs*, Burlingame, CA). Nikon Eclipse Ti-E inverted microscope or Nikon Confocal microscope with NIS-Elements imaging software (version 4.30) was used to capture images of primary cilia. Automated image acquisition was conducted in large image scan mode at 100 $\times$  magnification and Z-stacks of 0.1  $\mu\text{m}$  thickness. All images are shown as maximum intensity projections except confocal generated images or stated otherwise.

### 5. Flow-induced cytosolic calcium imaging

Cells were grown on glass-bottom plates. After treatment with the appropriate drug, the cells were incubated with 5  $\mu\text{M}$  Fura-2 AM (*TEFLabs*, Austin, TX) at 37°C for 30 minutes. After washing with DPBS, the cells were observed under a 40 $\times$  objective lens with a Nikon Eclipse Ti-E microscope. Fura-2 fluorescence images at excitation of 340/380 nm and emission of 510 nm were recorded. After equilibration under the microscope for 20 minutes, baseline calcium was recorded for 2 minutes and experimental data were acquired. Fluid-shear stress was then applied to cells with an Instech P720 peristaltic pump. The perfused fluid was pumped into the cell culture dish and retained at a shear stress of 1 dyne/cm<sup>2</sup> (for epithelial cells) or 8 dyne/cm<sup>2</sup> (for endothelial cells) with a constant flow rate of about 20 or 160  $\mu\text{l}/\text{sec}$ , respectively. At the end of each

experiment, the maximum calcium signal was obtained by perfusion of ATP (10  $\mu$ M) to confirm cell viability. In addition to autofluorescence, both minimum and maximum fluorescence was collected as previously described<sup>84</sup>. Conditions for all experiments were maintained at 37°C and 5% CO<sub>2</sub> in a stage top cage incubator (okoLab, Burlingame, CA). Calcium analysis was then followed a standard calculation as previously described<sup>84</sup>.

#### 6. Generation of V2R-knockdown in renal epithelial LL-CPK1 cells

Arginine vasopressin receptor type-2 (AVPR2 or V2R) targeting shRNA construct (5'-ATC GCC TTG ATG GTG TTT GTG GCA CCT GC-3': pAVP2Ra-C-shLenti) in a lentivirus backbone vector (TL513450) was ordered from Origene. Viral particles were generated in HEK cells using shRNA lentiviral packaging kit (TR30022) and passed through a 0.45-micron filter to remove cell debris. For transduction, epithelial cells were incubated with the collected viral particles and Polybrene (8 ug/ml; EMD Millipore).

For Western blot, total cell lysate was analyzed by SDS-PAGE on a 10% SDS-polyacrylamide gel. After separation, a semi-dry transfer was done using Bio-Rad system. The anti-V2R (1:1000 dilution) and anti- $\beta$ -actin (1:500 dilution) antibodies were incubated with the PVDF (Polyvinylidene difluoride) membrane. Each incubation was done at 4°C overnight. For visualization, horse radish peroxidase (HRP)-conjugated secondary antibodies anti-mouse (1:1000 dilution) or anti-rabbit (1:1000 dilution) were used. For dot blot experiment, cell or ciliary proteins were extracted in RIPA buffer with protease inhibitor. A 3  $\mu$ l of sample extract was spotted onto a nitrocellulose membrane. After drying the membrane, it was blocked in 5% BSA (bovine serum albumin; *Promega*) for 1 hour. Incubation with V2R antibody (1:1000 dilution) was done for 30 minutes at room temperature. The membrane was then incubated with an HRP conjugated anti-rabbit antibody for 30 minutes at room temperature. For both Western and dot blots, the membrane was incubated with ECL (Enhanced Chemiluminescent; *Thermo Scientific*) for 1 minute. Visualization of the protein signal was done in Bio-Rad Image analysis and imager.

#### 7. Cilia isolation

Cells were plated on 100 mm dishes (6 for each cell line) with 10% FBS supplemented DMEM at 37°C in 5% CO<sub>2</sub>. Cells were grown for 7 days and were starved overnight for differentiation as



outlined above in cell culture methods. Cells were rinsed gently with PBS for a brief period and 10 ml of PBS was added. The dish was then placed on a rotary shaker (*ThermoFisher Scientific* MaxQ 2508) and shaken for 4 minutes at 360 rpm, resulting in a shear stress of 10 dyn/cm<sup>2</sup>. PBS was collected and transferred to a 50 ml centrifuge tube and spun for 10 minutes at 1,000 xg at 4°C. After discarding the pellet, the supernatant was spun down in an ultracentrifuge (*ThermoFisher Scientific* Sorvall WX 100+ Ultracentrifuge) with a fixed angle rotor (*ThermoFisher Scientific*, T-647.5) at 40,000 xg for 45 minutes at 4°C. After discarding the supernatant, the remaining pellet containing primary cilia, was resuspended in either RIPA buffer or resuspension buffer as previously discussed<sup>43,44</sup>.

#### 8. cAMP imaging and quantification

Intracellular cyclic AMP (cAMP) was quantified using ELISA and live-cell imaging. The cAMP ELISA Kit from *Cayman Chemical* (Cat. No. 581001) was used to measure total cAMP from cell population. Samples were lysed according to manufacturing instructions in a 96-well plate format. After primary incubation for 18 hours, the plate was developed and read at 415 nm on a spectrophotometer.

For cAMP live-cell imaging, we tested both pc3.1-SSTR3-mICNBD-FRET and 5HT6-mCherry-cADDIs. The generation of pc3.1-SSTR3-mICNBD-FRET and 5HT6-mCherry-cADDIs have been previously described<sup>85,86</sup>. While both constructs worked fine in response to forskolin, we chose to use 5HT6-mCherry-cADDIs for the rest of our studies to obtain a relatively better transfection in our cell line. Of note is that pc3.1-SSTR3-mICNBD-FRET was introduced to the cells with chemical transfection (jetPRIME; *Polyplus*), whereas Baculovirus transduction was utilized to express 5HT6-mCherry-cADDIs (#D0211G; *Montana Molecular*). 2x10<sup>5</sup> cells were plated in 6 well plates and grown in conditions described above for 3 days. Baculovirus mediated transduction was then performed using a final concentration of 5x10<sup>5</sup> VG (viral genes)/ml and 4 mM sodium butyrate. 12 hours after initiation of viral transduction media was replaced with starvation media and incubated for another 16 hours before imaging. To enable us to monitor cilia and cell body concurrently, we used side-view imaging as previously described<sup>51</sup>. After infection, baseline fluorescence was examined for each cell. Those cells expressing the cAMP sensor in the cilia were used in our studies. In addition to cilia specific cAMP sensor, a global cytosolic sensor (#U0200R; *Montana Molecular*) was also used to validate our imaging system.



Fluorescence readings were taken on individually for mCherry and cADDIs (cAMP difference detector in situ) at excitation/emission wavelengths of 590/610 and 490/510 nm, respectively. A set of mCherry and cADDIs images were captured at 0.8 frames per second. The mCherry signal was used to correct fluorescence artifact. Because cADDIs is a downward cAMP reporter with a constant mCherry fluorescence, the mCherry/cADDIs ratio therefore depicted intracellular cAMP level and was used to quantify changes in cilioplasmic and cytoplasmic cAMP. For ease of understanding, the cADDIs signal was inverted to represent a direct relationship between cAMP level and cADDIs intensity in our figures (1/cADDIs). Time-lapse recordings were acquired on NIS-Elements imaging software (version 4.30) and fluorescence intensities were measured for the duration of the experiment.

## 9. Data analysis

All data are reported as a mean  $\pm$  standard error of mean (s.e.m). Statistical analysis was performed using ANOVA (analysis of variance) followed by Bonferroni post-hoc test or two way ANOVA when two factors were present followed by Sidak's multiple comparison test. Power analysis was determined from the coefficient variant. When our coefficient variant was above 15%, the number of experimental and corresponding control groups was increased. Because in all our studies both control and experimental groups were run in parallel, our control and experimental values represented matched number of observations. In some cases, all experimental groups (including the corresponding controls) were analyzed with the post-hoc test. In other cases, only selected pairs (control vs. experimental groups) were tested. Most of our statistical analyses were performed with *GraphPad Prism v.7* software. In some cases, Microsoft Excel v.15.4 was used for regression analyses. Linear regression was performed to obtain a standard calibration curve and linear equation. In this case, the analysis was done with the ordinary least squares (OLS) regression of  $y$  on  $x$ . A non-linear logarithmic regression was used to fit the sigmoidal trend-curve to show dose-response relationship. Asterisks (\*) denote statistically significant differences at various probability levels ( $P$ ). The  $P$  values of the significant differences are indicated in the figure legends.

When image analyses were done on fixed-specimen, images were taken at different focal planes (z-stack). If needed, a 3-dimensional image was constructed from the XY planes to validate XZ and YZ field for completion of analysis or measurement. Automated image acquisition with a thickness of 0.1  $\mu\text{m}$  were taken with Nikon A1R Confocal microscope and NIS-Elements imaging software v.4.30. This system was also used for image analyses (3D object reconstruction, image segmentation, etc.). For live-imaging, Nikon Eclipse Ti-E inverted microscope and Nikon NIS Element for Advanced Research software were used for image acquisition and analyses. Our live-imaging system with controlled environmental chamber allowed more flexibility for various excitation and emission spectra from a fast wavelength exchanger DG4/5 mirror reflection system. Images were not enlarged during image analysis to avoid a false empty magnification. Ciliary length measurements were done using the measurement tool in NIS-Elements imaging software on maximum intensity projections obtained from immunofluorescent images. All representative images and video frames are presented with scale bars to indicate the actual image reduction size at 0.8 frames per seconds (fps). Before Fura-2 experiments, a brightfield image focused on cell borders was obtained. Using intensity thresholds, a binary layer was created and overlaid with the Fura-2 images to create our representative images.

Free cytosolic calcium (Cyt  $\text{Ca}^{2+}$ ) concentrations were calculated with the formula  $[\text{Cyt } \text{Ca}^{2+} = K_d \times [(R - R_{\text{min}})/(R_{\text{max}} - R)] \times (F_{\text{max}}/F_{\text{min}})]$ , where  $K_d$  denotes the apparent dissociation constant of the Fura-2 indicator (145 nM),  $R$  is a ratio of 510 nm emission intensity with excitation at 340 and 380 nm, and  $R_{\text{max}}$  and  $R_{\text{min}}$  are fluorescence intensity ratios for the calcium-bound and calcium-unbound Fura-2 with excitation at 340 and 380, respectively. We determined the  $R_{\text{max}}$  and  $R_{\text{min}}$  values to be stable and independent of cell type.  $F_{\text{max}}$  and  $F_{\text{min}}$  were the fluorescence intensity values of Fura-2 with excitation at 380 nm under the same conditions. The calcium level was radiometrically calculated.  $R_{\text{min}}$  and  $R_{\text{max}}$  values denote the minimum and maximum radiometric signal ratios, respectively. At the end of each experiment, the minimum fluorescence ( $R_{\text{min}}$ ) was obtained by incubating the cells in calcium-free solution that contained 2 mM EGTA and 10  $\mu\text{M}$  ionomycin at pH 8.6 to optimize the ionomycin effect. After the minimum signal ratio was determined, the cells were incubated with excess calcium (10 mM) to obtain the maximum signal ratio ( $R_{\text{max}}$ ). Signal intensities were collected from individual cells, as well as from the

whole cell population/monolayer. All the fluorescence measurements were corrected for autofluorescence. Calcium analysis was then followed a standard calculation as previously described<sup>84</sup>.

## Results

### Tolvaptan increases ciliary length and enhances shear-stress induced cytosolic calcium increase.

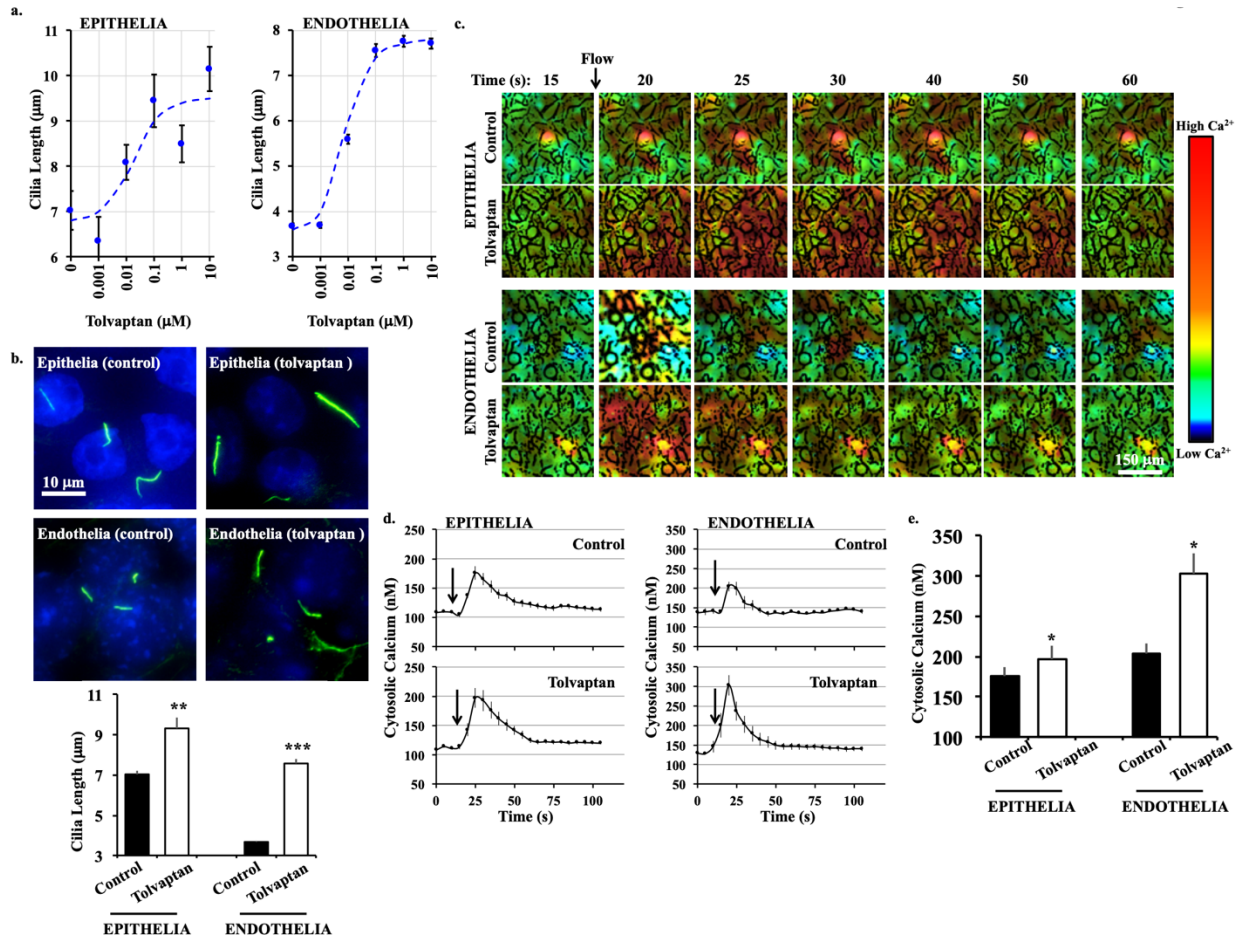


Figure 24. Tolvaptan increases cilia length and enhances mechanosensitivity. (a) Dose-response relationship between different concentrations of tolvaptan and ciliary length is shown in the Sigmoidal plot. Distribution of ciliary length for individual tolvaptan concentration is shown in Figure 25. (b) Representative immunostaining images of epithelial and endothelial cells treated without (control, vehicle) and with tolvaptan (0.1 μM) for 24 hours. Cilia (acetylated-α-tubulin) are shown in green and nucleus in blue. Corresponding bar graphs show ciliary length averages. (c) Time-lapse images represent the intracellular calcium level in response to fluid-shear stress (arrow) by epithelial and endothelial cells treated without (control, vehicle) and with tolvaptan (0.1 μM). Color bar indicates intracellular calcium level from low (black) to high (red). Corresponding brightfield images are shown in Figure 25. (d) Averaged intracellular calcium levels are plotted across time in second (s). Arrows indicate the start of fluid-shear stress. (e) Bar graph shows averaged intracellular calcium peak induced by fluid-shear. N=3 experiments

for each group. For each N, a minimum of 50 cells were analyzed. \* P<0.05, \*\*P<0.001, and \*\*\*P<0.0001 compared to the corresponding control groups.

To determine if tolvaptan could alter the ciliary length, we measured the ciliary length distribution in epithelial and endothelial cells after treatment with different concentrations of tolvaptan (Figure 25). Tolvaptan-treatment resulted in a dose-dependent increase in ciliary length in renal epithelial cells. The effect was maximal at 0.1  $\mu$ M and reached a steady-state at higher concentrations (Figure 24a, b). In renal epithelial cells, average ciliary length was  $7.05 \pm 0.15 \mu\text{m}$ . When treated with 0.1  $\mu$ M tolvaptan, ciliary length increased to  $9.34 \pm 0.51 \mu\text{m}$ . In vascular endothelial cells, which generally have shorter cilia than epithelial cells, ciliary length increased from  $3.67 \pm 0.06 \mu\text{m}$  to  $7.56 \pm 0.14 \mu\text{m}$  after treatment with tolvaptan.

Both epithelial and endothelial cilia function as mechanosensory organelles by increasing intracellular calcium in response to fluid-shear stress<sup>4-7</sup>. To test whether the increase in ciliary length translated to enhanced mechanosensitivity, cytosolic calcium levels in response to shear stress were measured with Fura-2 (Figure 24c & 25). After baseline measurement, cells were subjected to shear stress. Pre-treatment with tolvaptan significantly enhanced the calcium response to fluid flow in both epithelial and endothelial cells (Figure 24d, e). These results show that tolvaptan increases ciliary length and enhances cilia mechanosensitivity.

The cilia are also intertwined with the cell cycle and are usually resorbed during cell division<sup>38,39</sup>. We therefore examined if tolvaptan affected cell division using labeling with propidium iodide, a dye that binds stoichiometrically to DNA, to approximate the distribution of cells at different cell division stages. However, tolvaptan did not affect cell division stages in either epithelial or endothelial cells (Figure 25).

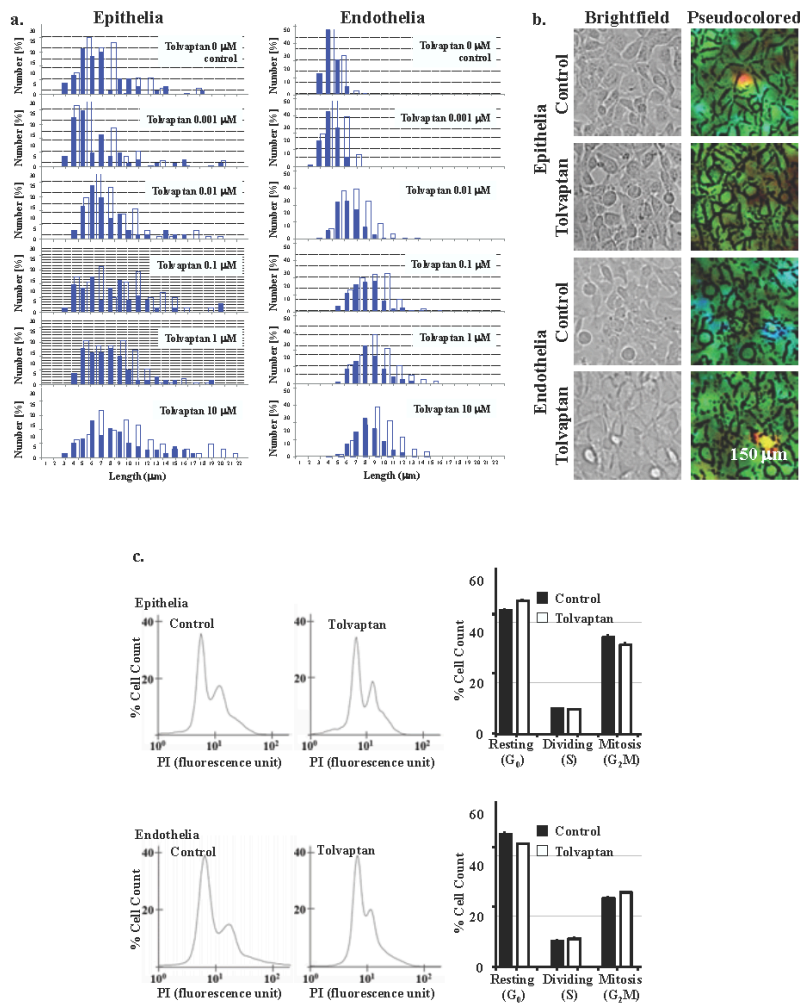


Figure 25. Tolvaptan increases ciliary length in the dose-dependent manner without affecting stages of cell division. (a) Ciliary length distribution in renal epithelial LL-CPK1 cells without (vehicle control) and with tolvaptan (1 nM to 10  $\mu$ M) treatment is shown in the histogram. Ciliary length (in  $\mu$ m) was plotted against the number of cells (in percent). 100 cells were randomly selected and measured from each preparation (N=3). (b) Before Fura-2 experiments, a brightfield image was obtained (left panel). Intensity thresholds were applied to create a binary layer highlighting cell border. The binary layer was overlaid with the Fura-2 images to create our representative images (right panel). (c) Flow cytometry analysis on cells without (vehicle control) and with tolvaptan (0.1  $\mu$ M) treatment was conducted in endothelia and epithelia with propidium iodide (PI). Averaged cell counts in each cell division stage are shown in bar graph. N=3 in each group and treatment.



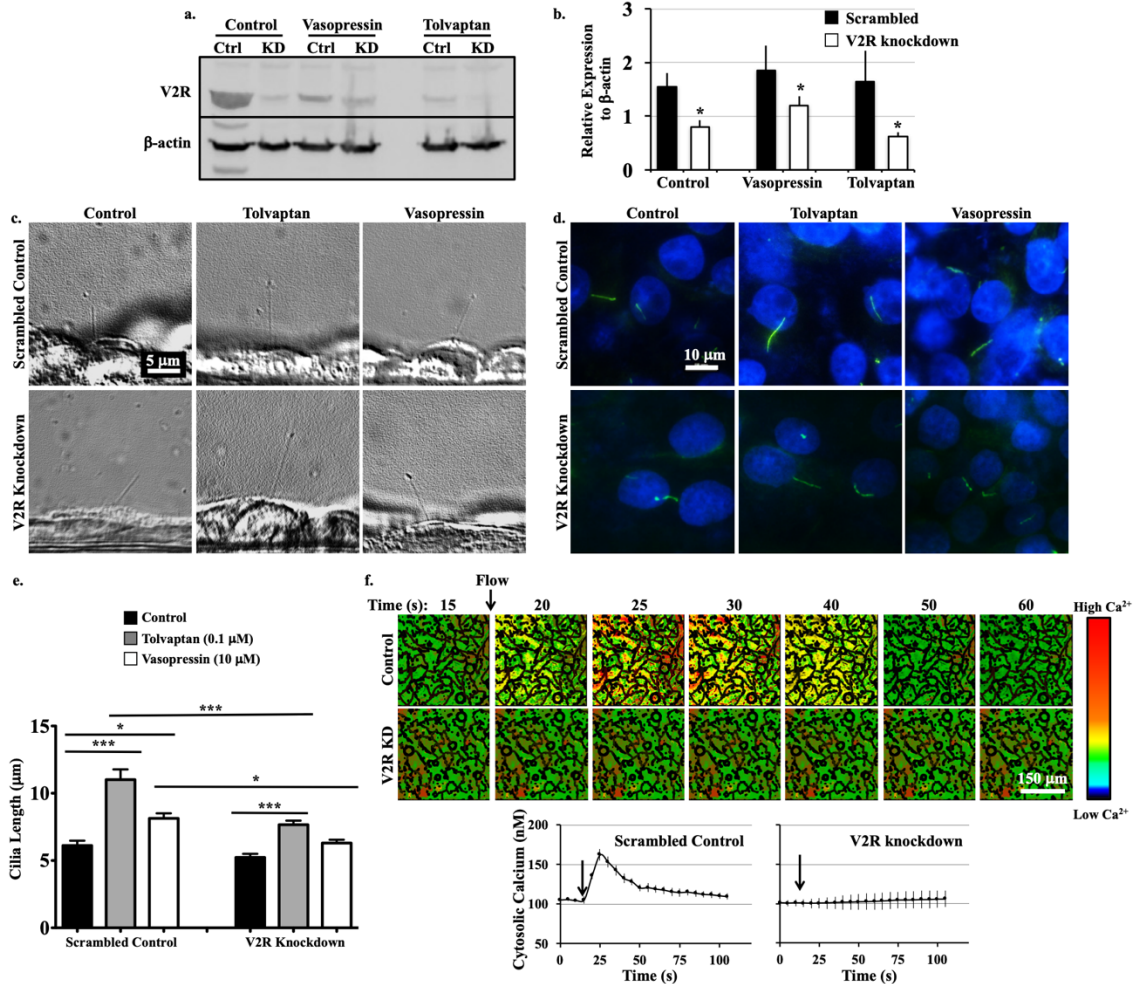


Figure 26. V2R modulates ciliary length and function. (a) Representative western blot image of scrambled control (Ctrl) and V2R-knockdown (KD) cells with vehicle (control), vasopressin (10  $\mu$ M) and tolvaptan (0.1  $\mu$ M) treatments. (b) Normalized V2R expression level is shown. Changes in ciliary length are observed from the phase contrast (side view, c) and immunostaining (top view, d) images. (e) Average ciliary length with two-way ANOVA was conducted on the influence of two independent variables i.e., cell type and type of treatment on the length of cilia. The cell type and treatment interaction were significant though it did not qualify the main effects,  $F(2, 533) = 5.009$ ,  $p < 0.01$ . Two-way ANOVA was followed by post hoc analysis with Sidak's multiple comparison test. (f) Time-lapse images represent intracellular calcium level in response to fluid-shear stress. Color bar indicates intracellular calcium level from low (black) to high (red). Averaged intracellular calcium levels are plotted across time in second (s). Arrows indicate the start of fluid-shear stress. Corresponding brightfield images are shown in Figure 27.  $N=3$  experiments for each group. For each  $N$ , a minimum of 50 cells were analyzed. \*  $P < 0.05$ , \*\*  $P < 0.001$ , and \*\*\*  $P < 0.0001$  compared to the corresponding control groups.

## Vasopressin receptor knockdown modulates ciliary length and function.

To further validate our results, we generated V2R-knockdown LL-CPK1 epithelial cells using lentiviral transfection. It has been reported that receptor activation or inhibition promotes receptor down-regulation<sup>38,39</sup>; thus, V2R expression was examined in cells with or without vasopressin (10  $\mu$ M) or tolvaptan (0.1  $\mu$ M) treatment for 24 hours (Figure 26a & 27). V2R expression was compared between V2R-knockdown cells and the corresponding scrambled control cells (Figure 26b). Ciliary length was determined in scrambled or V2R-knockdown treated cells in combination with addition of saline (control), tolvaptan, or vasopressin in live (Figure 26c) and fixed (Figure 26d) cells. Cilia in V2R-knockdown cells ( $5.23\pm 0.27$   $\mu$ m) appeared shorter than in scrambled control cells ( $6.11\pm 0.36$   $\mu$ m), but the difference was not significant (Figure 26e). Tolvaptan treatment caused a significant increase in ciliary length of both control cells ( $11.01\pm 0.76$   $\mu$ m) and V2R-knockdown cells ( $7.67\pm 0.30$   $\mu$ m). However, the increase was significantly less in the V2R-knockdown compared to controls. Cells treated with vasopressin displayed a significant increase in ciliary length in scrambled control cells ( $8.13\pm 0.38$   $\mu$ m vs.  $6.11\pm 0.36$   $\mu$ m in control), but not in V2R-knockdown cells ( $6.30\pm 0.25$   $\mu$ m vs.  $5.23\pm 0.27$   $\mu$ m in V2R-knockdown control).

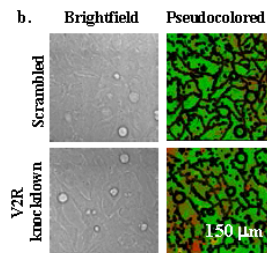
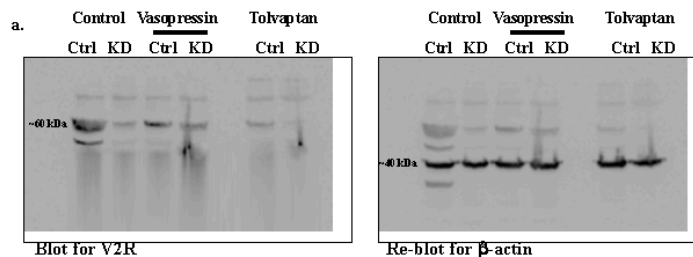




Figure 27. V2R knockdown cells show lower expression of receptor. (a) Using shRNA mediated silencing of strategy, V2R was knocked-down in LL-CPK1 cells (KD). The expression level of V2R was evaluated in response to vehicle (control), vasopressin (10  $\mu$ M) and tolvaptan (0.1  $\mu$ M) treatments in both scrambled control (Ctrl) and KD cells. Shown are full Western blot of V2R, in which the same membrane was reblotted for b-actin. (b) A brightfield image was obtained (left panel) to represent cells used in Fura-2 experiments of both scrambled and V2R-knockdown cells. Baseline Fura-2 intensity is shown for both cell lines with a binary layer highlighting cell border (right panel).

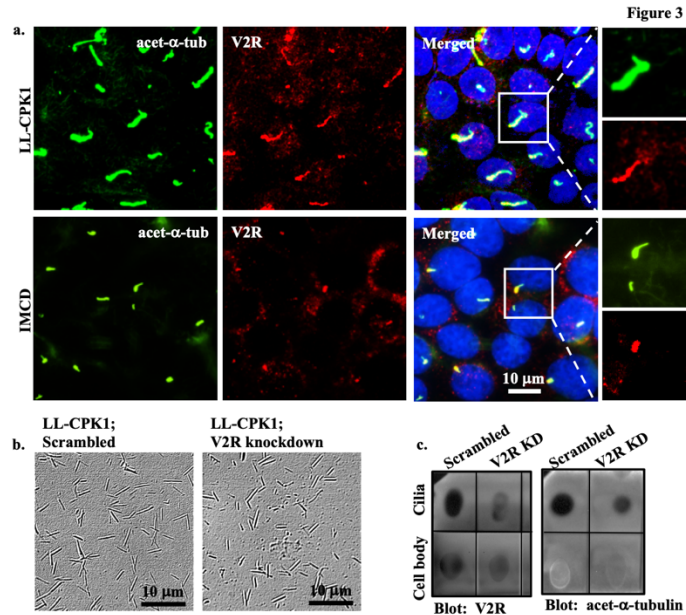


Figure 28. V2R is localized to primary cilia. (a) Confocal images of renal epithelial from pig (LL-CPK1) and dog (IMCD) show localization of V2R (red) at the base of cilia. Acetylated- $\alpha$ -tubulin (acet- $\alpha$ -tub) used as ciliary marker is shown in green and nucleus in blue. Maximum intensity projection images from accumulated z-stack for LL-CPK1 (scrambled and V2R-knockdown), IMCD and endothelial cells are shown in Figure 29 and 30. (b) Phase contrast images represent isolated cilia from scrambled control and V2R-knockdown LL-CPK1 cells. (c) Dot blot indicates the presence of V2R in both isolated-cilia and cell-body extracts. Isolated cilia extracts are confirmed by the presence of acetylated- $\alpha$ -tubulin.

To investigate the role of V2R-knockdown in fluid-sensing, calcium imaging in response to fluid flow was performed. Although the differences in ciliary length were negligible between the V2R-knockdown and control cells, the V2R-knockdown failed to show the characteristic peak of calcium influx upon fluid flow (Figure 26f & 27). Previous work has also shown that the V2R is

linked to calcium mobilization in rat IMCD cells, where activation of the V2 receptor results in a transient calcium increase, although the underlying mechanism has not been established<sup>40</sup>.

Next, immunolocalization was performed to reveal whether V2R localizes to primary cilia (Figure 28a). IMCD cells, which have been shown to contain V2R in the cilium, were used as a positive control<sup>41,42</sup>. In LL-CPK1, V2R localization was observed throughout the cilium and in IMCD cilium V2R was detected in the base of cilium (Figure 28a & 29). V2R-knockdown cells showed very little membrane localization of V2R (Figure 29). Because most endothelial cells did not show V2R localization to primary cilia (Figure 29), we only used LL-CPK1 in the remainder of our studies. Additionally, LL-CPK1 cells were grown on permeable supports and then used for immunolocalization. After scanning Z-stack images, XZ and XY planes were reconstructed which showed similar distribution of V2R in the apical and basolateral membrane (Figure 30).

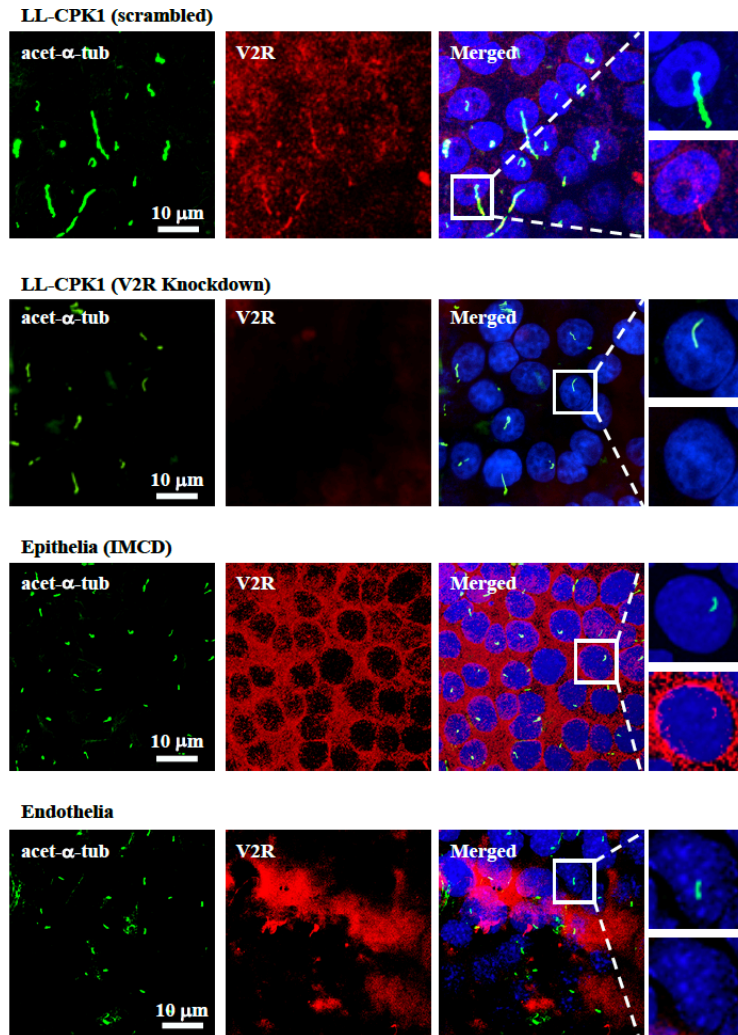


Figure 29. V2R is localized to primary cilia in renal epithelial cells. Renal epithelia from control LL-CPK1, V2R-knockdown LL-CPK1, IMCD and vascular endothelial cells were examined with ciliary marker acetylated- $\alpha$ -tubulin (acet- $\alpha$ -tub; green), V2R (red) and dapi (blue). Z-stack of confocal images at 0.1  $\mu$ m slices were taken, and a maximum intensity projection was obtained. Magnified view of single cell showing V2R (red) localization in the cilium (green) are on the rightmost panel.

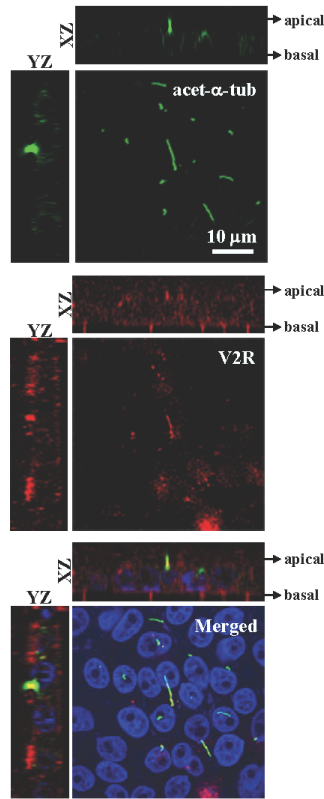


Figure 30. Apical and basolateral distribution of V2R in renal epithelial cells. Polarized LL-CPK1 cells grown on permeable support were examined with ciliary marker acetylated- $\alpha$ -tubulin (acet- $\alpha$ -tub; green), V2R (red) and dapi (blue). Z-stack of confocal images at 0.1  $\mu$ m increments were taken to create XZ and YZ axis plane. Apical and basal sides are labeled in the XZ view. The XY view shows a single focused plane of the cilia from the z-stack.

To further confirm the presence of V2R in the cilia, primary cilia were isolated using shear stress<sup>43,44</sup>. Isolated cilia from scrambled and V2R-knockdown cells were verified with a brightfield microscope (Figure 28b). Due to a low concentration of total protein collected in the isolated cilia extract, a dot blot was used (Figure 28c). The acetylated- $\alpha$ -tubulin blot was to indicate the purity of our cilia lysate and the corresponding V2R blot established that the V2R was associated with the cilia.

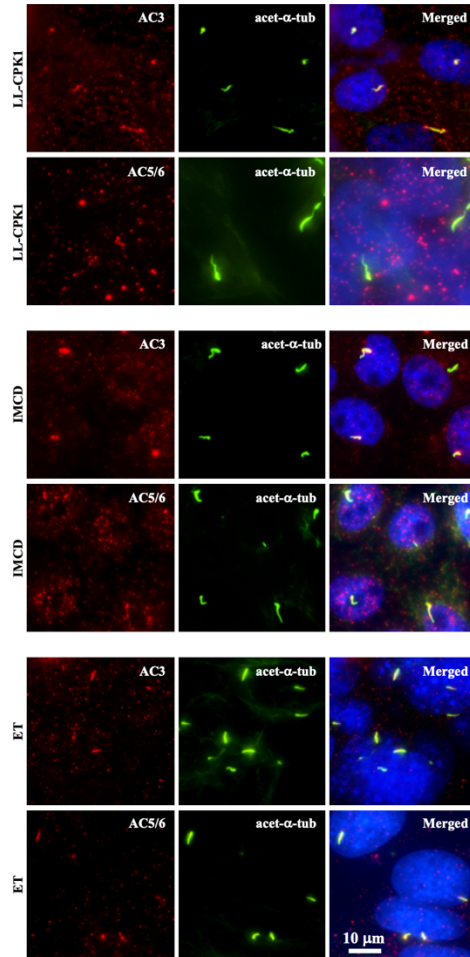


Figure 31. Adenylyl cyclase isoforms are differentially expressed to cilia in different cell lines. Adenylyl cyclase-3 (AC3; red) is localized to cilia in renal epithelial (LL-CPK1 and IMCD) and vascular endothelial (ET) cells (Figure 32 for an additional LL-CPK1 image). Adenylyl cyclase-5/6 (AC5/6; red) is localized to cilia in IMCD and ET cells, but not in LL-CPK1. Acetylated- $\alpha$ -tubulin (acet- $\alpha$ -tub) used as ciliary marker is shown in green and nucleus in blue. Additional images for other AC isoforms are shown in Supplementary Figure S5.

### Primary cilia are cAMP responsive microdomain.

V2R is a Gs-coupled GPCR, which activates AC and, thereby, increases intracellular cAMP levels<sup>45,46</sup>. AC3 has been reported to localize to neuronal primary cilia<sup>47,48</sup>, whereas AC5/6 are expressed in primary cilia of mouse renal epithelial and LL-CPK1 cells<sup>49,50</sup>. We analyzed AC expression in different cell lines and observed a differential expression pattern between the different AC isoforms (Figure 32). AC5/6 was not localized in cilia of LL-CPK1 cells, although

it was observed in IMCD and endothelial cilia (Figure 31). In contrast, AC3 was localized in cilia of LL-CPK1, IMCD, and endothelial cells (Figure 31 & 32).

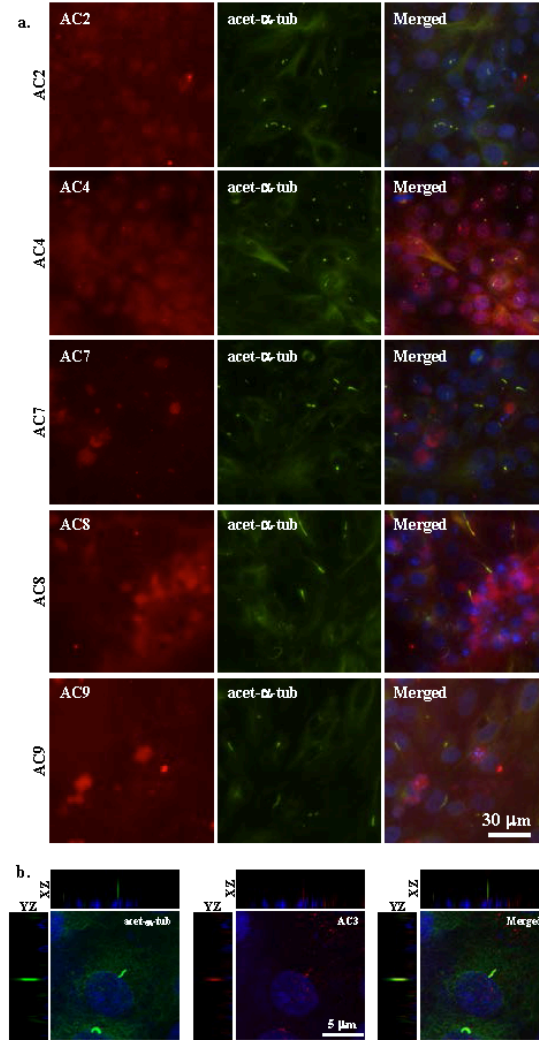


Figure 32. Among adenylyl cyclase (AC) isoforms-2, 3, 4, 7, 8 and 9 only AC3 is localized to the primary cilia of renal LL-CPK1 cells. (a) AC isoforms were examined for their ciliary immuno-localization. The first column of images shows AC isoforms (red) followed by ciliary marker acetylated- $\alpha$ -tubulin (acet- $\alpha$ -tub; green) and nucleus marker (merged; blue). (b) LL-CPK1 cells were examined with AC3 (red), ciliary marker acetylated- $\alpha$ -tubulin (acet- $\alpha$ -tub; green), and dapi (blue). Z-stack images at 0.1  $\mu$ m slices were taken and compiled to construct a 2D overlay, XZ and YZ axis views.

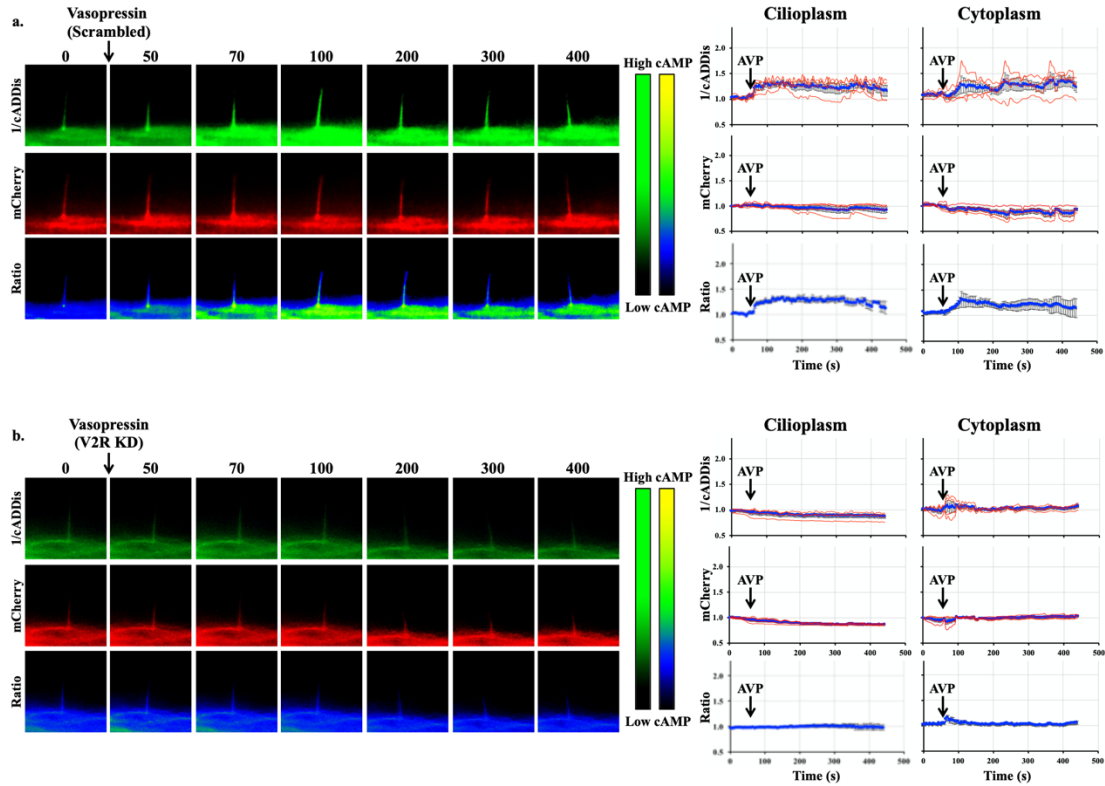


Figure 33. Vasopressin mediates cAMP signaling in cilia. Representative time-lapse images of 1/cADDIs, mCherry channels and Ratio (mCherry/cADDIs) with their corresponding line graphs showing cAMP levels in response to vasopressin (AVP) in (a) scrambled and (b) V2R-knockdown cells. Color bar on the left indicates cAMP level from low (black) to high (green) for 1/cADDIs channel. cAMP level from low (black) to high (yellow) are shown on the right color bar for the ratio images. Corresponding individual raw traces (red) and average signal (blue) are plotted in line graphs for 1/cADDIs, mCherry and ratio signals in the cilioplasm and cytoplasm. Arrows indicate stimuli. N=4 for each group.



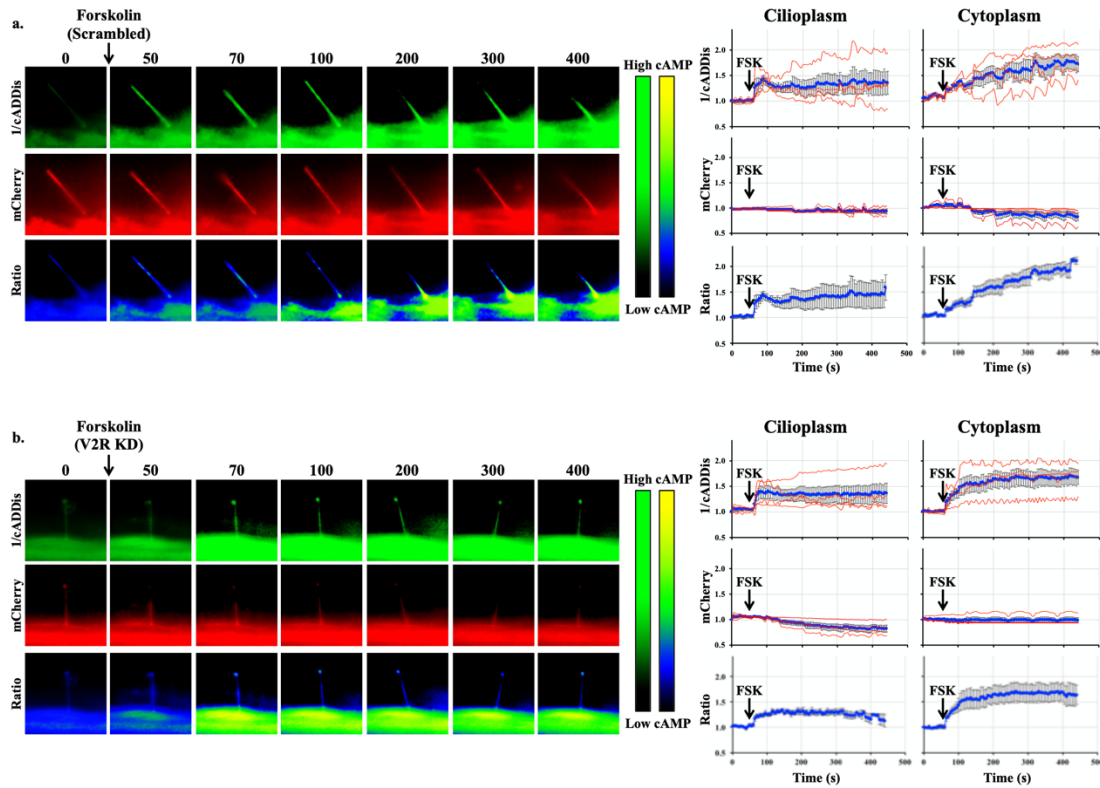


Figure 34. Forskolin increases cAMP level in cilioplasm and cytoplasm. Representative time-lapse images of 1/cADDIs, mCherry channels and Ratio (mCherry/cADDIs) with their corresponding line graphs showing cAMP levels in response to forskolin (FSK) in (a) scrambled and (b) V2R-knockdown cells. Color bar on the left indicates cAMP level from low (black) to high (green) for 1/cADDIs channel. cAMP level from low (black) to high (yellow) are shown on the right color bar for the ratio images. Corresponding individual raw traces (red) and average signal (blue) are plotted in line graphs for 1/cADDIs, mCherry and ratio signals in the cilioplasm and cytoplasm. Arrows indicate stimuli. N=4 for each group.



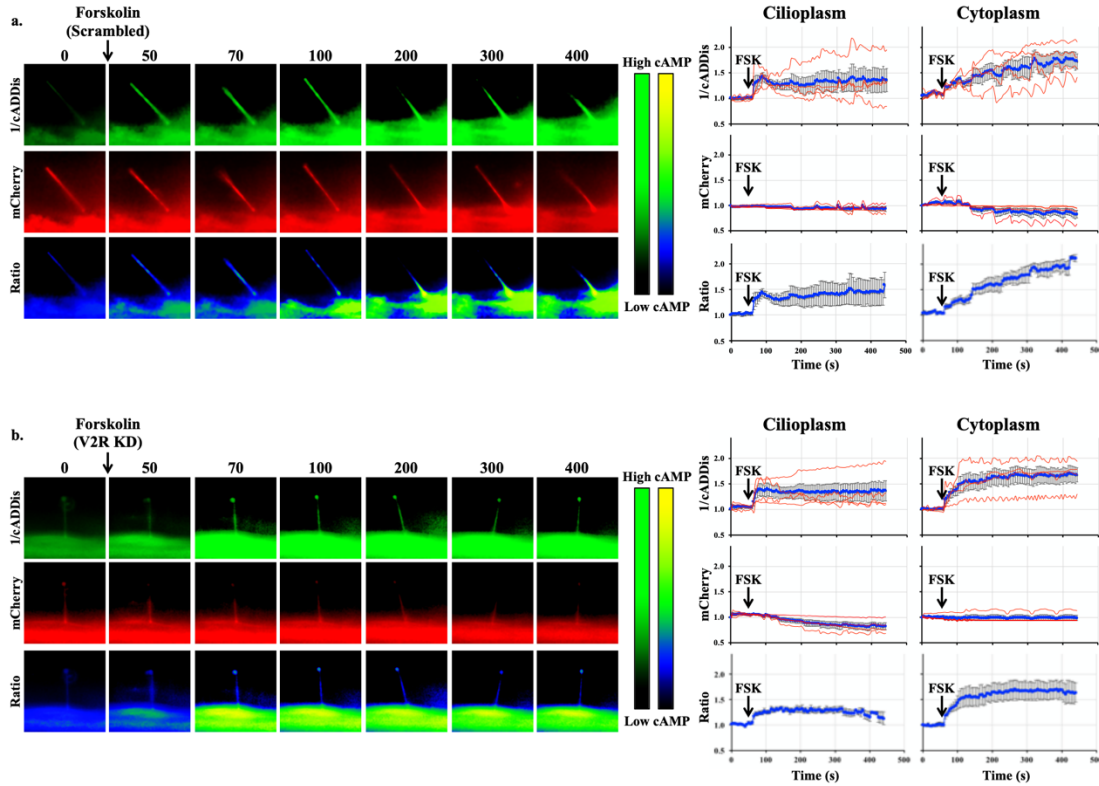


Figure 35. Tolvaptan increases cilioplasmic cAMP. Representative time-lapse images of 1/cADDis, mCherry channels and Ratio (mCherry/cADDis) with their corresponding line graphs showing cAMP levels in response to tolvaptan (Tvp) in (a) scrambled, (b) V2R-knockdown, and (c) verapamil-treated cells. Color bar on the left indicates cAMP level from low (black) to high (green) for 1/cADDis channel. cAMP level from low (black) to high (yellow) are shown on the right color bar for the ratio images. Corresponding individual raw traces (red) and average signal (blue) are plotted in line graphs for 1/cADDis, mCherry and ratio signals in the cilioplasm and cytoplasm. Arrows indicate stimuli. N=4 for each group.

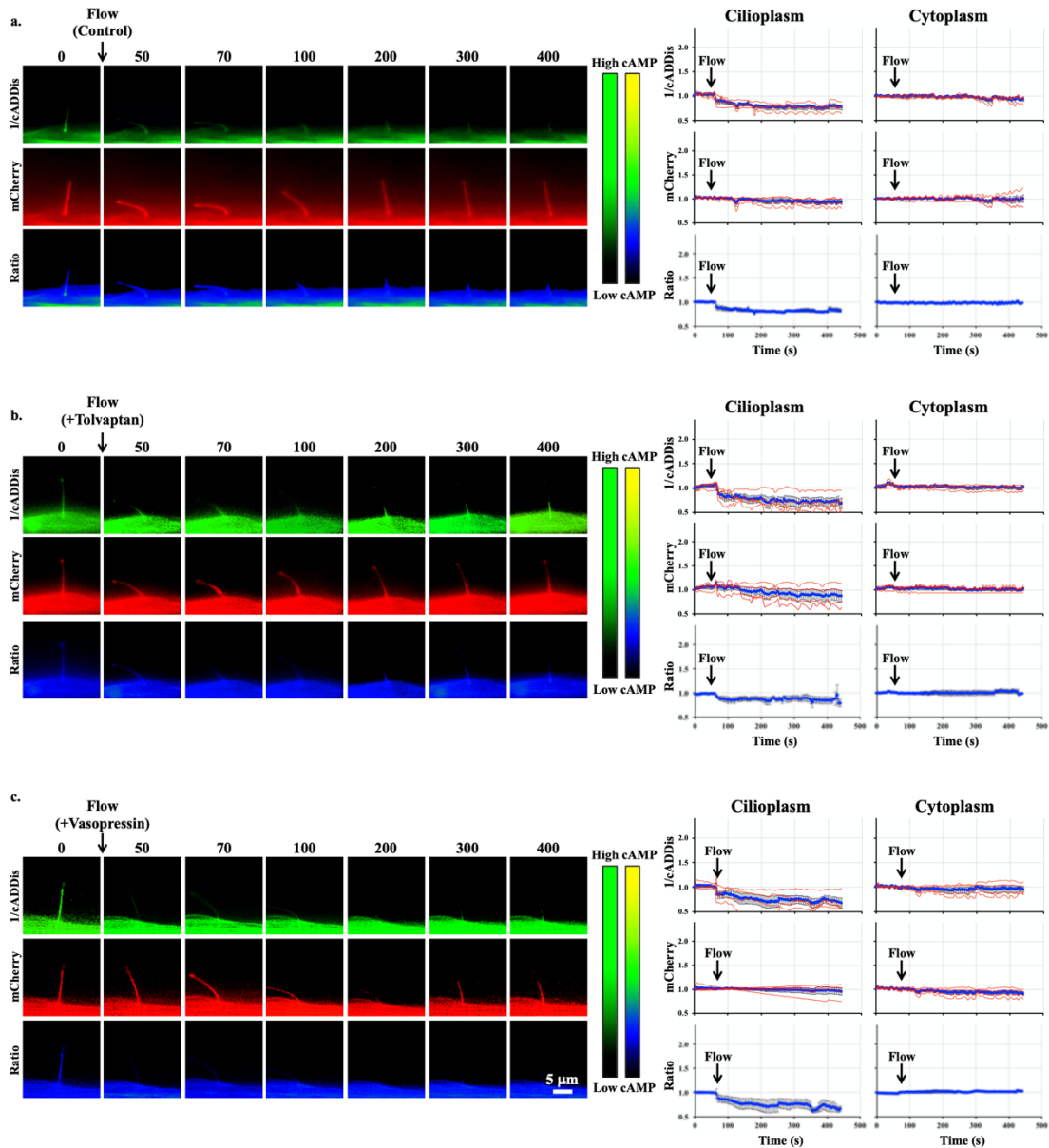


Figure 36. Flow decreases cilioplasmic cAMP level. Representative time-lapse images of 1/cADDis, mCherry channels and Ratio (mCherry/cADDis) in response to fluid-flow ( $1.0 \text{ dyne/cm}^2$ ) after treatment with (a) vehicle control, (b)  $0.1 \mu\text{M}$  tolvaptan (Tvp) or (c)  $10 \mu\text{M}$  vasopressin (AVP). Color bar on the left indicates cAMP level from low (black) to high (green) for 1/cADDis channel. cAMP level from low (black) to high (yellow) are shown on the right color bar for the ratio images. Corresponding individual raw traces (red) and average signal (blue) are plotted in line graphs for 1/cADDis, mCherry and ratio signals in the cilioplasm and cytoplasm. Arrows indicate stimuli. N=4 for each group.

Because cAMP measurement has traditionally been performed with a solid-phase enzyme immunoassay, we used this technique to measure cAMP levels after tolvaptan treatment or

induction of fluid-flow. Neither fluid flow nor tolvaptan treatment changed the cAMP levels, although a forskolin response was observed in both scrambled and V2R-knockdown cells (Figure 37). However, an immunoassay does not allow us to distinguish cilioplasmic from cytoplasmic cAMP changes. To monitor changes in ciliary cAMP levels, we used the ciliary-targeted cAMP sensor 5HT6-mCherry-cADDiS. We first confirmed that the kinetics between cilia-specific (5HT6-mCherry-cADDiS) and cytosolic (cAMP-cADDiS) reporters did not alter (Figure 37).

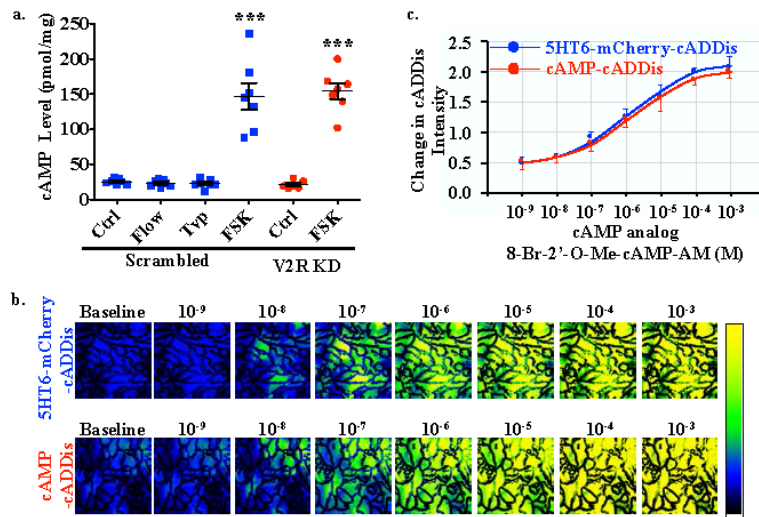


Figure 37. Global cAMP levels were measured using colorimetric competitive immunoassay, and 5HT6-mCherry-cADDiS and cAMP-cADDiS show similar dose response profiles. (a) Cell lysates collected from scrambled control and V2R-knockdown populations were used for cAMP quantification under different treatments (0.1  $\mu$ M tolvaptan or Tvp; 10  $\mu$ M vasopressin or AVP). Vehicle control with PBS (containing 0.005% DMSO) was used as a basal cAMP level. Fluid-shear stress was induced with 1.0 dyne/cm<sup>2</sup> for 5 minutes prior to the lysate collection. N=7 for each group. \*\*\*;  $p < 0.001$  compared to basal cAMP level. After expression of either 5HT6-mCherry-cADDiS or cAMP-cADDiS was confirmed in LL-CPK1 cells, cells were treated with adenylate cyclase inhibitor SQ22536 (10  $\mu$ M) for 24 hours to deplete intracellular cAMP. The cAMP reporter profiles were examined with different concentrations of cell permeable cAMP analog 8-Br-2'-O-Me-cAMP-AM (1 nM to 1 mM; 10<sup>-9</sup> to 10<sup>-3</sup> M). Changes in intracellular cAMP concentration are shown in (b) pseudocolored images after background subtraction and used to generate (c) dose-response curves. N=3 for each group.

Using imaging setup<sup>51</sup>, we were able to monitor both changes in the cytoplasmic and cilioplasmic cAMP levels. Vasopressin (10  $\mu$ M) elicited an increase in cAMP levels in the cilium and the cell body (Figure 33a). In the V2R-knockdown cells, this response was absent in

both the cytoplasm and the cilioplasm (Figure 33b). Forskolin (5  $\mu\text{M}$ ) also increased cAMP levels in the cytoplasm and cilioplasm of scrambled control and V2R-knockdown cells (Figure 34). Tolvaptan (0.1  $\mu\text{M}$ ) induced an increase cilioplasmic cAMP levels, but no significant change was observed in the cytoplasm (Figure 35a). Interestingly, tolvaptan also increased cilioplasmic cAMP in the V2R-knockdown cells (Figure 35b). To exclude potential involvement of extracellular calcium influx and the roles of calcium-regulated ACs, cells were preincubated with calcium channel blocker verapamil (2  $\mu\text{M}$ ) before being challenged with tolvaptan. Blocking verapamil-sensitive calcium channels had no effect on ciliary cAMP increase nor impacted tolvaptan-induced ciliary length increase (Figure 35c, Figure 38). In response to flow, the cilioplasmic cAMP underwent a significant decrease beyond the basal level (Figure 36a). The same response was not observed in the cytoplasm, where the cAMP remained at the basal level. Neither vasopressin (10  $\mu\text{M}$ ) nor tolvaptan (0.1  $\mu\text{M}$ ) affected the flow-induced repression of cilioplasmic cAMP (Figure 36b, c). In the cytoplasm, cAMP levels remained stable during flow. Taken together, certain stimuli modulated cAMP response differentially between cilioplasm and cytoplasm (Figure 39), which supports the idea of the cilium being a distinct cAMP microdomain.

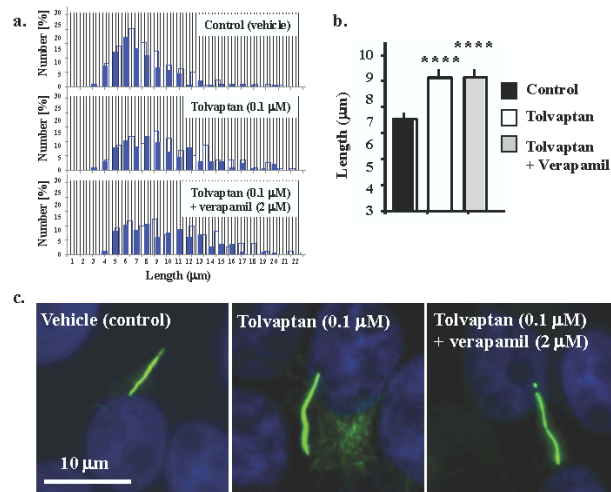


Figure 38. Calcium channel blocker, verapamil, does not affect increase in ciliary length induced by tolvaptan treatment. (a) Ciliary length distribution (in  $\mu\text{m}$ ) in response to vehicle (control) or tolvaptan (0.1  $\mu\text{M}$ ) after preincubation for 10 min in vehicle or verapamil (2  $\mu\text{M}$ ) was plotted against the number of cells (in percent). About 150 cells were randomly selected and

measured from each preparation (N=3). (b) Corresponding bar graphs show ciliary length averages. \*\*\*\*P<0.00001. c) Representative immunostaining images are shown where cilia are in green (acetylated- $\alpha$ -tubulin) and nucleus in blue.

## Discussion

Activation of V2R induces a GPCR signaling cascade, resulting in an intracellular cAMP increase. In turn, cAMP-dependent protein kinase (PKA) and other downstream signaling molecules are activated<sup>52,53</sup>. Ultimately, this leads to the insertion of AQP2 into the apical membrane<sup>54</sup>, increasing water reabsorption in the kidney collecting duct and enhancing urinary concentration in the thick ascending limb. Thus, the overall V2R function is to regulate body fluid homeostasis<sup>18</sup>.

Using PCK rats (orthologous to human PKD)<sup>26</sup> crossed with Brattleboro rats (without circulating vasopressin)<sup>27</sup>, Wang et. al. found that vasopressin is a powerful modulator of cystogenesis<sup>23</sup>. The PCK AVP<sup>-/-</sup> rats have lower renal cAMP level and show a marked reduction in renal cysts. Likewise, other animal studies show that inhibition of vasopressin-mediated signaling protects against cystogenesis<sup>24,25</sup>. The preclinical results support the idea of pursuing V2R antagonists like tolvaptan as a prospective treatment for PKD. Clinical data have also shown positive results with tolvaptan significantly reducing the rate of total kidney volume increase and slowing the estimated glomerular filtration rate (eGFR) decline in patients<sup>28-32</sup>. In April 2018, tolvaptan, under the trade name Jynarque was approved by the FDA to slow kidney function decline in adults with PKD. As a note, tolvaptan has been previously approved in 2008 by the FDA, marketed as Samsca, for treatment and prevention of hyponatremia<sup>55,56</sup>. Due to the potential of liver injury caused by tolvaptan, there is an FDA approved Risk Evaluation and Mitigation Strategy (REMS) program that needs to be followed when tolvaptan is prescribed to PKD patients<sup>57,58</sup>. The REMS include requirement of frequent tests for blood bilirubin-total (BT), alanine and aspartate aminotransferases (ALT and AST) levels to evaluate liver toxicity. Discontinuation of treatment can mitigate the hepatotoxic effects of tolvaptan when caught early hence emphasizing the requirement of frequent testing of liver function biomarkers<sup>57,59</sup>.

In our study, we examined the effect of tolvaptan on ciliary function because defects in ciliary function have been associated with PKD. Ciliary dysfunction that prevents sensation of fluid-flow in renal epithelia i.e. calcium fluxes generated in response to fluid-flow, contributes to cyst formation<sup>6,60</sup>. Kidney-specific inactivation of Kif3a, a ciliogenic gene, in newborn mice resulted in the loss of primary cilia and produced kidney cysts<sup>61</sup>. The loss of cilia resulted in aberrant

planar cell polarity as measured by the orientation of mitotic spindles in relation to the longitudinal axis of the collecting ducts. When complemented with increased rates of cell proliferation, like in cases of acute renal injury, the aberrant planar cell polarity randomizes orientation of cell division leading to tubular dilatation and kidney cyst formation<sup>62</sup>. Previous studies have shown that the ability of cilia to sense fluid-flow correlates with the ciliary length<sup>63</sup>. Upon treatment with tolvaptan, ciliary length was increased in both epithelial and endothelial cells. In turn, the mechanosensitivity of the cells was increased, as shown by cytosolic calcium measurements in response to fluid-flow. Endothelial cells displayed a more pronounced amplification of the calcium signal, which could be attributed to the more pronounced increase of ciliary length after tolvaptan treatment compared to epithelial cells.

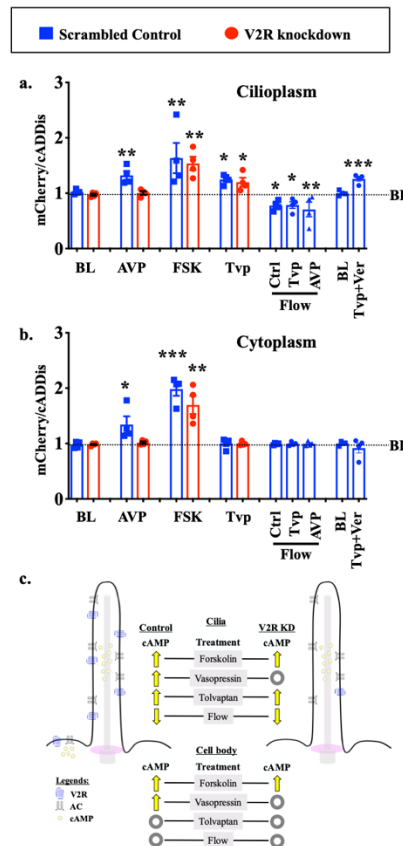


Figure 39. Cilioplasmic and cytoplasmic cAMP levels are differentially regulated. Peak cAMP increase in response to each stimulus is summarized in the bar graph for (a) cilioplasm and (b) cytoplasm. N=4 experiments for each group. \* P<0.05, \*\*P<0.001, and \*\*\*P<0.0001 compared to the baseline (BL) level prior to stimulus; AVP=arginine vasopressin; FSK=forskolin; Tvp=tolvaptan; Ctrl=control; Ver=verapamil. (c) Vasopressin receptor type-2 (V2R) is localized



to primary cilia in renal epithelia, and V2R activation with vasopressin increases adenylyl cyclase (AC) activity. Tolvaptan but not vasopressin elicits a cAMP increase in V2R-knockdown in primary cilium. Unlike tolvaptan which shows cilia-specific cAMP response, AC activator (forskolin) and vasopressin elicit cAMP responses in both cilioplasm and cytoplasm. Cilioplasmic but not cytoplasmic cAMP signaling is repressed below basal levels when cilia bend by fluid-flow. These responses indicate that a cilium may function as a distinct cAMP microdomain, independent from cytoplasmic cAMP.

Tolvaptan is a V2R antagonist, thus a V2R-knockdown would be expected to have similar effects as tolvaptan treatment. However, our results indicate that tolvaptan increases ciliary length, whereas V2R-knockdown does not affect ciliary length. Furthermore, tolvaptan also increases ciliary length in V2R-knockdown cells. This could be due to the incomplete deletion of V2R, which allows tolvaptan to act through V2R albeit at a lower magnitude, or the action of tolvaptan is independent of V2R. To this end, we analyzed localization of V2R receptors and observed similar V2R presence in apical and basolateral membranes. We see V2R expressed throughout the cilium in LL-CPK1, as also shown by Raychowdhury et. al.<sup>49</sup>, and in the basal bodies of primary cilia in IMCD renal epithelial cells. The exact mechanism by which tolvaptan increases ciliary length and function is not clear at present. However, our data indicate that such a mechanism very likely involves ciliary cAMP. The most recent study indicates that tolvaptan can inhibit potassium (K<sup>+</sup>) channels<sup>64</sup>. Thus, the potential of multiple targets or mechanisms of action of tolvaptan remains a possibility.

We performed functional studies to compare cAMP levels in V2R-knockdown cells in response to V2R agonist and antagonist. In our cilia imaging experiments, vasopressin, forskolin and tolvaptan increased cilioplasmic cAMP levels. Vasopressin stimulated cilioplasmic cAMP increases were absent in V2R-knockdown cells, whereas tolvaptan elicited a cilioplasmic cAMP increase independent of V2R. We propose that while vasopressin requires the presence of V2R to engage signaling in the cilium, tolvaptan acts in a V2R-independent manner on ciliary signaling.

Previous studies have shown that the ciliary V2R is coupled with a functional AC that increases cAMP levels in cilia upon vasopressin binding<sup>49</sup>. This is particularly interesting since localized cAMP responses could regulate ciliary function without stimulating global increases in cAMP



that would affect cell proliferation in cystic epithelia. V2R activation stimulates AC activity and studies have shown AC isoform 5/6 to be present in the cilia<sup>49,50</sup>. To verify this and discover if any other isoforms are present in the cilium, we immunostained for all AC isoforms. To our surprise we found AC3 in the cilia of LL-CPK1 cells, but there was no cilia localization of AC5/6 as previously reported<sup>49,50</sup>. Of note is that AC3 localization has been reported in neuronal cilia<sup>47,48</sup>. AC3 is one of the three CaM-sensitive AC isoforms although the effect is not as pronounced as seen in CaM activation of AC1 and AC8. Further, it is likely that AC3 is conditionally activated by calcium/ calmodulin (CaM) and also by PKC but inhibited by calcium/calmodulin-dependent protein kinase II (CaMK-II)<sup>65-67</sup>. Studies have shown CaM localization at the basal body as well as throughout the cilia in a punctate pattern<sup>68</sup>. In a 2011 study, Rothschild et. al. showed that CaMK-II is present in zebrafish cilia<sup>69</sup>. Morpholino mediated suppression of CaMK-II in zebrafish embryos induced hydrocephaly and pronephric cysts, and destabilized cloacal cilia. Furthermore, they establish that PKD2 and CaMK-II deficiencies are synergistic, where CaMK-II is a crucial effector of PKD2  $Ca^{2+}$  required for morphogenesis of the pronephric kidney and stabilization of primary cloacal cilia. This suggests that CaMK-II might play a key role in ciliary function and response to physiological stimuli.

Cyclic AMP signaling has the potential to regulate various pathways and cell functions but when restricted in a compartmentalization model, cAMP fluxes can result in specific responses. Based on our cAMP measurements, we noted that changes in cilioplasmic cAMP is independent from cytoplasm. We also found that while vasopressin and forskolin increase both cilioplasmic and cytoplasmic cAMP, tolvaptan and fluid-flow result in a discrete change only in cilioplasmic cAMP. In response to flow, the cilioplasmic cAMP underwent a significant decrease beyond basal levels. Pre-treatment with either vasopressin or tolvaptan does not affect the flow-induced cAMP decrease in the cilia, indicating the complexity of cAMP signaling within cilioplasm. These results support the idea that the cAMP signaling occurs in a compartmentalized manner such that numerous signaling pathways can utilize this biochemical signal and still achieve distinct cellular effects (Figure 39).

The concept of cAMP being synthesized in specific microdomains and spatially regulated is of growing interest. Studies with membrane microdomain specific sensors show that in addition to

the local phosphodiesterases, which control the levels of cAMP, there are specific arrangements of the cAMP signaling components<sup>70-73</sup>. Scaffold proteins, such as A-kinase anchoring proteins (AKAPs) and perhaps others, bring together GPCR, AC isoforms, phosphodiesterases and protein kinase A to create signaling complexes that regulate spatially constricted cAMP signaling cascades. The small cilia organelle enables enrichment of proteins with respect to the rest of the plasma membrane and may also restrict diffusion of second messengers with a transition zone that separates the cilioplasm from the cytoplasm<sup>74-78</sup>. These features make the cilia an effective signaling microdomain with the ability to generate a high local concentration of second messengers and effectors proteins. Studies have shown the presence of GPCR, AC isoforms and cAMP-mediated pathways present in the cilium<sup>49,79</sup>. It is plausible to contemplate that cAMP could play a role in the dynamic modulation of the cilia, which is linked to its functional efficiency.

In conclusion, we find that tolvaptan can modulate ciliary length and function. Interestingly, tolvaptan does not fit the mold of a traditional antagonist, at least not within the ciliary structure. The prospect of tolvaptan working through an off-target effect in the cilia might open new strategies targeting the cilia and PKD relationship. In studying effects V2R/tolvaptan in cilioplasmic cAMP, our data further establish the cilium as a cAMP microdomain that responds to physiologically relevant stimulus.

## References

1. Pazour, G. J. *et al.* Chlamydomonas IFT88 and its mouse homologue, polycystic kidney disease gene *tg737*, are required for assembly of cilia and flagella. *J. Cell Biol.* **151**, 709–18 (2000).
2. Nauli, S. M. Loss of Polycystin-1 in Human Cyst-Lining Epithelia Leads to Ciliary Dysfunction. *J. Am. Soc. Nephrol.* **17**, 1015–1025 (2006).
3. Vassilev, P. M. *et al.* Polycystin-2 is a novel cation channel implicated in defective intracellular Ca<sup>2+</sup> homeostasis in polycystic kidney disease. *Biochem. Biophys. Res. Commun.* **282**, 341–50 (2001).
4. Xu, C. *et al.* Human ADPKD primary cyst epithelial cells with a novel, single codon deletion in the PKD1 gene exhibit defective ciliary polycystin localization and loss of flow-induced Ca<sup>2+</sup> signaling. *AJP Ren. Physiol.* **292**, F930–F945 (2006).
5. Nauli, S. M. *et al.* Endothelial Cilia Are Fluid Shear Sensors That Regulate Calcium Signaling and Nitric Oxide Production Through Polycystin-1. *Circulation* **117**, 1161–1171 (2008).
6. Nauli, S. M. *et al.* Polycystins 1 and 2 mediate mechanosensation in the primary cilium of kidney cells. *Nat. Genet.* **33**, 129–37 (2003).
7. Praetorius, H. A. & Spring, K. R. Bending the MDCK cell primary cilium increases intracellular calcium. *J. Membr. Biol.* **184**, 71–9 (2001).
8. Spasic, M. & Jacobs, C. R. Lengthening primary cilia enhances cellular mechanosensitivity. *Eur. Cell. Mater.* **33**, 158–168 (2017).
9. Abdul-Majeed, S. & Nauli, S. M. Dopamine receptor type 5 in the primary cilia has dual chemo- and mechano-sensory roles. *Hypertens. (Dallas, Tex. 1979)* **58**, 325–31 (2011).
10. Kathem, S. H. *et al.* Ciliotherapy: a novel intervention in polycystic kidney disease. *J. Geriatr. Cardiol.* **11**, 63–73 (2014).
11. Choi, Y.-H. *et al.* Polycystin-2 and phosphodiesterase 4C are components of a ciliary A-kinase anchoring protein complex that is disrupted in cystic kidney diseases. *Proc. Natl. Acad. Sci. U. S. A.* **108**, 10679–84 (2011).
12. Siroky, B. J. *et al.* Loss of primary cilia results in deregulated and unabated apical calcium entry in ARPKD collecting duct cells. *Am. J. Physiol. Renal Physiol.* **290**, F1320–8 (2006).
13. Pala, R. *et al.* Personalized Nanotherapy by Specifically Targeting Cell Organelles To Improve Vascular Hypertension. *Nano Lett.* **19**, 904–914 (2019).
14. Pala, R. *et al.* Ciliotherapy: Remote Control of Primary Cilia Movement and Function by Magnetic Nanoparticles. *ACS Nano* acsnano.9b00033 (2019). doi:10.1021/acsnano.9b00033
15. Grantham, J. J., Ye, M., Gattone, V. H. & Sullivan, L. P. In vitro fluid secretion by epithelium from polycystic kidneys. *J. Clin. Invest.* **95**, 195–202 (1995).
16. Ye, M. & Grantham, J. J. The Secretion of Fluid by Renal Cysts from Patients with Autosomal Dominant Polycystic Kidney Disease. *N. Engl. J. Med.* **329**, 310–313 (1993).
17. Mangoo-Karim, R. *et al.* Renal epithelial fluid secretion and cyst growth: the role of cyclic AMP. *FASEB J.* **3**, 2629–32 (1989).
18. Fenton, R. A., Brønd, L., Nielsen, S. & Praetorius, J. Cellular and subcellular distribution of the type-2 vasopressin receptor in the kidney. *Am. J. Physiol. Renal Physiol.* **293**, F748–F760 (2007).
19. Ausiello, D. A., Skorecki, K. L., Verkman, A. S. & Bonventre, J. V. Vasopressin signaling in kidney cells. *Kidney Int.* **31**, 521–529 (1987).
20. Nagao, S. Increased Water Intake Decreases Progression of Polycystic Kidney Disease in the PCK Rat. *J. Am. Soc. Nephrol.* **17**, 2220–2227 (2006).
21. Gattone, V. H., Wang, X., Harris, P. C. & Torres, V. E. Inhibition of renal cystic disease development and progression by a vasopressin V2 receptor antagonist. *Nat. Med.* **9**, 1323–6 (2003).
22. Gattone, V. H., Maser, R. L., Tian, C., Rosenberg, J. M. & Branden, M. G. Developmental

- expression of urine concentration-associated genes and their altered expression in murine infantile-type polycystic kidney disease. *Dev. Genet.* **24**, 309–318 (1999).
23. Wang, X., Wu, Y., Ward, C. J., Harris, P. C. & Torres, V. E. Vasopressin directly regulates cyst growth in polycystic kidney disease. *J. Am. Soc. Nephrol.* **19**, 102–8 (2008).
  24. Reif, G. A. *et al.* Tolvaptan inhibits ERK-dependent cell proliferation, CF secretion, and in vitro cyst growth of human ADPKD cells stimulated by vasopressin. *Am. J. Physiol. Renal Physiol.* **301**, F1005-13 (2011).
  25. Wang, X., Gattone, V., Harris, P. C. & Torres, V. E. Effectiveness of vasopressin V2 receptor antagonists OPC-31260 and OPC-41061 on polycystic kidney disease development in the PCK rat. *J. Am. Soc. Nephrol.* **16**, 846–51 (2005).
  26. Lager, D. J., Qian, Q., Bengal, R. J., Ishibashi, M. & Torres, V. E. The pck rat: a new model that resembles human autosomal dominant polycystic kidney and liver disease. *Kidney Int.* **59**, 126–36 (2001).
  27. Kim, J. K. & Schrier, R. W. Vasopressin processing defects in the Brattleboro rat: implications for hereditary central diabetes insipidus in humans? *Proc. Assoc. Am. Physicians* **110**, 380–6 (1998).
  28. Torres, V. E. *et al.* Effect of Tolvaptan in Autosomal Dominant Polycystic Kidney Disease by CKD Stage: Results from the TEMPO 3:4 Trial. *Clin. J. Am. Soc. Nephrol.* **11**, 803–11 (2016).
  29. Torres, V. E. *et al.* Multicenter, open-label, extension trial to evaluate the long-term efficacy and safety of early versus delayed treatment with tolvaptan in autosomal dominant polycystic kidney disease: the TEMPO 4:4 Trial. *Nephrol. Dial. Transplant* **33**, 477–489 (2018).
  30. Torres, V. E. *et al.* Tolvaptan in Patients with Autosomal Dominant Polycystic Kidney Disease. *N. Engl. J. Med.* **367**, 2407–2418 (2012).
  31. Higashihara, E. *et al.* Tolvaptan in autosomal dominant polycystic kidney disease: three years' experience. *Clin. J. Am. Soc. Nephrol.* **6**, 2499–507 (2011).
  32. Torres, V. E. *et al.* Tolvaptan in Later-Stage Autosomal Dominant Polycystic Kidney Disease. *N. Engl. J. Med.* **377**, 1930–1942 (2017).
  33. Cheng, X., Ji, Z., Tsalkova, T. & Mei, F. Epac and PKA: a tale of two intracellular cAMP receptors. *Acta Biochim. Biophys. Sin. (Shanghai)*. **40**, 651–62 (2008).
  34. Besschetnova, T. Y. *et al.* Identification of signaling pathways regulating primary cilium length and flow-mediated adaptation. *Curr. Biol.* **20**, 182–7 (2010).
  35. Low, S. H. *et al.* Targeting of SNAP-23 and SNAP-25 in polarized epithelial cells. *J. Biol. Chem.* **273**, 3422–30 (1998).
  36. Abdul-Majeed, S., Moloney, B. C. & Nauli, S. M. Mechanisms regulating cilia growth and cilia function in endothelial cells. *Cell. Mol. Life Sci.* **69**, 165–173 (2012).
  37. Ou, Y. *et al.* Adenylate cyclase regulates elongation of mammalian primary cilia. *Exp. Cell Res.* **315**, 2802–17 (2009).
  38. Sorokin, S. Centrioles and the formation of rudimentary cilia by fibroblasts and smooth muscle cells. *J. Cell Biol.* **15**, 363–377 (1962).
  39. Rieder, C. L., Jensen, C. G. & Jensen, L. C. W. The resorption of primary cilia during mitosis in a vertebrate (PtK1) cell line. *J. Ultrastruct. Res.* **68**, 173–185 (1979).
  40. Ecelbarger, C. A., Chou, C. L., Lolait, S. J., Knepper, M. A. & DiGiovanni, S. R. Evidence for dual signaling pathways for V2 vasopressin receptor in rat inner medullary collecting duct. *Am. J. Physiol. Physiol.* **270**, F623–F633 (1996).
  41. Faust, D. *et al.* Culturing primary rat inner medullary collecting duct cells. *J. Vis. Exp.* (2013). doi:10.3791/50366
  42. Nonoguchi, H. *et al.* Immunohistochemical localization of V2 vasopressin receptor along the nephron and functional role of luminal V2 receptor in terminal inner medullary collecting ducts. *J. Clin. Invest.* **96**, 1768–1778 (1995).
  43. Mohieldin, A. M. *et al.* Protein composition and movements of membrane swellings associated with primary cilia. *Cell. Mol. Life Sci.* **72**, 2415–29 (2015).
  44. Mitchell, K. A. P. Isolation of primary cilia by shear force. *Curr. Protoc. cell Biol.* **Chapter 3**,

- Unit 3.42.1-9 (2013).
45. Nielsen, S. *et al.* Vasopressin increases water permeability of kidney collecting duct by inducing translocation of aquaporin-CD water channels to plasma membrane. *Proc. Natl. Acad. Sci.* **92**, (1995).
  46. Schlondorff, D. & Franki, N. Effect of vasopressin on cyclic AMP-dependent protein kinase in toad urinary bladder. *Biochim. Biophys. Acta* **628**, 1–12 (1980).
  47. Bishop, G. A., Berbari, N. F., Lewis, J. & Mykityn, K. Type III adenylyl cyclase localizes to primary cilia throughout the adult mouse brain. *J. Comp. Neurol.* **505**, 562–71 (2007).
  48. Wang, Z. *et al.* Adult Type 3 Adenylyl Cyclase–Deficient Mice Are Obese. *PLoS One* **4**, e6979 (2009).
  49. Raychowdhury, M. K. *et al.* Vasopressin receptor-mediated functional signaling pathway in primary cilia of renal epithelial cells. *Am. J. Physiol. Renal Physiol.* **296**, F87-97 (2009).
  50. Wang, Q. *et al.* Adenylyl cyclase 5 deficiency reduces renal cyclic AMP and cyst growth in an orthologous mouse model of polycystic kidney disease. *Kidney Int.* (2017). doi:10.1016/j.kint.2017.08.005
  51. Jin, X. *et al.* Cilioplasm is a cellular compartment for calcium signaling in response to mechanical and chemical stimuli. *Cell. Mol. Life Sci.* **71**, 2165–78 (2014).
  52. Yip, K.-P. Coupling of vasopressin-induced intracellular Ca<sup>2+</sup> mobilization and apical exocytosis in perfused rat kidney collecting duct. *J. Physiol.* **538**, 891–9 (2002).
  53. Chou, C.-L. *et al.* Non-muscle myosin II and myosin light chain kinase are downstream targets for vasopressin signaling in the renal collecting duct. *J. Biol. Chem.* **279**, 49026–35 (2004).
  54. Brown, D. The ins and outs of aquaporin-2 trafficking. *Am. J. Physiol. Renal Physiol.* **284**, F893-901 (2003).
  55. Verbalis, J. G. *et al.* Efficacy and safety of oral tolvaptan therapy in patients with the syndrome of inappropriate antidiuretic hormone secretion. *Eur. J. Endocrinol.* **164**, 725–732 (2011).
  56. Schrier, R. W. *et al.* Tolvaptan, a Selective Oral Vasopressin V<sub>2</sub> -Receptor Antagonist, for Hyponatremia. *N. Engl. J. Med.* **355**, 2099–2112 (2006).
  57. Watkins, P. B. *et al.* Clinical Pattern of Tolvaptan-Associated Liver Injury in Subjects with Autosomal Dominant Polycystic Kidney Disease: Analysis of Clinical Trials Database. *Drug Saf.* **38**, 1103–13 (2015).
  58. U.S. Food and Drug Administration. Drug Approval Package: Jynarque (tolvaptan). (2018). Available at: [https://www.accessdata.fda.gov/drugsatfda\\_docs/nda/2018/204441Orig1s000TOC.cfm](https://www.accessdata.fda.gov/drugsatfda_docs/nda/2018/204441Orig1s000TOC.cfm). (Accessed: 19th December 2018)
  59. Muto, S. *et al.* Long-term safety profile of tolvaptan in autosomal dominant polycystic kidney disease patients: TEMPO Extension Japan Trial. *Drug. Healthc. Patient Saf.* **9**, 93–104 (2017).
  60. Kuo, I. Y. *et al.* Cyst formation following disruption of intracellular calcium signaling. *Proc. Natl. Acad. Sci. U. S. A.* **111**, 14283–8 (2014).
  61. Lin, F. *et al.* Kidney-specific inactivation of the KIF3A subunit of kinesin-II inhibits renal ciliogenesis and produces polycystic kidney disease. *Proc. Natl. Acad. Sci. U. S. A.* **100**, 5286–5291 (2003).
  62. Fischer, E. *et al.* Defective planar cell polarity in polycystic kidney disease. *Nat. Genet.* **38**, 21–3 (2006).
  63. Upadhyay, V. S. *et al.* Roles of dopamine receptor on chemosensory and mechanosensory primary cilia in renal epithelial cells. *Front. Physiol.* **5**, 72 (2014).
  64. Lu, T.-L., Chang, W.-T., Chan, C.-H. & Wu, S.-N. Evidence for Effective Multiple K<sup>+</sup>-Current Inhibitions by Tolvaptan, a Non-peptide Antagonist of Vasopressin V<sub>2</sub> Receptor. *Front. Pharmacol.* **10**, 76 (2019).
  65. Halls, M. L. & Cooper, D. M. F. Regulation by Ca<sup>2+</sup>-signaling pathways of adenylyl cyclases. *Cold Spring Harb. Perspect. Biol.* **3**, a004143 (2011).
  66. Wei, J., Wayman, G. & Storm, D. R. Phosphorylation and inhibition of type III adenylyl cyclase



- by calmodulin-dependent protein kinase II in vivo. *J. Biol. Chem.* **271**, 24231–5 (1996).
67. Wei, J. *et al.* Phosphorylation and inhibition of olfactory adenylyl cyclase by CaM kinase II in Neurons: a mechanism for attenuation of olfactory signals. *Neuron* **21**, 495–504 (1998).
  68. Otto, E. A. *et al.* Nephrocystin-5, a ciliary IQ domain protein, is mutated in Senior-Loken syndrome and interacts with RPGR and calmodulin. *Nat. Genet.* **37**, 282–288 (2005).
  69. Rothschild, S. C., Francescato, L., Drummond, I. A. & Tombes, R. M. CaMK-II is a PKD2 target that promotes pronephric kidney development and stabilizes cilia. *Development* **138**, 3387–97 (2011).
  70. Agarwal, S. R., Miyashiro, K., Latt, H., Ostrom, R. S. & Harvey, R. D. Compartmentalized cAMP responses to prostaglandin EP2 receptor activation in human airway smooth muscle cells. *Br. J. Pharmacol.* **174**, 2784–2796 (2017).
  71. Wachten, S. *et al.* Distinct pools of cAMP centre on different isoforms of adenylyl cyclase in pituitary-derived GH3B6 cells. *J. Cell Sci.* **123**, 95–106 (2010).
  72. Agarwal, S. R. *et al.* Role of Membrane Microdomains in Compartmentation of cAMP Signaling. *PLoS One* **9**, e95835 (2014).
  73. Dessauer, C. W. Adenylyl cyclase--A-kinase anchoring protein complexes: the next dimension in cAMP signaling. *Mol. Pharmacol.* **76**, 935–41 (2009).
  74. Hu, Q. & Nelson, W. J. Ciliary diffusion barrier: The gatekeeper for the primary cilium compartment. *Cytoskeleton* **68**, 313–324 (2011).
  75. Hsiao, Y.-C., Tuz, K. & Ferland, R. J. Trafficking in and to the primary cilium. *Cilia* **1**, 4 (2012).
  76. Takao, D., Wang, L., Boss, A. & Verhey, K. J. Protein Interaction Analysis Provides a Map of the Spatial and Temporal Organization of the Ciliary Gating Zone. *Curr. Biol.* **27**, 2296–2306.e3 (2017).
  77. Bachmann-Gagescu, R. *et al.* The Ciliopathy Protein CC2D2A Associates with NINL and Functions in RAB8-MICAL3-Regulated Vesicle Trafficking. *PLOS Genet.* **11**, e1005575 (2015).
  78. Garcia-Gonzalo, F. R. *et al.* A transition zone complex regulates mammalian ciliogenesis and ciliary membrane composition. *Nat. Genet.* **43**, 776–784 (2011).
  79. Kwon, R. Y., Temiyasathit, S., Tummala, P., Quah, C. C. & Jacobs, C. R. Primary cilium-dependent mechanosensing is mediated by adenylyl cyclase 6 and cyclic AMP in bone cells. *FASEB J.* **24**, 2859–68 (2010).
  80. Bogard, A. S., Xu, C. & Ostrom, R. S. Human bronchial smooth muscle cells express adenylyl cyclase isoforms 2, 4, and 6 in distinct membrane microdomains. *J. Pharmacol. Exp. Ther.* **337**, 209–17 (2011).
  81. Hull, R. N., Cherry, W. R. & Weaver, G. W. The origin and characteristics of a pig kidney cell strain, LLC-PK1. *In Vitro* **12**, 670–677 (1976).
  82. Tahara, A. *et al.* Pharmacological characterization of the human vasopressin receptor subtypes stably expressed in Chinese hamster ovary cells. *Br. J. Pharmacol.* **125**, 1463–1470 (1998).
  83. Jin, X. *et al.* L-type calcium channel modulates cystic kidney phenotype. *Biochim. Biophys. Acta* **1842**, 1518–26 (2014).
  84. Nauli, S. M. *et al.* Non-Motile Primary Cilia as Fluid Shear Stress Mechanosensors. in *Methods in enzymology* **525**, 1–20 (2013).
  85. Mukherjee, S. *et al.* A novel biosensor to study cAMP dynamics in cilia and flagella. *Elife* **5**, 694–697 (2016).
  86. Tewson, P. H., Martinka, S., Shaner, N. C., Hughes, T. E. & Quinn, A. M. New DAG and cAMP Sensors Optimized for Live-Cell Assays in Automated Laboratories. *J. Biomol. Screen.* **21**, 298–305 (2016).

## Conclusion

Our knowledge of the primary cilium and its role in mechanotransduction among other functions has been advanced in the past decades. As a critical sensory organelle, the importance of cilium is highlighted by the multi-organ diseases that arise due to defective or absent cilia. Ciliary transduction of fluid flow stimulus regulates biochemical reactions, molecular responses, gene expressions regulating tissue development and physiological function. Here we covered approaches to study ciliary signaling and pathways that modulate mechanosensory primary cilia. Our aim is to be able to determine whether signals are arising from the cilioplasm or cytoplasm. This has been done using a side view modality, coupled with a high spatial-temporal resolution and high sensitivity fluorescent sensor. With our cilia targeted ratio-metric sensor and single cilia imaging we shed light on the dynamics of cAMP changes in the primary cilium. This is motivated by the involvement of cilia and aberrant signaling in ciliopathies since defects in the structure of cilia or protein complexes located in the primary cilia cause ciliopathies.

Along with the mechanical sensory functions, we tested whether the primary cilium has a role in sensing biochemical cues, more specifically its role in transducing pH changes of the extracellular milieu. We compared acidosis response using vascular endothelial cells in comparison to cilia-less *Tg737* cells. This allowed us to observe potential pathways that might be differentially regulated by the presence of the cilium. Using mitogen-activated protein kinase (MAPK) activation markers, we assessed acid-activation of p38- and ERK1/2-mediated signaling pathways, which were involved in regulating ion transport for acid-base homeostasis in endothelia. We established that the primary cilium influences pH sensing threshold with cilia-less *Tg737* requiring farther acidic condition to activate the same suite of MAPK proteins. However, intracellular pH homeostasis is not significantly different between the wild-type and *Tg737* cells with pH recovery occurring through a  $K^+$ -dependent process. Nonetheless, cells developed longer cilia when challenged with an acidic environment. It is interesting to note that cilia length has been speculated to increase in response to injury or environmental insults. Endothelial cilia, although having effect on acid-activated MAPK activation as well as modulating its length in response to acidosis, are unlikely to be the sole acid sensing organelle.



Our results also highlighted the limitation of our study in ciliary pH sensing since inherent mechanisms related to pH homeostasis could be disrupted in *Tg737* cells. IFT88 protein, which is deleted in *Tg737* cells, are involved in transport of proteins between cilium and cell body. IFT88 is not only limited to transporting but also is localized in proliferating mammalian cells at the centrosome and participates in cell cycle progression. Upon cilia resorption, the ciliary proteins get redistributed and IFT88 proteins become associated with the proximal end of centrioles. Inhibition of *IFT88* expression causes cell-cycle progression from G1 to S and G2/M phases. Therefore, in order to bypass possible cell cycle induced effects by *IFT88* deletion, either mechanical or chemical disruption of the cilium can be used to test ciliary pH sensing. Chloral hydrate has been used to de-ciliate cells but can also increase cell size, disrupt the cytoskeleton and has an inhibitive effect on mitosis. However, we are encouraged by other studies that have found acid stimulated ion channels (ASICs) in olfactory cilia as well as a mechanosensation related function for ASIC neuronal cells. Loss of ASIC in mice models reduced the sensitivity of a mechanoreceptor responding to noxious pinch. The ASIC knockout mice had decreased response to acid- and noxious heat stimuli. This leads to the possibility to study ASIC isoforms distribution in the cilia and tease out the nuanced contribution of primary cilia in acid sensation.

As a sensory organelle, the cilium utilizes secondary messengers such as calcium and cAMP to transmit stimuli and effect changes in the cell. cAMP signaling has the potential to regulate various pathways and cell functions. cAMP fluxes can initiate specialized responses with the help of cAMP pathway modulators organized in clusters. This is possible with scaffold proteins that bring together G-protein coupled receptor (GPCR), adenylyl cyclase (AC) isoforms, phosphodiesterases and protein kinase A to create signaling complexes dedicated to fine tune cAMP signaling cascades. Our interest in ciliary cAMP signaling was started with tolvaptan, a prospective drug for polycystic kidney disease, which acts on a GPCR located in the cilia and effects ciliary structure/function. After observation of tolvaptan induced ciliary length increase and functional enhancement, we investigated the ciliary vasopressin receptor 2 (V2R) signaling cascade. V2R, the target of tolvaptan, is activated by its natural ligand vasopressin leading to AC activity thus cAMP increase. With the help of targeted fluorescent sensors, our model of localized ciliary cAMP responses that regulates cilia structure and function was strengthened. Tolvaptan increased cilia specific cAMP and this occurred without stimulating global increases in

cAMP which could increase cell proliferation in cystic epithelia. Vasopressin and forskolin increased cilioplasmic and cytoplasmic cAMP while treatment with tolvaptan resulted in a discrete cAMP increase restricted to the cilioplasm. Demonstrating its function as a flow sensor, we found that the cilioplasmic cAMP is decreased beyond basal levels when fluid flow is applied. These results support compartmentalized cAMP signaling occurring in the cilium, independent from the cytosol.

Another plausible idea would be that tolvaptan acts as a partial agonist by itself although numerous studies that have shown tolvaptan dampens vasopressin mediated cAMP increase. An explanation could be receptor-based functional selectivity or “protean” agonism. As an example, dichloroisoproterenol acts stochastically as either a weak partial agonist or a weak inverse agonist for  $\beta_2$ -adrenergic receptor. However, after agonist-induced desensitization, dichloroisoproterenol switches fully to an inverse agonist. Chidiac P et al. in their study show that the initial state of the receptor can determine whether a ligand behaves as a partial agonist or an inverse agonist (Chidiac, Nouet, & Bouvier, 1996). In our case, a possible scenario *in vivo* might be that vasopressin induces desensitization of V2R affects tolvaptan interaction with the receptor and causes it to behave as an inverse agonist.

Studies have shown AC isoforms to be present in the cilia (Bishop, Barbari, Lewis, & Mykytyn, 2007; Raychowdhury et al., 2009; Q. Wang et al., 2017; Z. Wang et al., 2009) and we find ciliary localization of AC3 in LL-CPK1 cells. AC3 is one of the three Calmodulin(CaM)-sensitive AC isoforms and is likely to be conditionally activated by  $Ca^{2+}$ / CaM as well as PKC. Studies have shown CaM localization at the basal body as well as throughout the cilia (Otto et al., 2005). All these studies show how input synchronization of calcium and its binding partners with ciliary AC might affect the final cAMP levels. Animas models relevant to our study such as V2R deficient or AC KO mice show a high mortality after birth. The *V2R* genes are localized to the long arm of the X chromosome and loss of V2R function interferes with water uptake in the renal collecting duct system, polyuria accompanied by excessive thirst. The large output of urine can lead to severe hypernatremia and dehydration if water intake is not maintained. Adult females (*V2R*<sup>+/-</sup>) which have a functioning copy of V2R mice displayed a reduced urine-concentrating ability, polyuria, and polydipsia. *AC3* KO mice that survive suffer from anosmia,

cognitive failures and obesity but have no other perturbations of peripheral organs such as vessels, bone or cartilage. One hypothesis is that other isoforms from the AC pool might make up for the loss of AC3. Although these animal models are plagued by the induced disabilities these might help in studying the interrelationship between the cilia localized proteins, ciliary characteristics and development *in vivo*.

The cilium is an effective signaling microdomain with the ability to generate a high local concentration of second messengers and effectors proteins. Other structural features such as the transition zone of the cilium also restrict biomolecules to the cilium but still activate downstream effectors that have cell-wide consequences. Our studies indicate that sensory function of the cilium involves cAMP pathway in regulating ciliary structure and function where the cilium acts as a cAMP compartment that responds to physiological stimulus. Overall, it is important to understand the complex molecular composition of the cilia, appreciate the diverse functions attributed to it and the pathways contained within it.

## References

1. Bishop, G. A., Berbari, N. F., Lewis, J., & Mykityn, K. (2007). Type III adenylyl cyclase localizes to primary cilia throughout the adult mouse brain. *The Journal of Comparative Neurology*, 505(5), 562–571. <https://doi.org/10.1002/cne.21510>
2. Chidiac, P., Nouet, S., & Bouvier, M. (1996). Agonist-induced modulation of inverse agonist efficacy at the beta 2-adrenergic receptor. *Molecular Pharmacology*, 50(3), 662–669. Retrieved from <http://www.ncbi.nlm.nih.gov/pubmed/8794908>
3. Otto, E. A., Loeys, B., Khanna, H., Hellemans, J., Sudbrak, R., Fan, S., ... Hildebrandt, F. (2005). Nephrocystin-5, a ciliary IQ domain protein, is mutated in Senior-Loken syndrome and interacts with RPGR and calmodulin. *Nature Genetics*, 37(3), 282–288. <https://doi.org/10.1038/ng1520>
4. Pala, R., Mohieldin, A. M., Shamloo, K., Sherpa, R. T., Kathem, S. H., Zhou, J., ... Nauli, S. M. (2019). Personalized Nanotherapy by Specifically Targeting Cell Organelles To Improve Vascular Hypertension. *Nano Letters*, 19(2), 904–914. <https://doi.org/10.1021/acs.nanolett.8b04138>
5. Raychowdhury, M. K., Ramos, A. J., Zhang, P., McLaughlin, M., Dai, X.-Q., Chen, X.-Z., ... Cantiello, H. F. (2009). Vasopressin receptor-mediated functional signaling pathway in primary cilia of renal epithelial cells. *American Journal of Physiology. Renal Physiology*, 296(1), F87-97. <https://doi.org/10.1152/ajprenal.90509.2008>
6. Wang, Q., Cobo-Stark, P., Patel, V., Somlo, S., Han, P.-L., & Igarashi, P. (2017). Adenylyl cyclase 5 deficiency reduces renal cyclic AMP and cyst growth in an orthologous mouse model of polycystic kidney disease. *Kidney International*. <https://doi.org/10.1016/j.kint.2017.08.005>
7. Wang, Z., Li, V., Chan, G. C. K., Phan, T., Nudelman, A. S., Xia, Z., & Storm, D. R. (2009). Adult Type 3 Adenylyl Cyclase-Deficient Mice Are Obese. *PLoS ONE*, 4(9), e6979. <https://doi.org/10.1371/journal.pone.0006979>